**Linköping University**

Department of Management and Engineering

Division of Fluid and Mechanic Systems


Master Thesis in Aerospace Engineering

# Implementation of Flight Mechanical Evaluation Criteria in an Aircraft Conceptual Design Tool with Focus on Lateral Motion

*Author*
García Garre, Ricardo - ricardogarciagarre@gmail.com

*Supervisor*: Jonas Stålhand
*Examiner*: Lars Johansson

Linköping Universitet, May 2023
SE-581 83 Linköping, Sverige
013-28 10 00, www.liu.se

**Abstract**

This thesis addresses the modeling of the main lateral aerodynamic characteristics of a conventional aircraft in the subsonic flight regime, to be implemented within the data model of the Pacelab APD program. The main objective is to use semi-empirical methods available in the existing literature to estimate the behavior of a conventional aircraft during the conceptual design stage. Due to the nature of this phase, the methods employed must be such that they allow for quick calculations using little computational power to perform multiple iterations within a small time frame.

The thesis provider, Saab AB, requires that these methods be digitized within the software Pacelab APD, used by the company for the conceptual modeling of new aircraft. Thus, the geometric and aerodynamic definition of the aircraft model provided by Pacelab APD are used as input parameters for the implemented methods and criteria related to flight mechanics.

This thesis analyzes, studies, and presents basic foundations and advanced concepts of flight mechanics available in the literature, the methodology adopted for its digitization in Pacelab APD, the results obtained from the use of such methods, and a final discussion on their accuracy and reliability, comparing them with other known methods and software programs to calculate, among other things, aerodynamic derivatives. The results of this project will contribute to the development of new aircraft designs in a more efficient way by providing a tool to predict their lateral flight characteristics during the conceptual design phase.

Simultaneously, two master theses are conducted to achieve this objective, with a division of workload focusing on the longitudinal and lateral dynamics of the aircraft. This thesis specifically focuses on the lateral motion.

**Key words:** lateral flight mechanics, subsonic flight, conceptual design criteria, aircraft, aerodynamics, data modeling, Pacelab APD, empirical methods, method digitization, computational efficiency, flight characteristics, aerodynamic derivatives

# Contents

# List of Figures

# List of Tables

# List of Symbols

## Acronyms

| | |
|---|---|
| AB | Aktiebolag (Limited Company) |
| AD | Aerodynamic Derivatives |
| APD | Aircraft Preliminary Design |
| AR | Aspect Ratio |
| CAD | Computer aided design |
| CFD | Computational fluid dynamics |
| CG | Center of Gravity |
| DATCOM | Data Compendium |
| EO | Engineering Object |
| EWB | Engineering Workbench |
| FEM | Finite Element Method |
| FO | Functional Object |
| GmbH | Gesellschaft mit beschränkter Haftung (Limited Liability Company) |
| KD | Knowledge Designer |
| LiU | Linköping University |
| LCDP | Lateral Control Departure Parameter |
| USAF | United States Air Force |
| VLM | Vortex Lattice Method |

# Roman letters

| | |
|---|---|
| b | Span |
| | Body |
| C | Coefficient |
| D | Drag |
| i | Any aerodynamic variable (velocity, rate, deflection etc.) |
| $I_{xx}$ | Airplane moment of inertia about x axis |
| $I_{yy}$ | Airplane moment of inertia about y axis |
| $I_{zz}$ | Airplane moment of inertia about z axis |
| L | Lift |
| | Roll moment |
| m | Aircraft's mass |
| M | Mach |
| | Pitch Moment |
| N | Yaw Moment |
| O | Origin |
| p | Rolling rate |
| q | Pitching rate |
| $\bar{Q}$ | Dynamic pressure |
| r | Yawing rate |
| R | Various physical quantities (force, moment, etc.) |
| S | Wing surface area |
| V | Velocity |
| w | Wing |
| u | Forward velocity |
| v | Side velocity |
| V | Airplanes airspeed |
| w | Vertical velocity |
| X | Axis pertaining to a triad type coordinate system |
| | Force in the X axis |
| Y | Axis pertaining to a triad type coordinate system |
| | Force in the Y axis |
| Z | Axis pertaining to a triad type coordinate system |
| | Force in the Z axis |

# Greek letters

| | |
|---|---|
| $\alpha$ | Longitudinal angle of attack |
| $\beta$ | Lateral angle of attack (a.k.a sideslip angle) |
| $\delta$ | Deflection of an aerodynamic surface |
| $\phi$ | Roll angle |
| $\psi$ | Yaw angle |
| $\theta$ | Pitch angle |
| $\Lambda$ | Sweep angle |
| $\Gamma$ | Dihedral angle |

# Subscript

| | |
|---|---|
| a | Referred to aerodynamic<br>Aileron |
| b | Referred to the body / fuselage |
| c/0 | At the leading edge of the chord |
| c/4 | At one fourth of the chord |
| c/2 | At the half of the chord |
| e | Elevator |
| eff | Effective |
| f | Flap |
| h | Referred to the horizontal stabilizer |
| l | Roll Moment |
| m | Pitch Moment |
| n | Yaw Moment |
| r | Rudder |
| v | Referred to the vertical tail (fin) |
| w | Referred to the wing |
| $\infty$ | Referred to free stream conditions |

# Chapter 1

# Introduction

A crucial phase in the aircraft design process is the conceptual design stage, where many iterations of a concept aircraft are simulated in order to yield the optimum configuration to meet given requirements for a specific mission. This phase involves the creation of a preliminary design that outlines the fundamental characteristics of an aircraft. Therefore, the selection of the best configuration, both in geometric and aerodynamic terms, is paramount to lay the foundation for the aircraft's ultimate success. This is done through an iterative process that involves multiple trade studies, and analysis to identify the best design options and trade-offs.

During this first design stage, it is also of special relevance to make an initial estimation of the flight characteristics that a specific iteration of a concept aircraft will have, predicting how the new design will behave during the flight. This aims to ensure that the aircraft meets the expected requirements and is safe to fly. Here is where the field of flight mechanics comes into play. Flight mechanics is concerned with generating models of forces, momentum, and dimensionless factors that help designers evaluate the feasibility of a project and the flying qualities of an aircraft. It also provides criteria that help to carry out a better design and sizing of the lifting and aerodynamic control surfaces.

It is evident that flight mechanics is important at the conceptual design stage, as it plays a critical role in ensuring the aerodynamic behavior of the aircraft is well understood. A comprehensive study of the aircraft's aerodynamics enables the proper sizing of its main aerodynamic surfaces, resulting in good aerodynamic performance, reduced drag, good flying qualities and enhanced economic viability of the project. This underscores the importance of effective flight mechanics analysis and design in optimizing the overall performance of an aircraft.

Given the critical role of flight mechanics in the aircraft conceptual design stage, this thesis endeavors to examine how the field of flight mechanics can be

effectively integrated into the design iteration process of new aircraft models, such that it can be practically applied by aerospace design companies.

## 1.1 Thesis motivation

This master's thesis is proposed by the Swedish aircraft design and manufacturing company, Saab AB (Saab) [1]. One of the digital programs that Saab employs for the conceptual design of new aircraft prototypes is Pacelab Aircraft Preliminary Design, abbreviated as Pacelab APD, developed by the German company PACE Aerospace Engineering and Information Technology GmbH (PACE).

Pacelab APD is presented as an alternative that "allows evaluating alternative aircraft configurations in terms of performance, economics and technical risk and helps to assess the impact of technological innovations early in the design process" [2]. It is a program that allows, among other things, parametric modeling of aircraft.

One of the capabilities of Pacelab APD is the analysis of masses and weights of the various components that make up the geometry. This is especially useful for calculating aspects such as the necessary lift that the wing must generate to maintain level flight at a certain altitude. Weight estimation also allows for the calculation of other basic aspects of particular importance, such as the center of gravity or the moments of inertia of the aircraft, critical for conducting flight mechanics studies, as will be discussed later. Pacelab APD also estimates the aerodynamic characteristics of the models, such as the lift generated by the aerodynamic surfaces and the drag produced by the various components of the aircraft, such as the fuselage, wing, or tail stabilizers.

However, Pacelab APD has significant limitations that directly affect the preliminary design phase. Firstly, it lacks the ability to model some of the main aerodynamic control surfaces, such as ailerons and elevator. Similarly, it lacks methods that allow for the estimation of forces and moments generated by the aircraft geometry itself by the aerodynamic and control surfaces.

These two limitations render it unfeasible to implement any sizing criteria for surfaces related to flight mechanics. However, this limitation can be overcome by using so-called rules of thumb, which consist of a factor that relates or estimates the size that certain surfaces should have compared to others whose dimensions are known. These methods generally work well when the aircraft to be designed has a design very similar to those with which the corresponding rule of thumb has been developed. In any other case, the use of this technique could result in very imprecise results that tend to overestimate or underestimate the necessary size of a component. In any case, there are other options to address this problem, which will be part of the objective of this project.

In addition to being used to perform proper sizing of the aerodynamic control and lifting surfaces, the implementation of flight mechanics criteria is used to conduct stability studies of the aircraft, both static and dynamic.

In summary, this master's thesis is proposed by Saab to evaluate the implementation of flight mechanics criteria within the Pacelab APD program in the conceptual design phase of new aircraft. While this program offers a wide range of capabilities for the analysis and parametric modeling of aircraft, it has some limitations in modeling aerodynamic control surfaces, estimating the external moments and forces and determining the stability of the model. The objective of this thesis is to address these limitations and implement flight mechanics criteria that are use during the design stage.

## 1.2 Objective

The primary aim of this master's thesis is to establish the necessary theoretical and practical groundwork for applying flight mechanics criteria that enable precise sizing and placement of aerodynamic control and lifting surfaces on aircraft. Additionally, this work seeks to comprehend the aerodynamic behavior of an aircraft during flight, encompassing its stability and flying characteristics. To accomplish this objective, the Pacelab APD software will be utilized, which currently lacks design criteria pertaining to flight mechanics.

Furthermore, the pursuit of this primary objective entails acquiring a range of knowledge, skills, and collateral objectives that can be summarized through the following enumeration:

- Conducting a bibliographic study of the available methods and criteria in the literature.
- Selecting those that are implementable, taking into account their complexity, precision, and feasibility for implementation in Pacelab APD.
- Understanding the functioning and capabilities of Pacelab APD. Additionally, it is an essential requirement to have knowledge of programming in the C# language.
- Implementation of those coefficients that model the main aerodynamic forces and moments generated by the aircraft. These will be calculated based on semi-empirical low computational cost methods.
- Evaluation and validation of both the code and the methods implemented in Pacelab APD.
- Implementation of flight mechanics criteria that intervene in the loop of aircraft sizing and design. The criteria selected for this project are:

  - One engine inoperative
  - Steady roll
  - Departure criteria

- To extract and compare the results with existing methods and programs to evaluate the accuracy and reliability of the results.

Of the above objectives that are implicit in this thesis, the implementation of aerodynamic coefficients stands out. Its development and motivation are detailed later in the document. However, should be noted that its high complexity of implementation entails a high cost in resources, in terms of the time required for its implementation, testing, and validation. Consequently, this process represents approximately 80% of the available time for the completion of the project.

Furthermore, this work will address the following research questions regarding the methodology used.

- To what extent are the selected methods efficient and accurate in estimating the aerodynamic coefficients of the aircraft?
- What are the most important and commonly used criteria that can be derived from the aerodynamic derivatives and coefficients of the aircraft?

## 1.3 Limitations

This work is presented as the first in a series of projects that aim to achieve the complete integration of flight mechanics criteria employed during the conceptual design phase for proper sizing of aircraft surfaces and components, as well as stability analysis, without restrictions on configuration, speed, or any other aspect that directly affects the methods used for calculating these criteria.

Given the nature of this thesis, which is intended to lay the groundwork for future projects, it is necessary to significantly limit the scope of analysis and study. This allows for the effective computation and presentation of the most fundamental and necessary factors prior to the calculation of more complex ones. This section goes on to discuss the complexity of the flight mechanics field and establishes the general scope and framework on which the following work is based.

Flight mechanics is a vast field of study concerned with the analysis and design of aircraft systems and their behavior in flight. It is complex and multifaceted, and as such, requires a deep understanding of the physics and engineering principles that govern aircraft motion and performance.

One important aspect of flight mechanics is the study of different speed regimes. Aircraft can operate at various speeds, ranging from subsonic (below the speed of sound), transonic (close to the speed of sound), and supersonic (above the speed of sound). Each speed regime has unique characteristics and presents different challenges to aircraft designers and operators.

A more detailed and quantitative discretization of the different flight regimes under which an aircraft, and basically any moving body, can operate is found in reference [3]. The following are these flight regimes in a quantitative form, and in image figure 1.1, this description is graphically represented.

- When the local Mach number is less than 1.0 everywhere in the flowfield, the flow referred to as subsonic.
- When the local Mach number is greater than 1.0 everywhere in the flowfield, the flow is supersonic.
- If a flowfield has areas where the speed of the air is both below and above the speed of sound (subsonic and supersonic), then it is referred to as transonic. Transonic flow usually happens at Mach numbers between 0.8 and 1.2 in the freestream, depending on the body geometry and airspeed.
- Finally, hypersonic speed refers to speeds that are extremely fast, typically starting at around Mach 5. At such speeds, the air around the object moving through it becomes ionized, and the object experiences extremely high temperatures and pressures [4].

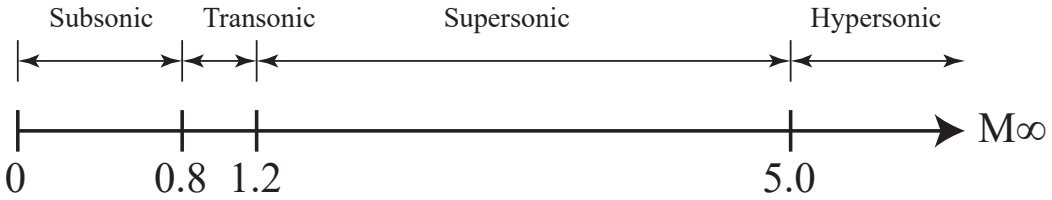


Figure 1.1: Aerodynamic flight regimes

In addition to intended speed regime, aircraft can be configured in a variety of ways. Conventional aircraft, such as commercial airliners, have a classic wing and tail design. Fighter aircraft, on the other hand, have a more compact and maneuverable design. Flying wings, as the name suggests, do not have a distinct fuselage or tail and are primarily composed of the wing. Canard aircraft feature a small wing near the nose of the aircraft and a larger wing at the rear. An illustration of these configurations is shown in figure 1.2.

The study of flight mechanics involves developing models and equations to describe the behavior of aircraft in various speed regimes and configurations. Different authors may propose different methods for calculating flight mechanic

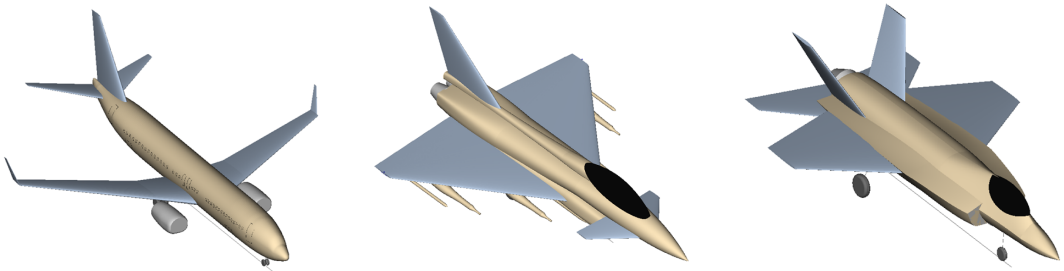

(a) Boeing 737-800 (Conventional)

(b) Eurofighter Typhoon (Canard)

(c) Lockheed Martin F-35A (Fighter)

Figure 1.2: Model representation of different aircraft configurations

criteria, depending on the focus of their research and the assumptions they make about the aircraft and its environment.

Despite the wealth of knowledge and research in the field of flight mechanics, this project is limited to some extent. The scope of the study is limited to a particular aspect of flight mechanics, and as such, may not cover all aspects of aircraft behavior, configuration, and flight envelope performance. Additionally, the calculations and models presented rely on certain assumptions and simplifications that may not be applicable in all scenarios. It is important to keep these limitations in mind when interpreting the results and conclusions of this project.

Firstly, this project solely deals with the analysis and implementation of the aerodynamic characteristics of **lateral dynamics** of aircraft, thus excluding those corresponding to the longitudinal part. The latter is developed in parallel in a separate master's thesis. Also, the study is limited to those aircraft that have a **traditional configuration**, i.e., aircraft consisting of the following set of parts: fuselage, wing, horizontal and vertical tail stabilizers (see figure 1.2). Finally, the study region is limited to **subsonic flight**, i.e., up to a Mach number close to 0.8. In figure 1.3, a brief outline of the scope of flight dynamics is presented, where the analyzed study path has been highlighted in green.

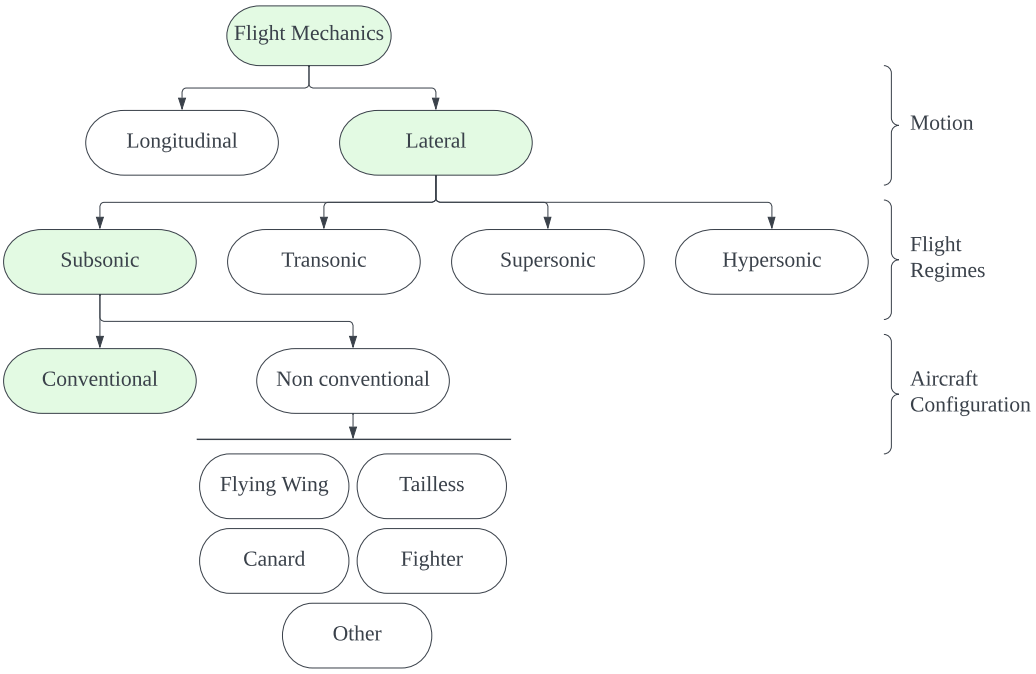


Figure 1.3: Flight mechanics categorization scheme

# Chapter 2

# Background

## 2.1 Aircraft design process

An aircraft design starts identifying the need for a new product because of new or stricter requirements, legal or technical, new available technologies, new challenges, new applications or new mission requirements. Once a new aircraft is set to be defined, the design process can be divided into three phases according to Raymer [5]:

1. **Conceptual Design**: This stage sets the beginning of the design process of any aircraft and thus, requires addressing several fundamental questions that will drive the design process.

   First, it is essential to identify the requirements that will guide the design process. These requirements may include factors such as performance, safety, regulatory compliance, customer preferences, and market trends.

   Second, it is necessary to determine the physical characteristics of the aircraft, such as its size, weight, and cost, based on the identified requirements.

   The third question to be addressed is related to the tradeoffs that must be made to achieve the desired performance, while considering factors such as cost, weight, and complexity.

   Fourth, selecting the appropriate technologies to be used is critical, and the design team should have a comprehensive understanding of the available options and their respective benefits and limitations.

   Finally, it is important to assess whether the requirements produce a viable and salable aircraft that will meet the customer's needs and compete effectively in the market. Answering these questions adequately will enable the design team to make informed decisions, optimize the design, and ultimately achieve a successful outcome.

2. **Preliminary Design**: This stage involves freezing the configuration of the aircraft, developing the surface definition, creating a test and analytical database, designing major items, and producing an initial cost estimation of the project based on statistical data.

3. **Detail Design**: During this stage, the design team focuses on converting the preliminary design into a fully detailed and feasible design that can be manufactured. The main objectives of this stage are to design the actual pieces that will be built, develop tooling and fabrication processes, test major items such as structure and landing gear, and finalize weight and performance estimates. The successful completion of the Detail Design stage is crucial to ensure that the aircraft meets all requirements and performs as expected.

4. **Fabrication**

This project addresses the stage of conceptual design, and it is further detailed below.

### 2.1.1 Conceptual design stage

The conceptual design phase is when the designers have freedom to perform trade studies with the designs and requirements to define one selected design according to desired characteristics.

This thesis sets its focus on the conceptual design phase's stability & control, where tradeoffs for configuration arrangement, size, weight and performance are still into perspective. Of major importance of the conceptual design phase is that changes in the layout can always happen because of newly learned points from previous design iterations.

Due to the aforementioned reasons, it is expected that during the initial design phase, numerous changes and iterations will take place that affect the design. These changes will occur at a high frequency, and therefore the calculation of the aircraft's data model must be optimized to be performed as quickly as possible. Equally important is the sensitivity analysis of a variable with respect to the parameters that affect it. Thus, the preview of the evolution of a variable with the change in magnitude of a parameter is often represented in graphs that aim to identify relevant minima or maxima that can optimize the geometry or represent a geometric or aerodynamic limitation.

All of this requires short resolution times of the equations that make up the data model, and should require low to moderate computational power. This aspect is particularly relevant and should be considered as one of the fundamental factors that directly affect the methodology to be followed to implement flight mechanics criteria.

The flow of stages in a conceptual design phase can be described as in figure 2.1

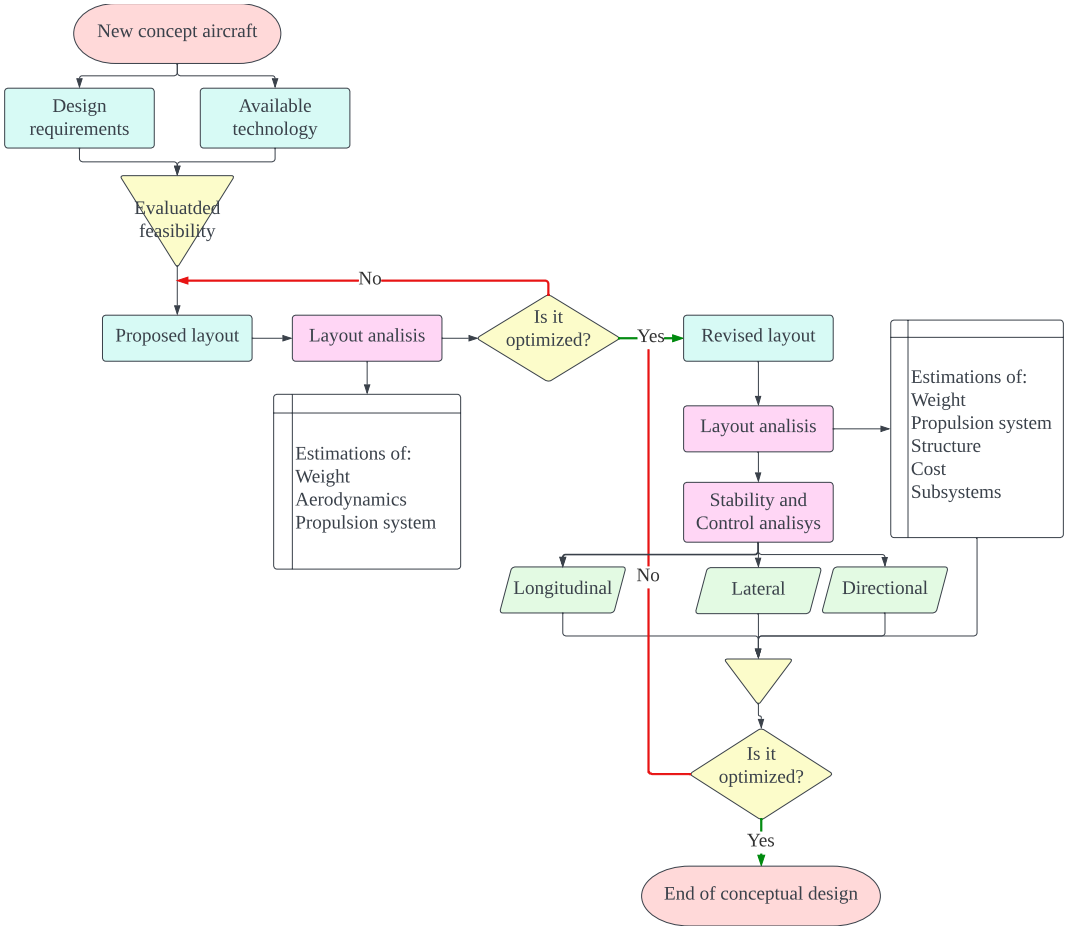


Figure 2.1: Conceptual design workflow for an aircraft according to Raymer [5]. Modified to illustrate the scope of the thesis during the stability & control estimation within the detailed analysis.

# Chapter 3

# Theoretical framework

## 3.1 Reference coordinate systems and angles

In order to obtain and set a frame of reference for the study of flight mechanics, the definition of reference systems is essential, where positions, velocities, and accelerations are defined through an orthogonal triad of axes.

### 3.1.1 Coordinate systems

There are numerous coordinate systems with respect to which the position and orientation of aircraft in space can be defined. Some of these include body axes, wind axes, fixed axes on the ground, or a system based on local horizon axes [6]. Below are two of the most commonly used coordinate systems:

#### Body Axis

Body axis reference systems (Ob, Xb, Yb, Zb) refer to the rigid body of the aircraft, with the origin (Ob) located at the center of mass and the axes fixed with respect to the aircraft geometry. The three mutually perpendicular axes rotate with the aircraft.

There can be different body axis systems, but they always form a right-handed trihedron. The Xb-axis represents the longitudinal axis of the aircraft, generally pointing forward. The Yb-axis is perpendicular to the plane of symmetry of the aircraft, with the positive direction pointing towards the right when viewed from the center of gravity of the aircraft towards the nose [6]. Finally, the Zb-axis is perpendicular to the other two, with positive sign when pointing downwards. This description is graphically represented in figure 3.1.

Notice how more than one possible coordinate system is presented in the figure.

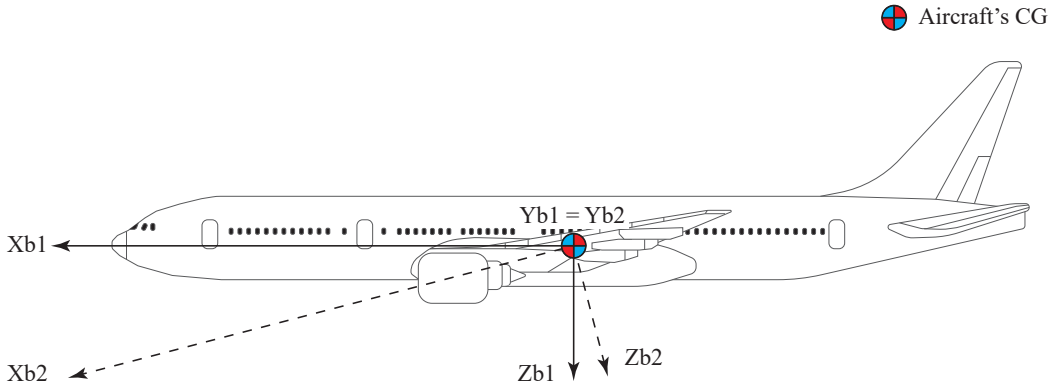


Figure 3.1: General scheme of body axis coordinate system

As previously mentioned, there can be many body axes systems. Three have special importance:

- Principal inertia axes. In this case (Xb, Yb, Zb) are principal inertia axes and the inertia products are zero [6].
- Stability axes. Used to study small disturbances from certain stationary flight reference conditions. Xb has the direction of the aircraft's aerodynamic velocity in the initial stationary conditions.
- The term *wind axes* is occasionally used for a body axes system in which the Xb axis coincides with the flight velocity.

### Wing axes

Wind axes reference system (Ow, Xw, Yw, Zw) is related to the instantaneous aerodynamic velocity of the aircraft and is only fixed to the aircraft at the point Ow = CG. It is related to the body axes through the attack and sideslip angles, which are fundamental independent variables for expressing aerodynamic forces and moments.

In wind axes, the Xw axis is directed according to the aerodynamic velocity vector *Va* of the aircraft, with the same direction: forward. The Zw axis is located in the plane of symmetry of the aircraft and is downward (in normal flight). The component of the velocity along this axis is always zero.Finally, the Yw axis forms a right-handed triad with the previous ones. As well as the Zw component, the velocity component along Yw is always zero. A graphical representation of this description is shown in figure 3.2.

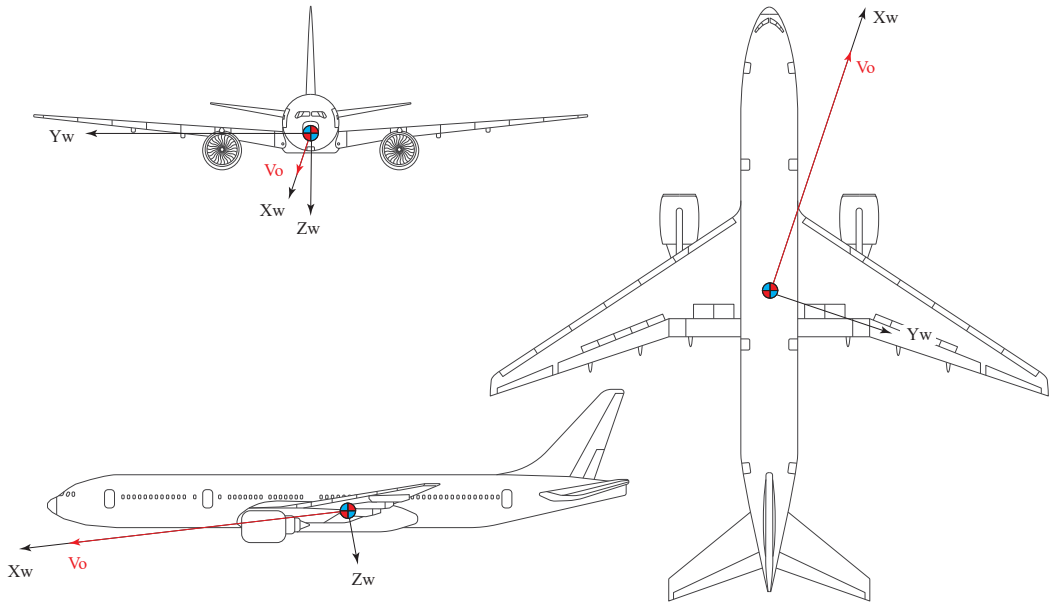


Figure 3.2: General scheme of wind axis coordinate system

### 3.1.2 Aerodynamic angles

The forces and moments that act on an airplane in flight are generated by its motion relative to the air and are influenced by the orientation of the aircraft in relation to the direction of airflow. If the airflow is uniform, these forces and moments remain unchanged when the airplane is rotated around the direction of the air flow [7]. Therefore, to describe the aerodynamic forces and moments, only two orientation angles with respect to the relative wind, referred to as the aerodynamic angles, are required: the angle of attack ($\alpha$) and the sideslip angle ($\beta$).

The angle of attack, commonly denoted as $\alpha$, is the angle formed between the lateral projection X in wind axes (Xw) and the longitudinal reference line of the fuselage. This reference line can be defined in different ways, including: the Xb axis belonging to the principal axis of inertia in body axes or the zero-lift line of the fuselage, among others. For the development of this project, the longitudinal reference line of the fuselage is taken as the one that passes through its center of gravity and has a horizontal parallel direction to the fuselage centerline.

On the other hand, the sideslip angle, denoted as $\beta$, is the angle formed between the vertical projection of the reference line of the fuselage defined above and the vertical projection of the Xw axis.

The definition of these two angles is reflected in figure 3.3.

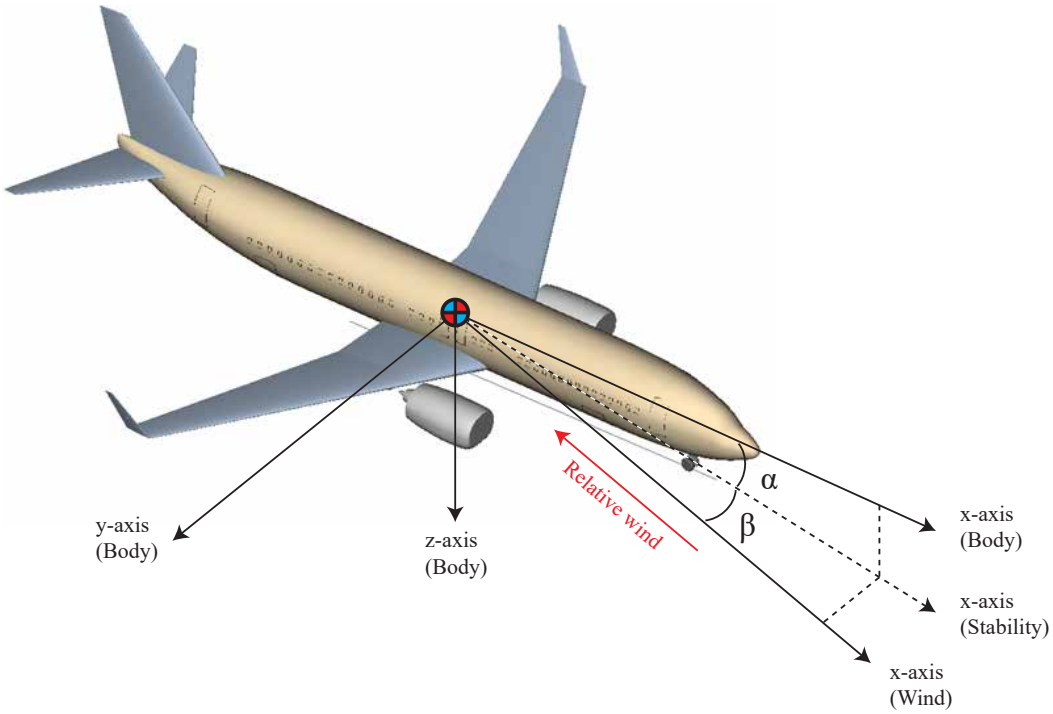


Figure 3.3: Definition of axes and aerodynamic angles

## 3.2 Nomenclature

In flight mechanics, there is a general nomenclature for expressing the linear and angular forces, moments, displacements, velocities, and accelerations of an aircraft. The purpose of this section is to present this nomenclature.

The rotation of an aircraft around its three principal axes in body axes is a fundamental concept in aeronautics. These rotations have specific names which are widely used in the field. The three rotational motions are:

- Roll: This is the rotation around the longitudinal axis of the aircraft. It is also known as bank and is controlled by the ailerons. When an aircraft rolls, one halve of the wing goes up while the other goes down. To establish a convention, a positive roll occurs when the right side of the wing goes down (right aileron up) and the left part moves up (left aileron down). The rolling moment is denoted by the letter L, the rolling angle is defined by $\phi$ and the rolling rate by p ($\dot{\phi} = \mathrm{p}$).

- Pitch: This is the rotation around the lateral axis of the aircraft. It is also known as attitude and is controlled by the elevator. When an aircraft pitches, the nose either points up or down. A positive pitch occurs when the the nose points upwards (elevator up). The pitching moment is denoted by the letter M and the pitch angle by $\theta$ and the pitching rate by q ($\dot{\theta} = \mathrm{q}$).

- Yaw: This is the rotation around the vertical axis of the aircraft. It is also known as heading and is controlled by the rudder. When an aircraft yaws, the nose moves left or right. A positive yaw occurs when the aircraft rotates clockwise, (nose points to the right and the rudder turns right). The yawing moment is denoted by the letter N and the yaw angle by $\psi$ and the yawing rate by r ($\dot{\psi} = \mathrm{r}$).

Similar to what was done previously with moments, rotational speeds, and angles, the same can be done with linear forces and speeds. These are, for a body axes coordinate system:

- Forward (Xb axis): Forward velocity is denoted as u and the axial force is X. Positive when moving forward.
- Lateral (Yb axis): Lateral or side velocity is referred to as v and the side force is Y. Positive when directed to the right.
- Vertical (Zb axis): Vertical velocity is denoted as w and vertical force is Z. Positive when directed downwards.

Figure 3.4 illustrates the aforementioned description for all velocities, forces and moments corresponding to the 6 degrees of freedom of the aircraft. Also the positive direction for all of them is shown.

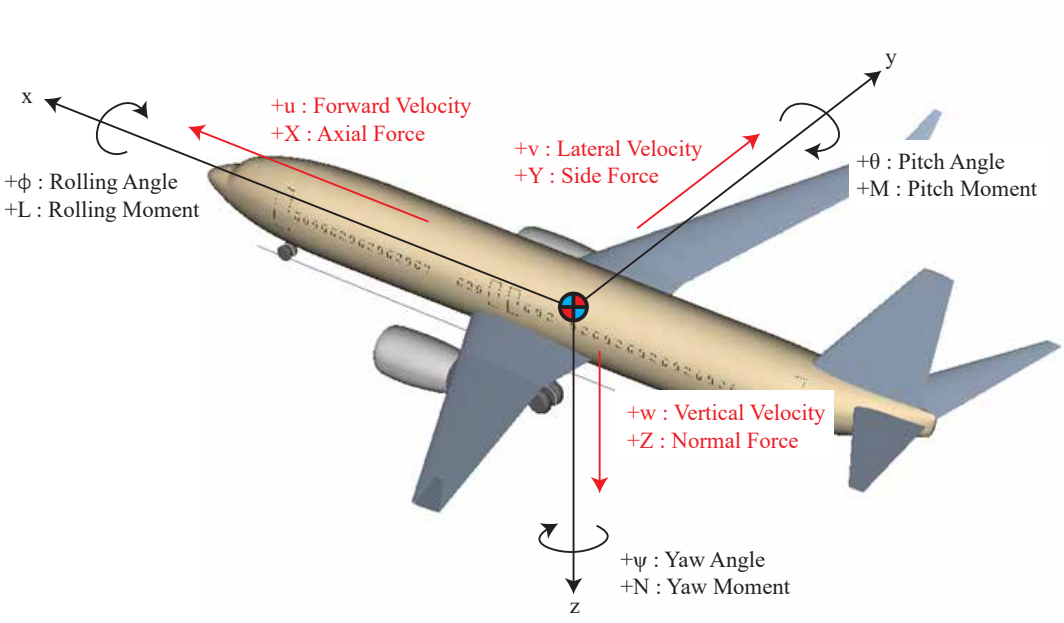


Figure 3.4: Sign and nomenclature convention used in flight mechanics

A summary of the nomenclature presented in this section and used throughout this document and is collected in table 3.1.

| | Linear | | |
|---|---|---|---|
| | Velocity | Force | Distance |
| Forward | U | X | x |
| Lateral | V | Y | y |
| Vertical | W | Z | z |
| | Angular | | |
| | Rate | Moment | Angle |
| Roll | p | L | $\phi$ |
| Pitch | q | M | $\theta$ |
| Yaw | r | N | $\psi$ |

Table 3.1: Flight mechanic nomenclature

## 3.3 The aerodynamic derivatives

### 3.3.1 Introduction

Flight mechanics is the branch of engineering that deals with the analysis and prediction of the forces and moments acting on an aircraft and its response to them.

One of the key components of flight mechanics are the aerodynamic derivatives, also frequently called, stability derivatives. As described by Napolitano [8], "Stability derivatives are the coefficients that relate the changes in aerodynamic forces and moments to changes in aircraft motion".

For a conventional stable aircraft, the aerodynamic derivatives provide valuable information that can help engineers assess and predict the stability and controllability characteristics of an aircraft. For unstable configurations, these aerodynamic derivatives become essential parameters for establishing and designing control laws that aim to ensure stability and controllability. Therefore, they are fundamental for the automatic control of the aircraft [9].

Stability derivatives can help the aircraft designer in the conceptual design phase by providing a quick and easy way to evaluate different design options and trade-offs. For example, by changing some parameters such as wing shape, aspect ratio, sweep angle, dihedral angle, etc., the designer can see how they affect the stability derivatives and hence the stability and controllability characteristics of the aircraft. This can help select the most suitable configuration that meets the design objectives and constraints.

The importance of stability derivatives in aircraft design is highlighted by Raymer [5], where the author states that "The aircraft designer needs to be

able to predict stability and control derivatives early in the design process, to help guide decisions on major design parameters". By understanding the stability derivatives, the designer can make informed decisions about wing and tail sizing, control surface placement, and other key design parameters.

### 3.3.2 Aerodynamic derivatives classification

Aerodynamic derivatives can be classified in the following groups [9]:

- Velocity derivatives. These are derivatives with respect to the aircraft linear velocities, i.e. u, v and w.
- Static derivatives, obtained with respect to the aerodynamic angles $\alpha$ and $\beta$. These ones govern the aircraft's static stability.
- Dynamic derivatives. The aerodynamic derivatives with respect to the rotational motion variables p, q, and r usually imply a dampening into their respective axis.
- Control derivatives, express the capability or effectiveness of the control surfaces' movements to alter the moments and forces acting on the aircraft. They also includes the engine throttle lever.

### 3.3.3 Aerodynamic derivatives generalities

Aerodynamic physical quantities, such as force or moment (provided in table 3.1), can have as many first-order partial derivatives as the number of variables they contain. Assuming a physical quantity $R$, its corresponding aerodynamic derivatives would be defined by means of equation equation 3.1.

$$\begin{aligned} R_i &= \left(\frac{\partial R}{\partial i}\right) \\ &\text{with:} \\ &\quad i \in \{\text{u},\ \text{v},\ \text{w},\ \text{p},\ \text{q},\ \text{r},\ \alpha,\ \beta,\ \delta_A,\ \delta_E,\ \delta_R\} \\ &\quad R \in \{\text{X},\ \text{Y},\ \text{Z},\ \text{L},\ \text{M},\ \text{N}\} \end{aligned} \tag{3.1}$$

Due to the fact that a rigid aircraft can be subject to 3 forces (X, Y, Z), three moments (L, M, N), and has 6 dynamic variables (u, v, w, p, q, r) plus three aerodynamic control variables ($\delta_a$, $\delta_e$, $\delta_r$), it is possible to establish 54 ($6 \cdot 9 = 54$) aerodynamic partial derivatives, to which those that accept linear and angular accelerations $\dot{v}$, $\dot{w}$, $\dot{\alpha}$, and $\dot{\beta}$ as variables could be added.

Due to the longitudinal symmetry of an aircraft and the mode of action of the aerodynamic controls, the value of a large number of these derivatives is particularly small or even zero [9], excluding aircraft with propellers.

The numerical value of a specific aerodynamic derivative indicates the intensity of dependence of the physical quantity ($R$ in equation 3.1) on the respective aerodynamic variable ($i$ in equation 3.1), assuming that the remaining variables remain constant [9]. Additionally, their units depend on the quantities they are composed of. Regarding the magnitude and sign of an aerodynamic derivative, the following can be established:

- If the magnitude of the value is large, $i$ has a significant influence on $R$. In case the value is small (close to 0), $i$ does not have a significant influence on $R$.
- If the sign of the value is positive (+), the variable $i$ increases the value of the derivative, while if it is negative (−), it decreases the value of the derivative as the variable increases.

### 3.3.4 Lateral Aerodynamic derivatives and dimensionless coefficients

The dimensional aerodynamic coefficients, explained previously in section 3.3.3, represent the influence of the different aerodynamic variables over the direct forces and moments acting on an aircraft. As their name suggest, these are dimensional and are influenced by various factors, including aircraft size, speed, and atmospheric conditions.

On the other hand, dimensionless aerodynamic coefficients, also known as non-dimensional coefficients, are derived from dimensional coefficients and provide a normalized representation of the aerodynamic characteristics. These coefficients eliminate the dependence on physical units and allow for comparisons across different aircraft types and scales.

The relationship between dimensional and dimensionless coefficients is established through appropriate reference quantities. By dividing the dimensional coefficient by the relevant reference quantity, such as dynamic pressure or aircraft characteristics, the corresponding dimensionless coefficient is obtained. This process enables a normalization of aerodynamic coefficients, facilitating comparisons across different flight conditions, aircraft sizes, and configurations.

This also enables the development of methods that allow for the estimation of dimensional coefficients through semi-empirical computations based on established techniques for estimating dimensionless coefficients. Subsequently,

the importance of being able to estimate aerodynamic coefficients from the calculation of dimensionless derivatives is further elaborated.

Below, equations 3.2 to 3.10 detail the main lateral aerodynamic derivatives and how they relate to their corresponding dimensionless coefficients [10]. Among the parameters that relate them are:

- $\bar{Q}$: Dynamic pressure [lbs/ft$^2$].
- $S$: Reference area [ft$^2$].
- $b$: Wing span [ft].
- $m$: Aircraft mass [slugs].
- $V_\infty$: Airplane true airspeed [ft/sec].
- $I_{xx}$: Airplane moments of inertia about x-axis [slugs $\cdot$ ft$^2$].
- $I_{zz}$: Airplane moments of inertia about z-axis [slugs $\cdot$ ft$^2$].

**Side-force dimensional/dimensionless coefficients relationship**

$$Y_\beta = \frac{\bar{Q} \cdot S}{m} Cy_\beta \quad \left[\frac{\text{ft/sec}^2}{\text{rad}}\right] \tag{3.2}$$

$$Y_p = \frac{\bar{Q} \cdot S \cdot b}{2 \cdot m \cdot V_\infty} Cy_p \quad \left[\frac{\text{ft/sec}^2}{\text{rad/sec}}\right] \tag{3.3}$$

$$Y_r = \frac{\bar{Q} \cdot S \cdot b}{2 \cdot m \cdot V_\infty} Cy_r \quad \left[\frac{\text{ft/sec}^2}{\text{rad/sec}}\right] \tag{3.4}$$

**Rolling moment dimensional/dimensionless coefficients relationship**

$$L_\beta = \frac{\bar{Q} \cdot S \cdot b}{I_{xx}} Cl_\beta \quad \left[\frac{\text{rad/sec}^2}{\text{rad}}\right] \tag{3.5}$$

$$L_p = \frac{\bar{Q} \cdot S \cdot b^2}{2 \cdot I_{xx} \cdot V_\infty} Cl_p \quad \left[\frac{\text{rad/sec}^2}{\text{rad/sec}}\right] \tag{3.6}$$

$$L_r = \frac{\bar{Q} \cdot S \cdot b^2}{2 \cdot I_{xx} \cdot V_\infty} Cl_r \quad \left[\frac{\text{rad/sec}^2}{\text{rad/sec}}\right] \tag{3.7}$$

**Yawing moment dimensional/dimensionless coefficients relationship**

$$N_\beta = \frac{\bar{Q} \cdot S \cdot b}{I_{zz}} Cn_\beta \quad \left[\frac{\text{rad/sec}^2}{\text{rad}}\right] \tag{3.8}$$

$$N_p = \frac{\bar{Q} \cdot S \cdot b^2}{2 \cdot I_{zz} \cdot V_\infty} Cn_p \quad \left[\frac{\text{rad/sec}^2}{\text{rad/sec}}\right] \tag{3.9}$$

$$N_r = \frac{\bar{Q} \cdot S \cdot b^2}{2 \cdot I_{zz} \cdot V_\infty} Cn_r \quad \left[\frac{\text{rad/sec}^2}{\text{rad/sec}}\right] \tag{3.10}$$

### 3.3.5 Significance of aerodynamic derivatives

Napolitano, in chapter 4.8 of [8], provides a qualitative analysis where he presents the significance of different lateral aerodynamic derivatives. He classifies these derivatives into seven groups, ordered from most to least relevant. In table 3.2, a similar representation is presented, showcasing only the lateral aerodynamic coefficients, organized into four groups.

| Relative Importance | Lateral Stability Derivatives |
|---|---|
| Group #1 | $Cl_\beta$, $Cn_\beta$ |
| Group #2 | $Cl_p$, $Cn_r$ |
| Group #3 | $Cy_\beta$, $Cy_p$, $Cy_r$, $Cn_p$, $Cl_r$ |
| Group #4 | $Cy_{\dot{\beta}} \approx Cl_{\dot{\beta}} \approx Cn_{\dot{\beta}} \approx 0$ |

Table 3.2: Classification of the lateral directional stability derivatives according to their relative importance

The values of the aerodynamic derivatives in Group #1 directly affect the overall stability of the aircraft, whereas the values of derivatives in Group #2 primarily impact the handling qualities and the aerodynamic characteristics of the aircraft perceived by the pilot [8]. Regarding Groups #3 and #4, they have limited to moderate significance in the aerodynamic modeling of the aircraft.

## 3.4 Comparison of approaches for estimating aerodynamic derivatives

The previously presented dimensionless coefficients can be calculated, or rather, estimated, by using different approaches, such as wind tunnel testing, flight testing, Computational Fluid Dynamics simulations (CFD) or semi-empirical

methods like DATCOM. Each approach has its advantages and limitations in terms of accuracy, cost, and applicability.

Wind tunnel testing involves placing a scaled model of the aircraft in a controlled airflow and measuring the forces and moments using sensors or balances. It can provide accurate data for a range of conditions, but it is expensive and time-consuming, and may not replicate all the effects of the actual flight environment. Furthermore, it requires a scaled physical model of the concept aircraft to be manufactured, which significantly increases the cost and time to simulate each iteration.

Computational Fluid Dynamics (CFD), on the other hand, possesses the ability to capture intricate flow features, non-linearities, and complex phenomena with a remarkable degree of fidelity. The utilization of CFD enables a detailed analysis of the aerodynamic characteristics, providing insights into the flow behavior and associated forces acting upon the aircraft. However, such simulations demand substantial computational resources and expertise to set up and execute the simulations effectively. Additionally, uncertainties and errors in the modeling, such as turbulence modeling or mesh resolution, may introduce inaccuracies in the results. In conclusion, the time required to perform a single CFD simulation and the energy and computational resources that it demands makes them unsuitable for the aerodynamic characterization of aircraft in conceptual design.

Finally, analytical methods, such as DATCOM, rely on simplified assumptions and idealized models of aircraft geometry and aerodynamics. These methods are valuable in providing preliminary estimates and conducting parametric studies during the conceptual design phase. However, it is important to acknowledge their inherent limitations. Analytical methods often fall short in capturing the full range of non-linearities and complexities inherent in real flow phenomena. The simplifying assumptions made in these methods may overlook intricate details, resulting in potential discrepancies between the analytical predictions and real-world observations. Consequently, while analytical methods offer a practical means of rapidly assessing the aircraft's aerodynamic behavior, they should be used carefully.

Taking the aforementioned considerations into account, it becomes evident that the use of analytical techniques based on semi-empirical methods is opportune during the conceptual design phase. These methods provide quick estimations of the aerodynamic behaviour of an aircraft while requiring minimal energy, computational resources, and technical knowledge of complex fluid simulation programs. Despite their limited precision and reliability, this approach has been chosen for estimating aerodynamic coefficients due to its particular suitability for the conceptual design phase, where the accuracy of the aircraft's aerodynamic characteristics are not critical in determining the project's success.

# Chapter 4

# Aerodynamic derivatives methods

While various approaches exist for calculating stability derivatives, this chapter focuses on semi-empirical methods.

Semi-empirical methods for stability derivative estimation can be found in prominent references such as Roskam [11], Napolitano [8], and the United States Air Force's DATCOM [12]. However, this thesis primarily relies on the methods and equations outlined in the book "*Methods for estimating stability and control derivatives of conventional subsonic airplanes*" by Jan Roskam [11]. Roskam's work not only builds upon the DATCOM methodology but also offers clearer explanations and more comprehensive definitions, making it a valuable resource for the proposed analysis.

It is important to note that due to the complexity of implementation and the limited time available, the focus is primarily on calculating the aerodynamic stability derivatives. Control derivatives, which describe the effects of control surfaces on aircraft dynamics, will be addressed in a separate project and assumed as user input in Pacelab APD.

The lateral motion related derivatives discussed in this chapter are divided into:

- Sideslip angle ($\beta$) derivatives
  - $Cy_\beta$ (section 4.1.1) - Variation of side force coeff. with $\beta$
  - $Cl_\beta$ (section 4.1.2) - Variation of rolling moment coeff. with $\beta$
  - $Cn_\beta$ (section 4.1.3) - Variation of yawing moment coeff. with $\beta$
- Roll Rate (p) derivatives
  - $Cy_p$ (section 4.2.1) - Variation of side force coeff. with p

  - $Cl_p$ (section 4.2.2) - Variation of rolling moment coeff. with p
  - $Cn_p$ (section 4.2.3) - Variation of yawing moment coeff. with p

- Yaw Rate (r) derivatives
  - $Cy_r$ (section 4.3.1) - Variation of side force coeff. with r
  - $Cl_r$ (section 4.3.2) - Variation of rolling moment coeff. with r
  - $Cn_r$ (section 4.3.3)- Variation of yawing moment coeff. with r

## 4.1 Sideslip angle derivatives

### 4.1.1 $Cy_\beta$ - Variation of side force coefficient with sideslip angle

For a conventional, tail-aft airplane, this derivative is divided into the contributions from wing, even though its significance is small unless in cases where the wing has a nonzero dihedral angle, body and vertical tail as:

$$Cy_\beta = Cy_{\beta_w} + Cy_{\beta_b} + Cy_{\beta_v} \tag{4.1}$$

The wing contribution is, at the present level of approximation, only dependent on the dihedral angle of the wing ($\Gamma$) and is set as in equation 4.2. Note that the value for the dihedral angle is expected to be in degrees and the factor 57.3 converts it to radians.

$$Cy_{\beta_w} = -0.0001 \cdot |\Gamma| \cdot 57.3 \quad \left[\text{rad}^{-1}\right] \tag{4.2}$$

The contribution of the fuselage is estimated as:

$$Cy_{\beta_b} = -2 \cdot K_i \cdot \left(\frac{S_0}{S}\right) \quad \left[\text{rad}^{-1}\right] \tag{4.3}$$

Where,

- $K_i$ is a factor presented in figure A.1 accounting for the distance between the body's center line to quarter-chord point of exposed wing root chord over the maximum body height at wing-body intersection.
- $S_0$ is the cross sectional area of the fuselage measured at the point in the x-axis where the flow ceases to be potential [11]. This point, denoted as

$x_0$ is function of the fuselage's length ($l_b$) and the x-coordinate $x_1$, which is the body station where $\partial S_x/\partial dx$ (with $S_x$ being the cross sectional area of the fuselage at a given x-coordinate) first reaches its maximum negative value. Distances $x_0$ and $x_1$ are correlated by equation 4.4.

$$x_0 = l_b \cdot \left(0.378 + 0.527 \cdot \left(\frac{x_1}{l_b}\right)\right) \tag{4.4}$$

The contribution of the vertical stabilizer is described as in 4.5.

$$Cy_{\beta_v} = -k \cdot C_{L_{\alpha_v}} \left(1 + \frac{d\sigma}{d\beta}\right) n_v \cdot \frac{S_v}{S} \quad [\text{rad}^{-1}] \tag{4.5}$$

Where,

- $k$ is an empirical factor defined in figure A.2.
- $\left(1 + \frac{d\sigma}{d\beta}\right) n_v$ can be calculated from equation 4.6.

$$\left(1 + \frac{d\sigma}{d\beta}\right) n_v = 0.724 + 3.06 \cdot \frac{S_v/S}{1 + \cos(\Lambda_{c/4})} + 0.4 \cdot \frac{Z_w}{d} + 0.009 \cdot A \tag{4.6}$$

  Where

  - $Z_w$ is the vertical distance from the wing root quarter chord point to the fuselage center line (regarded as positive downward).
  - $d$ is the maximum fuselage height along the chord-line of the wing-fuselage intersection.

- $C_{L_{\alpha_v}}$, is the vertical tail lift-curve slope. It can be calculated by the Polhamus equation 4.7 taking into account that the aspect ratio A is considered to be the effective aspect ratio ($A_{V_{\text{eff}}}$) because of the interference of the horizontal tail as in 4.8.

$$C_{L_\alpha} = \frac{2\pi \cdot A_{V_{\text{eff}}}}{2 + \sqrt{\left(\frac{AR \cdot \beta}{\kappa}\right)^2 \left(1 + \frac{\tan^2(\Lambda_{C/2})}{\beta^2}\right) + 4}} \tag{4.7}$$

$$A_{V_{\text{eff}}} = \left(\frac{A_{V(B)}}{A_V}\right) A_V \left\{1 + K_H \left(\frac{A_{V(HB)}}{A_{V(B)}} - 1\right)\right\} \tag{4.8}$$

Where,

- $A_V$ is the geometric aspect ratio $\frac{b_v^2}{S_v}$ for the isolated vertical tail as defined with the vertical tail span measured from the digitized plot that related the vertical stabilizer span by fuselage depth at quarter chord-point of vertical panels.
- $\left(\frac{A_{V(B)}}{A_V}\right)$ is the ratio of the aspect ratio of the vertical panel in the presence of the body to that of the isolated panel, given by figure A.3, which relates the fuselage depth in region of vertical tail and vertical tail taper ratio based on surface measured from fuselage center line.
- $\left(\frac{A_{V(HB)}}{A_{V(B)}}\right)$ is the ratio of the vertical panel aspect ratio in the presence of the horizontal rail and body to that of the panel in the presence of the body alone, given by the figure A.4.
- $K_H$ is a factor accounting for the relative size of the horizontal and vertical tails. Given in A.5.

It is worth mentioning that the method defined is only valid for the case in which the vertical fin is placed in the aircraft's longitudinal plane of symmetry. For twin vertical tails, refer to equation 7.7 of [11].

### 4.1.2 $Cl_\beta$ - Variation of rolling moment coefficient with sideslip angle

Considering a conventional, tail-aft airplane, this derivative is divided as in equation 4.9.

$$Cl_\beta = Cl_{\beta_{wb}} + Cl_{\beta_h} + Cl_{\beta_v} \tag{4.9}$$

The wing body contribution is defined as 4.10:

$$\begin{aligned} Cl_{\beta_{wb}} = 57.3 \cdot \Bigg[ & C_{L_{wb}} \left\{ \left(\frac{Cl_\beta}{C_L}\right)_{\Lambda_{c/2}} \cdot K_{M_\Lambda} \cdot K_f + \left(\frac{Cl_\beta}{C_L}\right)_A \right\} \\ & + \Gamma \left\{ \frac{Cl_B}{\Gamma} \cdot K_{M_\Gamma} + \frac{\Delta Cl_\beta}{\Gamma} \right\} + (\Delta Cl_\beta)_{Z_w} \\ & + \theta \cdot \tan(\Lambda_{c/4}) \left( \frac{\Delta Cl_\beta}{\theta \tan(\Lambda_{c/4})} \right) \Bigg] \quad [\text{rad}^{-1}] \end{aligned} \tag{4.10}$$

Where,

- $C_{L_{wb}} \approx C_L$ is the airplane steady state lift coefficient.
- $\left(\frac{Cl_\beta}{C_L}\right)_{\Lambda_{c/2}}$ is the wing sweep contribution obtained from figure A.6, relating the sweep angle of the half chord, taper ratio and the aspect ratio of the wing.
- $K_{M_\Lambda}$ is the compressibility (Mach number) correction to sweep obtained from figure A.9 relating the mach number and the half chord sweep angle of the wing.
- $K_f$ is a fuselage correction factor obtained from figure A.8. This relates the aspect ratio, the half chord sweep angle of the wing, the wing span and the distance in x-direction between the start of the fuselage to the half tip chord.
- $\left(\frac{Cl_\beta}{C_L}\right)_A$ is the aspect ratio contribution obtained from figure A.9.
- $\Gamma$ is the wing geometric dihedral angle, positive up (wing tip above the root chord), expressed in degrees.
- $\frac{Cl_B}{\Gamma}$ is the wing dihedral effect obtained from figure A.10 relating aspect ratio, taper ratio and the half chord sweep angle.
- $K_{M_\Gamma}$ is the compressibility correction to dihedral obtained from figure A.11 relating mach number, aspect ratio and half chord sweep angle.
- $\frac{\Delta Cl_\beta}{\Gamma}$ is the body-induced effect on the wing height and is give by 4.11.

$$\frac{\Delta Cl_\beta}{\Gamma} = -0.0005 \cdot \sqrt{A} \cdot \left(\frac{d}{b}\right)^2 \quad [\text{rad}^{-2}] \tag{4.11}$$

  Where,

  - $b$ is the wing span.
  - $d$ is obtained with 4.12.

$$d = \sqrt{\frac{\text{Average fuselage cross sectional area}}{0.7854}} \tag{4.12}$$

- $(\Delta Cl_\beta)_{Z_w}$ is another body-induced effect on the wing height given by equation 4.13.

$$(\Delta Cl_\beta)_{Z_w} = -\frac{1.2 \cdot \sqrt{A}}{57.3}\left(\frac{Z_w}{b}\right)\left(\frac{2 \cdot d}{b}\right) \quad [\text{deg}^{-1}] \tag{4.13}$$

  Where,

  - $Z_w$ is defined for equation 4.6.
  - $d$ is given by equation 4.12.

- $\frac{\Delta Cl_\beta}{\theta \tan(\Lambda_{c/4})}$ is a wing twist correction factor obtained from figure A.12 relating aspect ratio and taper ratio.
- $\theta$ is the wing aerodynamic twist between the root and tip sections of the wing, negative for washout.

The contribution of the horizontal tail, $Cl_{\beta_h}$ can be approximated by equation 4.14.

$$Cl_{\beta_h} = Cl_{\beta_{hb}} \frac{S_h \cdot b_h}{S_b} \quad [\text{rad}^{-1}] \tag{4.14}$$

Where,

- $Cl_{\beta_{hb}}$ is the given by equation 4.10 by considering the fuselage-horizontal tail the same way as the fuselage-wing.
- The magnitude of $\frac{S_h \cdot b_h}{S_b}$ determines the significance of $Cl_{\beta_h}$.

The contribution of the vertical tail, $Cl_{\beta_v}$ can be estimated from equation 4.15.

$$Cl_{\beta_v} = \left( \frac{Z_v \cos\alpha - l_v \sin\alpha}{b} \right) \quad [\text{rad}^{-1}] \tag{4.15}$$

Where,

- $Z_v$ is the distance in the z-axis between the vertical tail aerodynamic center and the airplane CG.
- $l_v$ is the distance in the x-axis between the vertical tail aerodynamic center and the airplane CG.

### 4.1.3 $Cn_\beta$ - Variation of yawing moment coefficient with sideslip angle

Considering a conventional, tail-aft airplane, this derivative can be estimated from the contributions of wing, body and vertical tail as in equation 4.16.

$$Cn_{\beta} = Cn_{\beta_w} + Cn_{\beta_b} + Cn_{\beta_v} \tag{4.16}$$

The wing contribution is considered negligible except for high angle of attack and therefore is dismissed from Roskam's methods.

The body-wing interference effect can be applied to all subsonic Mach numbers and it is estimated from 4.17.

$$Cn_{\beta_b} = -57.3 \cdot K_N \cdot K_{R_l} \cdot \frac{S_{b_S}}{S} \cdot \frac{l_b}{b} \quad [\text{rad}^{-1}] \tag{4.17}$$

Where,

- $K_N$ is an empirical factor for body + wing obtained from figure A.13 relating the fuselage maximum height, fuselage maximum width, the fuselage height at 1/4 of the length, at 3/4 of the length, the body side area and the x-coordinate of the CG position distance from the origin of the aircraft.
- $K_{R_l}$ is the empirical factor for the effect of the Reynolds number on the wing-body. Originally, this variable can be calculated by using figure 7.20 in Roskam's book [11], however, since the plot showed a linear tendency when the y-axis was set as logarithmic, a linear-logarithmic regression was carried out by using the digital tool developed by ATT Bioquest [13] to simply the implementation in Pacelab APD. The obtained equation was approximated as shown in equation 4.18. Where $Re_f$ is the fuselage's Reynolds number at a given flight condition (Mach and altitude).

$$K_{R_l} = 0.4716855 \cdot \log(Re_f) - 1.83 \tag{4.18}$$

- $S_{b_S}$ and $l_b$ are defined as the body side area and the fuselage length respectively.

The vertical tail contribution, $Cn_{\beta_v}$ is estimated by 4.19.

$$Cn_{\beta_v} = -Cy_{\beta_v} \left( \frac{l_v \cos\alpha - Z_v \sin\alpha}{b} \right) \quad [\text{rad}^{-1}] \tag{4.19}$$

Where,

- $Cy_{\beta_v}$ is obtained from equation 4.5.
- $Z_v$ is the vertical distance between the vertical tail aerodynamic center and the airplane CG.

- $l_v$ is the horizontal distance between the vertical tail aerodynamic center and the airplane CG.

## 4.2 Roll Rate derivatives

### 4.2.1 $Cy_p$ - Variation of side force coefficient with roll rate

According to Roskam, this derivative is negligible to estimate the airplane dynamic stability characteristics and the vertical tail is the dominating factor and therefore its contribution is considered as the full contribution 4.20.

$$Cy_p \approx Cy_{p_v} = 2\left(\frac{Z_v \cos\alpha - l_v \sin\alpha}{b}\right) \quad [\text{rad}^{-1}] \tag{4.20}$$

Where $Z_v$ and $l_v$ are already defined in sections 4.1.2 and 4.1.3.

### 4.2.2 $Cl_p$ - Variation of rolling moment coefficient with roll rate

This derivative is estimated as the contribution of the wing-body, horizontal tail and vertical tail of the aircraft as shown in equation 4.21.

$$Cl_p = Cl_{p_{wb}} + Cl_{p_h} + Cl_{p_v} \tag{4.21}$$

The wing-body contribution is estimated from equation 4.22.

$$Cl_{p_{wb}} \approx Cl_{p_w} = \left(\frac{\beta Cl_p}{k}\right) \cdot \frac{k}{\beta} \quad [\text{rad}^{-1}] \tag{4.22}$$

Where,

- $\left(\frac{\beta Cl_p}{k}\right)$ is the roll damping parameter from figure A.14 that relates the sweep angle, the aspect ratio and the sideslip angle of the airplane during the flight.
- $k$ is the ratio of the average wing section lift curve slope $Cl_{\alpha_w}$ to $2\pi$.

The contribution of the horizontal tail is estimated from equation 4.23.

$$Cl_{p_h} = 0.5 \cdot (Cl_p)_h \cdot \frac{S_h}{S} \cdot \left(\frac{b_h}{b}\right)^2 \tag{4.23}$$

Where $(Cl_p)_h$ is the horizontal tail contribution to $Cl_p$ based on its own reference geometry and found also from equation 4.22.

The contribution of the vertical tail may be approximated from 4.24

$$Cl_{p_v} = 2 \cdot \left(\frac{Z_v}{b}\right)^2 \cdot Cy_{\beta_v} \tag{4.24}$$

Where $Z_v$, $l_v$ and $Cy_{\beta_v}$ are already defined from section 4.1.2.

### 4.2.3 $Cn_p$ - Variation of yawing moment coefficient with roll rate

This derivative can be approximated from the contribution of the wing and the vertical tail 4.25.

$$\begin{aligned} Cn_{p_w} = -Cl_{p_w} \cdot \tan(\alpha) - \left[-Cl_p \cdot \tan(\alpha) - \left(\frac{Cn_p}{C_L}\right)_{C_L=0} \cdot C_L\right] \\ + \left(\frac{\Delta Cn_p}{\theta}\right)\theta + \left(\frac{\Delta Cn_p}{\alpha_{\delta_f}\delta_f}\right)\alpha_{\delta_f}\delta_f \quad [\text{rad}^{-1}] \end{aligned} \tag{4.25}$$

Where

- $Cl_{p_w}$ is found from equation 4.23.
- $\alpha$ is the wing angle of attack.
- $C_L$ is the wing lift coefficient .
- $\left(\frac{Cn_p}{C_L}\right)_{C_L=0}$ is the slope of the yawing moment due to rolling at zero lift given by 4.26.

$$\left(\frac{Cn_p}{C_L}\right)_{C_L=0} = \frac{A + 4 \cdot \cos\left(\Lambda_{c/4}\right)}{A \cdot B + 4\cos\left(\Lambda_{c/4}\right)} \cdot \left[\frac{A \cdot B + \frac{1}{2}\left[A \cdot B + 4\cos\left(\Lambda_{c/4}\right)\right] \cdot \tan^2\left(\Lambda_{c/4}\right)}{A + \frac{1}{2}\left(A + 4\cos\left(\Lambda_{c/4}\right)\right) \cdot \tan^2\left(\Lambda_{c/4}\right)}\right] \cdot \left(\frac{Cl_p}{C_L}\right)_{\substack{C_L=0 \\ M=0}} \tag{4.26}$$

Where,

- $B$ is a compressibility correction factor obtain from equation 4.27.

$$B = \sqrt{1 - M^2 \cos^2 \Lambda_{C/4}} \tag{4.27}$$

- $\left(\frac{Cl_p}{C_L}\right)_{\substack{C_L=0 \\ M=0}}$ is the slope of the low-speed yawing moment due to rolling at zero light given by equation 4.28.

$$\left(\frac{Cl_p}{C_L}\right)_{\substack{C_L=0 \\ M=0}} = -\frac{1}{6} \cdot \frac{A + 6\left(A + \cos\left(\Lambda_{c/4}\right)\right)}{\left(A + \cos\left(\Lambda_{c/4}\right)\right)} \cdot \left[\left(\frac{\bar{x}}{\bar{c}}\right) \cdot \frac{\tan\left(\Lambda_{c/4}\right)}{A} + \frac{\tan^2\left(\Lambda_{c/4}\right)}{12}\right] \quad [\text{rad}^{-1}] \tag{4.28}$$

Where,

  - $\bar{x}$ is the horizontal distance from the CG to the AC, positive when the AC is further (or closer to the tail) than the CG.
  - $\bar{c}$ is the wing mean aerodynamic chord.

- $\left(\frac{\Delta Cn_p}{\theta}\right)$ is the effect of linear wing twist from figure A.15 that relates the wing aspect ratio and taper ratio.
- $\theta$ is the wing aerodynamic twist angle between the root and tip stations in degrees.
- $\left(\frac{\Delta Cn_p}{\alpha_{\delta_f}\delta_f}\right)$ is obtained from figure 8.3 in Roskam's book [11]. Since the geometrical modeling of the flap is not currently defined inside Pacelab APD, a clean aircraft configuration is assumed, where flap deflection $\delta_f = 0$ and thus, none of the terms $\alpha_{\delta_f}$, $\left(\frac{\Delta Cn_p}{\alpha_{\delta_f}\delta_f}\right)$ modeling is needed.

The vertical tail contribution can be described as 4.29.

$$Cn_{p_v} = -\frac{2}{b} \cdot (l_v \cos\alpha - Z_v \sin\alpha) \left( \frac{Z_v \cos\alpha - l_v \sin\alpha}{b} \right) \cdot Cy_{\beta_v} \tag{4.29}$$

Where $Z_v$, $l_v$ and $Cy_{\beta_v}$ are defined in section 4.1.2.

## 4.3 Yaw Rate derivatives

### 4.3.1 $Cy_r$ - Variation of side force coefficient with yaw rate

According to Roskam, this derivative is of very minor importance and may be found from 4.30.

$$Cy_r = -\frac{2}{b} \cdot (l_v \cos\alpha - Z_v \sin\alpha) \cdot Cy_{\beta_v} \tag{4.30}$$

Where $Z_v$, $l_v$ and $Cy_{\beta_v}$ are found from section 4.1.2.

### 4.3.2 $Cl_r$ - Variation of rolling moment coefficient with yaw rate

This derivative can be estimated by the contribution of the wing and vertical stabilizer as in 4.31.

$$Cl_r = Cl_{r_w} + Cl_{r_v} \tag{4.31}$$

The variation of the wing yawing derivative $Cl_{r_w}$ with lift-coefficient is given by 4.32

$$Cl_{r_w} = C_L \left( \frac{Cl_r}{C_L} \right)_{C_L=0} + \left( \frac{\Delta Cl_r}{\Gamma} \right) \Gamma + \left( \frac{\Delta Cl_r}{\theta} \right) \theta \quad [\text{rad}^{-1}] \tag{4.32}$$

Where,

- $\left(\frac{Cl_r}{C_L}\right)_{C_L=0}$ is the slope of the rolling moment due to yawing at zero lift given by equation 4.33.

$$\left(\frac{Cl_r}{C_L}\right)_{C_L=0} = \frac{1 + \frac{A\,(1-B^2)}{2B\left(A\,B + 2\cos(\Lambda_{c/4})\right)} + \frac{A\,B + 2\cos(\Lambda_{c/4})}{A\,B + 4\cos(\Lambda_{c/4})}\frac{\tan^2(\Lambda_{c/4})}{8}}{1 + \frac{A + 2\cos(\Lambda_{c/4})}{A + 4\cos(\Lambda_{c/4})}\frac{\tan^2(\Lambda_{c/4})}{8}} \cdot \left(\frac{Cl_r}{C_L}\right)_{\substack{C_L=0 \\ M=0}} \tag{4.33}$$

  Where,

  - $B$ is a compressibility correction factor obtain from equation 4.27.
  - $\left(\frac{Cl_r}{C_L}\right)_{\substack{C_L=0 \\ M=0}}$ is the slope of the low-speed rolling moment due to yawing at zero lift, obtained from figure A.17 as a function of aspect ratio, sweep angle of the quarter chord and taper ratio.

- $C_L$ is the wing lift coefficient.
- $\frac{\Delta Cl_r}{\Gamma}$ is the increment in $\Delta Cl_r$ due to dihedral, given by 4.34.

$$\frac{\Delta Cl_r}{\Gamma} = \frac{1}{12} \cdot \frac{\pi A \sin(\Lambda_{c/4})}{A + 4\cos(\Lambda_{c/4})} \quad [\text{rad}^{-2}] \tag{4.34}$$

- $\Gamma$ is the dihedral angle in radians.
- $\left(\frac{\Delta Cl_r}{\theta}\right)$ is the increment in $Cl_r$ due to wing twist obtained from a digitized plot as a function of aspect ratio and the flap chord ratio to the wing's chord.
- $\theta$ is the wing aerodynamic twist between the root and tip sections in degrees.

The vertical tail contribution is given by 4.35.

$$Cl_{r_v} = -\frac{2}{b^2} \cdot (l_v \cos\alpha - Z_v \sin\alpha)\,(Z_v \cos\alpha - l_v \sin\alpha) \cdot Cy_{\beta_v} \tag{4.35}$$

Where $Z_v$, $l_v$ and $Cy_{\beta_v}$ are found from section 4.1.2.

### 4.3.3 $Cn_r$ - Variation of yawing moment coefficient with yaw rate

This derivative can be estimated from 4.36,

$$Cn_r = Cn_{r_w} + Cn_{r_v} \tag{4.36}$$

The wing contribution can be found with 4.37.

$$Cn_{r_w} = \left(\frac{Cn_r}{C_L^2}\right) \cdot C_L^2 + \left(\frac{Cn_r}{C_{D_0}}\right) \cdot \bar{C}_{D_0} \tag{4.37}$$

Where,

- $\left(\frac{Cn_r}{C_L^2}\right)$ is calculated from figure A.18 obtained as a function of the aspect ratio, sweep angle and taper ratio.
- $\left(\frac{Cn_r}{C_{D_0}}\right)$ is calculated from figure A.19 obtained as a function of the aspect ratio, sweep angle at the quarter chord and the static margin
- $\bar{C}_{D_0}$ is defined as as in equation 4.38.

$$C_D = \bar{C}_{D_0} + \frac{C_L^2}{\pi \cdot A \cdot e} \tag{4.38}$$

Where,

  - $C_D$ is the drag coefficient.
  - $C_L$ is the lift coefficient.
  - $e$ is the Oswald efficiency factor of the wing.

Since Mach number significantly affects $Cn_{r_w}$ through the parameter $\bar{C}_{D_0}$ this value should be evaluated from the drag polar at hte right Mach number [11].

The vertical tail contribution follows from 4.39.

$$Cn_{r_v} = -\frac{2}{b^2} \cdot (l_v \cos\alpha - Z_v \sin\alpha)^2 \cdot Cy_{\beta_v} \tag{4.39}$$

Where $Z_v$, $l_v$ and $Cy_{\beta_v}$ are found from section 4.1.2.

# Chapter 5

# Flight mechanics criteria for conceptual design

In this chapter, three flight mechanics related criteria have been chosen to be implemented in Pacelab APD. These are: steady roll, departure criteria, and one engine inoperative.

The criteria, belonging to the lateral motion of the aircraft, enable a quantitative assessment of the proper sizing of the aerodynamic and control surfaces defined during the conceptual design phase.

The following is a detailed description of the selected criteria.

## 5.1 Steady roll rate

The steady roll of an airplane is determined solely by the inputs of the ailerons deflections and main wing angle of attack. According to Raymer [5], the roll one-DOF equation for roll can be found as 5.1:

$$I_{xx} \cdot \ddot{\phi} = \bar{Q} \cdot S \cdot b \cdot (C_l + C_{l_p} \cdot \dot{\phi}) \tag{5.1}$$

Where,

- $I_{xx}$ is the moment of inertia along the roll (x) axis.
- $\ddot{\phi} = \dot{p}$ is the variation roll rate over time (roll angular acceleration).
- $\dot{\phi} = p$ is the roll rate.
- $\bar{Q}$ is the dynamic pressure.

- $S$ is the wing reference area.
- b is the wing span.
- $C_l$ is the rolling moment coefficient.
- $C_{l_p}$ is the variation of rolling moment coefficient with roll rate.

As its name suggest, steady roll implies that the aircraft is not in angular acceleration in roll ($\ddot{\phi} = \dot{p} = 0$), thus the steady roll is found by setting equation 5.1 equal to zero. Since equation 5.2 below indicates that the only rolling moment term that remains when the sideslip is equal to zero ($\beta = 0$) is the roll due aileron deflection, equation 5.1 can be written as equation 5.3 and the roll rate is defined by 5.4:

$$Cl = \frac{L}{q \cdot S \cdot b} = Cl_{\beta_w} \cdot \beta + Cl_{\delta_a} \cdot \delta_a + Cl_{\beta_v} \cdot \beta \tag{5.2}$$

Where,

- $Cl_{\delta_a}$ is the rolling coefficient due to aileron deflection.

$$I_{xx} \cdot \ddot{\phi} = \bar{Q} \cdot S \cdot b \cdot (Cl_{\delta_a} \cdot \delta_a + C_{l_p} \cdot \dot{\phi}) = 0 \tag{5.3}$$

$$\dot{\phi}_{ss} = -\frac{L_{\delta_\alpha} \cdot \delta_\alpha}{L_p} \tag{5.4}$$

## 5.2 Departure criteria

The departure criteria is an important tool to evaluate the handling qualities and behavior of an aircraft for high angles of attack. According to Raymer [5], as the angle of attack increases, a well designed airplane should experience mild buffeting to warn the pilot and retain control about all axes. Recovery should be immediate and there should be no tendency to enter a spin.

The most important coefficients to establish if an airplane is prone to any of the mentioned unwanted behaviors are $Cn_\beta$, $Cn_{\delta_\alpha}$, $Cl_\beta$ and $Cl_{\delta_\alpha}$. $Cn_{\beta\,\text{dynamic}}$ represents the variation of yawing moment coefficient with sideslip angle by the variation of rolling moment coefficient with roll rate with the yaw and roll moments of inertia and angle of attack. The lateral control departure parameter (LCDP) focus on the relationship between adverse yaw and directional

stability. Weissman [14] proposes the use of LCDP and its contributions to this criteria.

Raymer [5] describes two departure parameters to be evaluated, $Cn_{\beta\,\text{dynamic}}$ and LCDP.

The departure parameter $Cn_{\beta\,\text{dynamic}}$ is calculated as equation 5.5:

$$Cn_{\beta_{\text{dynamic}}} = Cn_{\beta} \cdot \cos(\alpha) - \frac{I_{zz}}{I_{xx}} \cdot Cl_{\beta} \cdot \sin(\alpha) \tag{5.5}$$

Where,

- $\alpha$ is the angle of attack.
- $I_{xx}$ is the moment of inertia along the roll axis.
- $I_{zz}$ is the moment of inertia along the yaw axis.

The lateral control departure parameter (LCDP) focuses on adverse yaw and directional stability and it is given by equation 5.6:

$$\text{LCDP} = Cn_{\beta} - Cl_{\beta} \cdot \frac{Cn_{\delta_a}}{Cl_{\delta_a}} \tag{5.6}$$

Where,

- $Cn_{\beta}$ is the variation of yawing moment coefficient with sideslip angle.
- $Cl_{\beta}$ is the variation of rolling moment coefficient with sideslip angle.
- $Cn_{\delta_\alpha}$ is the variation of yawing moment coefficient with aileron deflection angle.
- $Cl_{\delta_\alpha}$ is the variation of rolling moment coefficient with aileron deflection angle.

## 5.3 One engine inoperative

One engine inoperative is a flight condition that occurs when an aircraft is operating with one of its engines out, either due to engine failure or intentional shutdown. This condition has a significant impact on the performance and handling characteristics of the aircraft. During the conceptual design phase, it

is particularly relevant to consider this aspect as it directly affects the sizing of certain aerodynamic and control surfaces, such as the vertical tail, ailerons, and rudder.

When this situation arises, a series of moments around the x and z axes are generated. Firstly, the imbalance due to thrust asymmetry, depicted in figure 5.1, creates a yawing moment around the z-axis that needs to be compensated for by rudder deflection. Moreover, this moment will be greater when the operating symmetric engine produces more power and is located further from the aircraft's center of gravity. Secondly, the increased thrust on one side and the resulting yawing moment cause the section of the wing where the operating engines are located to advance, resulting in higher speed and consequently greater lift. Conversely, the section of the wing where the inoperative engine is situated will lag behind, leading to lower speed and reduced lift. Due to the imbalance in lift between the two wing sections, in conjunction with the yawing moment, a rolling moment occurs, which must be counteracted by the ailerons.

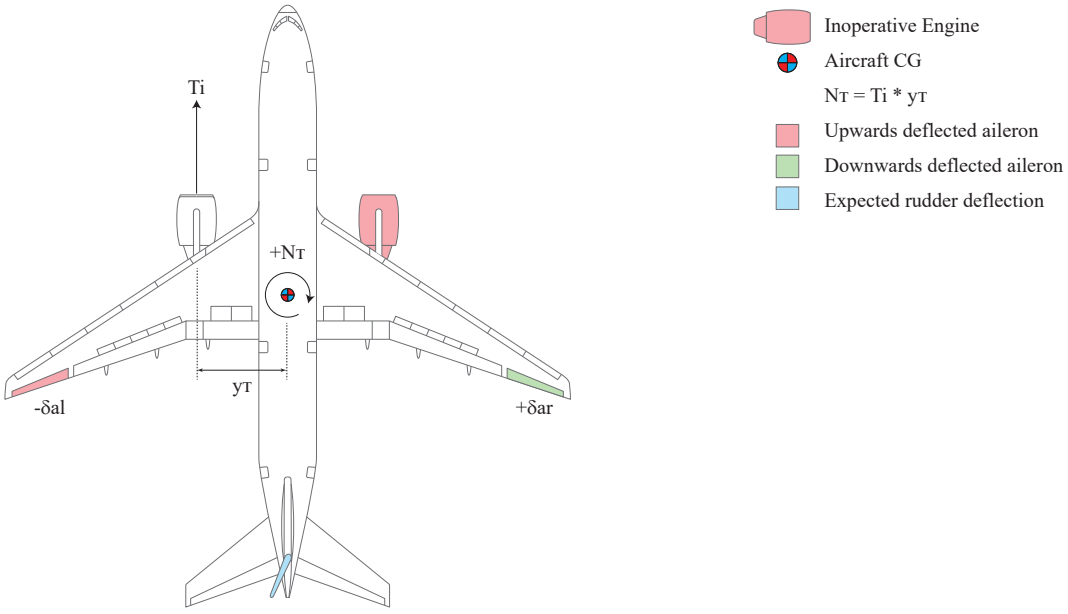


Figure 5.1: Modeling of the forces and moment acting on an engine out condition and the expected control surfaces deflections

To calculate the necessary deflections of the ailerons and rudder to maintain level flight with one engine inoperative, the following procedure, as defined in Napolitano [8], is followed.

First instance, it is assumed that when an aircraft engine fails, an immediate rolling and yawing moment is generated due to the thrust asymmetry produced by the engines, that is:

$$L_T \neq 0, \quad N_T \neq 0 \tag{5.7}$$

The modeling of the directional lateral dynamics corresponding to the flight condition of one engine inoperative starts with the analysis of the linearized equation governing the yawing and rolling moments. Equation 5.8 refers to the modeling of the yawing moment generated by trust asymmetry and equation 5.9 represents the rolling moment.

$$N_T = -\bar{Q} \cdot S \cdot b \cdot (Cn_\beta \cdot \beta + Cn_{\delta a} \cdot \delta a + Cn_{\delta r} \cdot \delta r) \tag{5.8}$$

$$L_T = -\bar{Q} \cdot S \cdot b \cdot (Cl_\beta \cdot \beta + Cl_{\delta a} \cdot \delta a + Cl_{\delta r} \cdot \delta r) \tag{5.9}$$

Due to the possibility that the pilot may not be aware of the engine malfunction that has occurred, a certain sideslip angle develops for a brief moment. It is assumed that during these brief seconds, all aerodynamic controls of the lateral dynamics are in their trim positions, i.e., $\delta_a \approx 0$ and $\delta_r \approx 0$. Thus, the aircraft rolls and yaws, resulting in a sideslip angle modeled by equation 5.10.

$$\beta|_{\text{Engine Out}} = \beta|_{\text{EO}} = -\frac{N_T}{Cn_\beta \cdot \bar{Q} \cdot S \cdot b} \tag{5.10}$$

Next, the pilot will try to compensate for the rolling and yawing moments by modifying the deflection of the control surfaces. Considering Equation 5.9 and solving for the aileron deflection, assuming that the rudder has not been modified ($\delta r = 0$) and that the sideslip angle $\beta = \beta|_{\text{EO}}$, we obtain Equation 5.11.

$$\delta a|_{\text{EO}} = \frac{\left(-Cl_\beta \cdot \beta|_{\text{EO}} - \dfrac{L_T}{\bar{Q} \cdot S \cdot b}\right)}{Cl_{\delta_a}} \tag{5.11}$$

Inserting the previously calculated value of $\beta|_{\text{EO}}$ (equation 5.10) into equation 5.11, equation 5.12 is derived.

$$\delta a|_{\text{EO}} = \frac{\left(\dfrac{Cl_\beta \cdot N_T}{Cn_\beta} - L_T\right)}{Cl_{\delta_a} \cdot \bar{Q} \cdot S \cdot b} \tag{5.12}$$

Next, the deflection of the rudder is calculated, by using equation 5.13, taking into account the previously calculated values for the sideslip angle ($\beta|_{\text{EO}}$) and the deflection of the ailerons ($\delta a|_{\text{EO}}$).

$$N_T = -\bar{Q} \cdot S \cdot b \cdot (Cn_\beta \cdot \beta|_{\text{EO}} + Cn_{\delta a} \cdot \delta a|_{\text{EO}} + Cn_{\delta r} \cdot \delta r) \tag{5.13}$$

And solving for the rudder deflection, equation 5.14 is obtained.

$$\delta r|_{\text{EO}} = \frac{-\left(Cn_\beta \cdot \beta|_{\text{EO}} + Cn_{\delta_a} \cdot \delta_a|_{\text{EO}} + \dfrac{N_T}{\bar{Q} \cdot S \cdot b}\right)}{Cn_{\delta_r}} \tag{5.14}$$

Finally, in cases where the factor $Cn_{\delta r}$ has a high value, an additional correction for the aileron deflection angle $\Delta\delta_a|_{\text{EO}}$ may be required, as shown in equation 5.15. Thus, the final value of the aileron deflection is determined by equation 5.16.

$$\Delta\delta_a|_{\text{EO}} = \frac{-Cl_{\delta r} \cdot \delta_r|_{\text{EO}}}{Cl_{\delta_a}} \tag{5.15}$$

$$\begin{aligned} \Delta\delta_a|_{\text{EO}_{\text{FINAL}}} &= \Delta\delta_a|_{\text{EO}} + \Delta\delta_a|_{\text{EO}} \\ &= \frac{\left(-Cl_\beta \cdot \beta|_{\text{EO}} - \dfrac{L_T}{\bar{Q} \cdot S \cdot b}\right)}{Cl_{\delta_a}} + \frac{-Cl_{\delta r} \cdot \delta_r|_{\text{EO}}}{Cl_{\delta_a}} \end{aligned} \tag{5.16}$$

To implement the one engine inoperative criterion, equations 5.12, 5.14, and 5.15 must be evaluated consecutively. Through the latter two equations, the necessary deflection angles of the rudder and ailerons can be obtained to maintain level flight with one engine inoperative.

It is important to note that there are physical limitations that prevent infinite deflection of the ailerons and rudder. Generally, for the ailerons, there is a restriction of $\pm 20°$. For the rudder, a typical maximum deflection of $\pm 25°$ is established.

This criterion will assist the aircraft designer during the conceptual phase in evaluating whether the sizing of the vertical stabilizer, rudder, and ailerons is sufficient to meet the required safety requirements.

# Chapter 6

# Implementation framework: Pacelab APD

## 6.1 Software overview

The implementation and evaluation of the methods presented in section 4 is carried out within the context of the Pacelab APD software package. Pacelab APD is comprised of two distinct programs that function in conjunction to enable the effective modeling of aircraft systems and the creation and storage of the data model that facilitate the computation of their relevant characteristics.

Specifically, these programs are denoted as PACE Engineering Workbench (EWB) and PACE Knowledge Designer (KD), respectively. Together, these software components facilitates the modeling, analysis, and design of aircraft systems in a comprehensive and efficient manner.

PACE Engineering Workbench is where the geometrical modeling of the aircraft is done and all the data resulting from solving the data model is displayed. It allows for the aircraft designer to change the design as well as the performance variables to evaluate the behavior according to the requirements. On the other hand, Knowledge Designer is the software where new feature implementation is done and contains the aircraft's data model. It stores the necessary methods to perform all calculations and estimations for mass, aerodynamics, control and any other variable of interest that should be displayed in Engineering Workbench. Due to the nature of Knowledge Designer, the software's end user is able to implement new chapters with methods and formulas that enables to extend the capabilities of the data model, and thus, the program with new features specifically tailored to the mission or application of the aircraft to be designed.

In order to correctly understand how the project has been organized within

Pacelab KD (Knowledge Designer), it is useful to first address the internal structure of the program, how the information is stored and structured, as well as the possibilities and projects that can be created within it. Access to information and the various internal parameters of the program is also a key aspect to take into account, since full knowledge of the available data will ultimately help reduce the amount of duplicated code, a critical aspect in such extensive software as is Pacelab APD.

To ensure efficient functioning of the program, there is a master file that holds the directory information for all the sub-files comprising the data model. When the program is initially provided to the end user, it comes preloaded with a default data model called *APDComplete* for the Knowledge Designer workspace.

The aforementioned files are divided into three main groups: Engineering Objects (EO), Functional Objects (FO) and Smart Formulas (SF).

Engineering Objects (EO) represent a parametric description of a real world engineering object, e.g. a wing, fuselage etc, however, they can also represent more abstract concepts such as aerodynamics or stability. An engineering object consists of parameters, methods, formulas, constraints and relationships between parameters.

To better understand the concept of Engineering Object, consider the case of a wing as an example. An aircraft's wing is made up of various parameters that define it parametrically, some of these are: the coordinate reference frame, wingspan, chord at the tip and root, sweep / dihedral angle or the airfoil. These parameters can be entered directly as an input by the user, as would be the case of the span, however, on occasions, it can happen that the parameters are calculated indirectly from others, as it is the case of the taper ratio, computed by the dimensions of the chords at the root and at the tip of the wing. Also, EOs can inherit or copy attributes (parameters) or characteristics from other EOs. For instance, the wing's position in space parameter may come from a parent EO called *PhysicalObject* with a parameter called *coordinates*.

A Functional Object (FO) is a reusable piece of code that performs a specific task or function within a larger program. It is designed to be modular and independent, making it easier to maintain, modify, and reuse in different parts of the program or in other programs altogether. This means that the FO can be used in different parts of the program where that calculation is needed, without having to rewrite the code each time. Furthermore, organizing the FO within a project item or folder enhances code accessibility and organization. This practice also helps developers locate the necessary code quickly and efficiently. Moreover, if there exist multiple methods for calculating a certain derivative, creating a separated FO with a different method from some other source, e.g. DATCOM, would enable to switch between methods depending on which is most suitable for a specific application. This FO switching is defined

inside the EO, offering increased flexibility and adaptability to the software.

Smart Formulas (SF) are a useful tool for locating and processing parameters in a dynamic environment, where users can load Engineering Objects at their disposal and fit them together according to their design requirements. This makes unfeasible to predict the number or even the existence of certain components or parameters in the current data model. Smart Formulas solve this problem by using, the so called, *Navigator* service to locate EOs, components, and parameters in the dynamic environment. The *Navigator* service returns the EOs and parameters located by the service according to a specified pattern coded by the developer, which ultimately allows for more efficient processing of the data.

Smart Formulas offer several advantages over EO formulas, including the ability to feature blocks of code, not just a single line expression, and a collection of output parameters determined by the *Navigator*. Nevertheless, due to the flexibility of C# programming language, a workaround has been found to overcome the restriction of having only one line of code in EO formulas, thus making the use of Smart Formulas outdated.

## 6.2 APD project structure

So far, a high-level overview of the primary options available in Pacelab APD for project creation has been provided in section 6.1. In this section, a general example is presented that illustrates how the implementation of the various aerodynamic derivatives for lateral motion has been carried out. Through this general explanation, it is intended that the reader can understand how other projects beyond the calculation of these derivatives are organized, such as the other implemented criteria.

By default, the base data model of Pacelab APD, *APDComplete*, is shipped with an already existing EO named *StabilityAndControl*. For this thesis it has been decided that no additional EO should be created since the existing one fitted the purpose of the task.

Inside the *StabilityAndControl* EO, a new project item is created with the purpose of storing all the data regarding the lateral aerodynamic derivatives. This new project item is made up parameters, which are all the derivatives for the lateral motion of the aircraft, that are ultimately displayed in EWB.

To calculate the lateral aerodynamic derivatives it is mandatory to create a dedicated formula linked to each one of them. The formula consists of a single line of code, as defined in section 6.1, and is in charge of updating the value of its correlated parameter every time the user executes the *solve* command in Pacelab Engineering Workbench.

The computation of an aerodynamic derivative is a complex task that involves the use of multiple equations, geometrical and aerodynamic input parameters, summations from the different contributions of the aircraft components (i.e. wing, fuselage, fin, stabilizer...) and in some cases, also requires using and interpolating two, three and even four dimensional plots. As it may seem evident, the use of a single line of code to perform such complex operations is not sufficient.

As a workaround, EO components also offer the possibility of implementing methods that can contain as many lines of code as necessary to complement the formulas. In this way, the parameter or aerodynamic derivative calls its corresponding formula, which in turn calls the corresponding method to perform the calculation.

Delving into the content and function of the EO methods, they are solely responsible for collecting the necessary inputs contained in the data model. Once obtained, they execute an FO function that requires those inputs and returns the expected value for the corresponding EO parameter. The implementation of such methods provides a powerful tool for enhancing the functionality of the underlying calculations and represents a key feature of the EO framework.

At this juncture, Functional Objects come into play, offering dedicated methods that can be reused throughout the entire data model. To facilitate the process of calculating the lateral derivatives, a new FO has been developed and named as *AerodynamicDerivativesMethods_ROSKAM*. It is noteworthy that the source from which all the methods inside the FO are derived has been appended to the end of its name, Roskam [11] in this case. This categorization of different methods from literature into separated projects eases the task of the end user in selecting the desired method. If a new developer wishes to add other methods from a different source, such as DATCOM, for instance, a new FO should be created with a similar name while changing only the name of the source from which the methods are derived.

The FO contains the multidimensional data tables that must be interpolated as well as the mathematical modeling of each aerodynamic derivative. Furthermore, each coefficient has been divided into their separate components. This is, let's say a given coefficient is made up of different contributions from the aircraft components, i.e. wing, body and vertical tail, then, there will be a dedicated method inside the FO project item that would calculate each of those individually and later on will be summed up by a more general method.

After defining all the aforementioned aspects, the workflow proceeds as follows and is illustrated in figure 6.1.

1. Initially, the user commands to solve the data model that contains an instance of the EO *StabilityAndControl*.

2. Subsequently, the parameters are updated by calling their respective formulas, which call the corresponding method (inside the EO).

3. These methods gather all necessary inputs to compute the dimensionless coefficients from the entire data model. Obtaining some of these inputs may be overly complicated and can pertain to various types such as geometrical or aerodynamic.

4. Once all inputs are gathered, each EO method invokes its corresponding FO coefficient methods, which perform the necessary calculations and returns the computed value.

5. Finally, the aerodynamic derivative parameter is updated with the value returned by the FO method and displayed to the user in EWB.

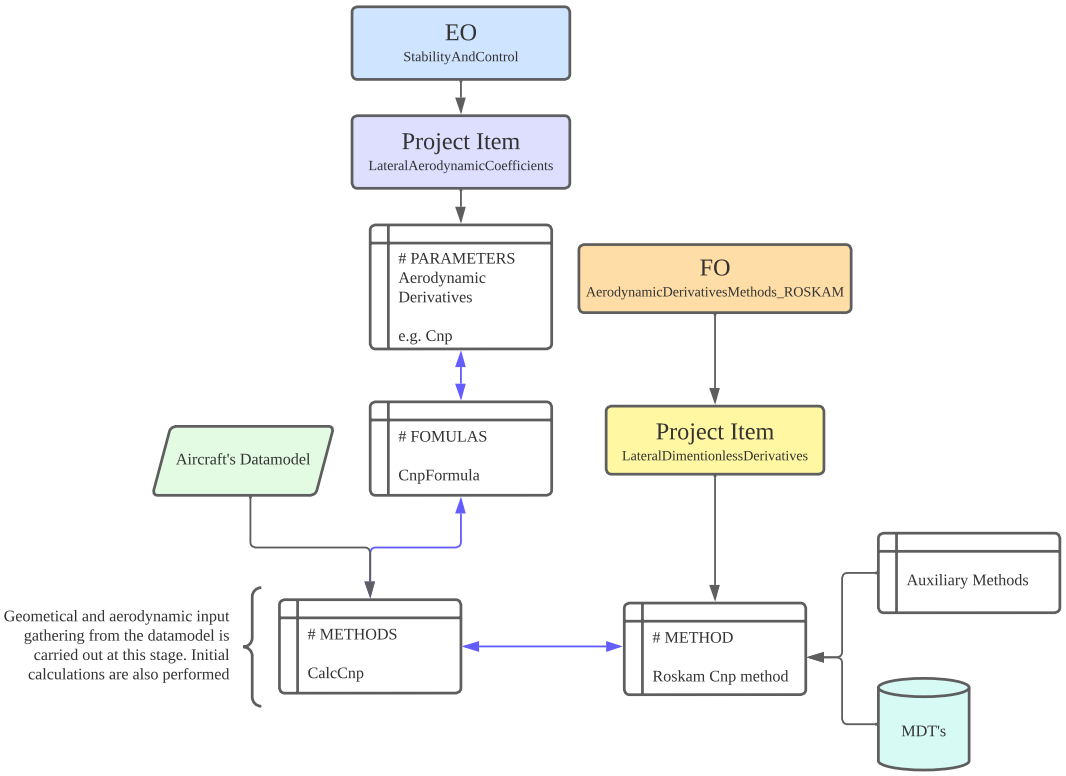


Figure 6.1: Flowchart for calculation of the aerodynamic derivatives inside Pacelab KD

# Chapter 7

# Pacelab APD Engineering Workbench output results

## 7.1 Flight conditions for stability derivatives calculation

The static stability derivatives for both the Boeing 747-400 and Boeing 737-800 were calculated using the flight conditions in table 7.1.

Table 7.1: Flight conditions for stability derivatives calculation

| **Flight Condition** | **Values** | **Unit** |
|---|---|---|
| Altitude | 100 | ft |
| Mach | 0.2, 0.4, 0.5, 0.6, 0.7 | - |
| Angle of Attack | -16, -8, -6, -4, -2, 0, 2, 4, 8, 8.5,10, 12, 14, 16, 18, 19, 20, 21, 22, 24 | deg |

## 7.2 Stability derivatives calculation: B747-400

Once all the flight conditions have been updated in Pacelab APD Engineering Workbench, the lateral static stability derivatives for the Boeing 747-400 were provided as follows in figure 7.1.

$Cl_\beta$ has a tendency to decrease its value with higher angles of attack. This derivative represents the variation of the rolling moment coefficient with respect to the sideslip angle ($\beta$). A positive value of $Cl_\beta$ indicates that an increase in sideslip angle will generate a rolling moment in the opposite direction.

$Cl_p$ represents the variation of the rolling moment coefficient with respect

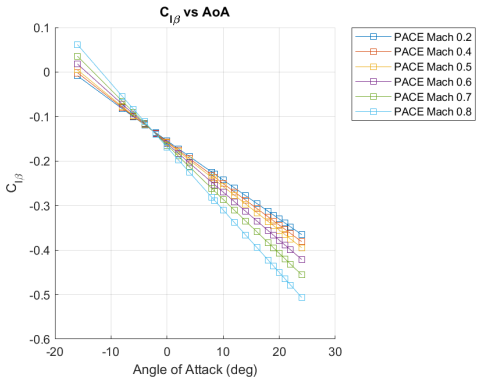


(a) Variation of rolling moment coefficient with sideslip angle.

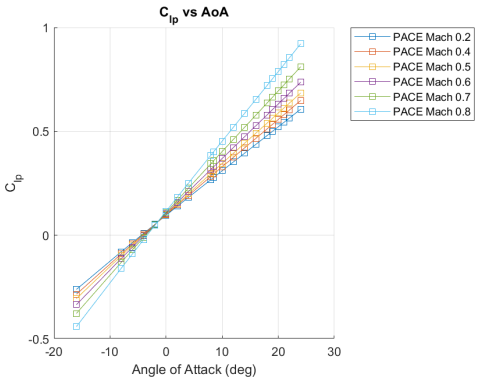


(b) Variation of rolling moment coefficient with roll rate.

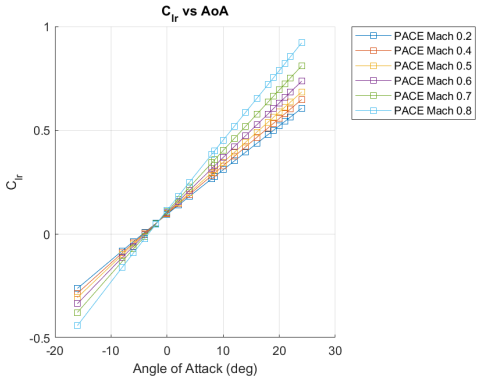


(c) Variation of rolling moment coefficient with yaw rate.

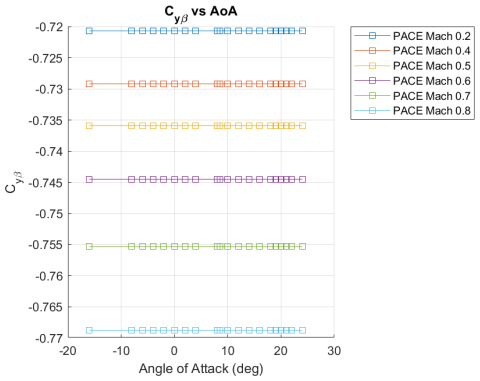


(d) Variation of side force coefficient with sideslip angle.

Figure 7.1: Pacelab APD Workbench Boeing 747-400 model's aerodynamic derivatives results

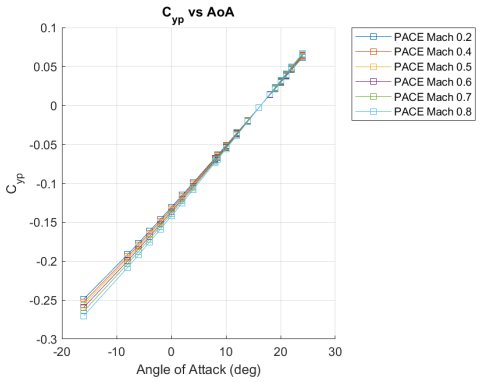


(e) Variation of side force coefficient with roll rate.

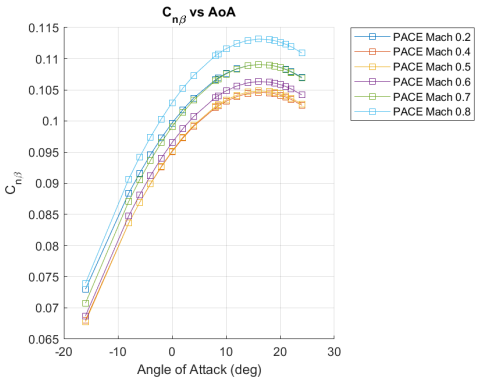


(f) Variation of yawing moment coefficient with sideslip angle.

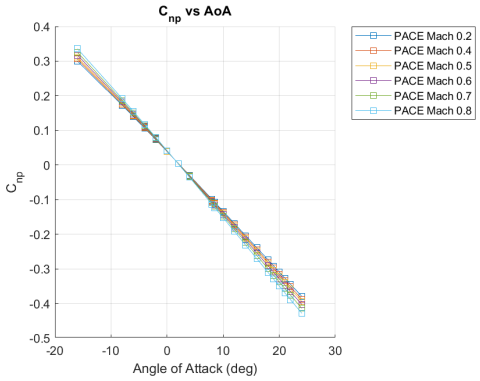


(g) Variation of yawing moment coefficient with roll rate.

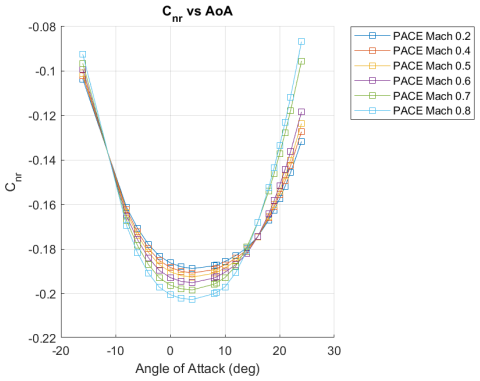


(h) Variation of yawing moment coefficient with yaw rate.

Figure 7.1: Pacelab APD Workbench Boeing 747-400 model's aerodynamic derivatives results

to the roll rate (p). A positive value of $Cl_p$ indicates that an increase in roll rate will generate a rolling moment in the same direction. This derivative affects the roll control and stability of the airplane. This derivative is important to estimate the roll rate of the aircraft and a negative value can cause a roll departure susceptibility that will be discussed further in this thesis.

The derivative $Cl_r$ represents the variation of the rolling moment coefficient with respect to the yaw rate (r). A positive value of $Cl_r$ indicates that an increase in yaw rate will generate a rolling moment in the same direction. This derivative along $Cn_r$ influence the Dutch-Roll and Spiral modes of the airplane since they are considered cross-coupled derivatives.

The derivative $Cy_\beta$ represents the variation of the side force coefficient with respect to the sideslip angle ($\beta$). A positive value of $Cy_\beta$ indicates that an increase in sideslip angle will result in an increase in the side force.

$Cy_p$ represents the variation of the side force coefficient with respect to the roll rate (p). A positive value of $Cy_p$ indicates that an increase in roll rate will generate a side force in the opposite direction. According to Roskam [11], this derivative has little effect on the overall flight characteristics of the airplane.

$Cn_\beta$ represents the variation of the yawing moment coefficient with respect to the sideslip angle ($\beta$). A positive value of $Cn_\beta$ indicates that an increase in sideslip angle will generate a yawing moment in the opposite direction. As previously mentioned, this is considered as a cross-coupled derivative that can influence the Dutch-Roll and Spiral modes of the airplane.

$Cn_p$ represents the variation of the yawing moment coefficient with respect to the roll rate (p). A positive value of $Cn_p$ indicates that an increase in roll rate will generate a yawing moment in the opposite direction. This derivative affects the directional stability of the airplane.

$Cn_r$ represents the variation of the yawing moment coefficient with respect to the yaw rate (r). A positive value of $Cn_r$ indicates that an increase in yaw rate will generate a yawing moment in the same direction.

## 7.3 Stability derivatives calculation: B737-800

Similarly to the previous model, the lateral static stability derivatives for the Boeing 737-800 were provided as follows in figure 7.2.

The results from the Boeing 737-800 calculations show a similar behavior in terms of variation of the stability derivatives by angle of attack besides the results for $Cl_p$, in which the Boeing 737-800 values remain constant while in the Boeing 747-800 those values increase with the angle of attack.

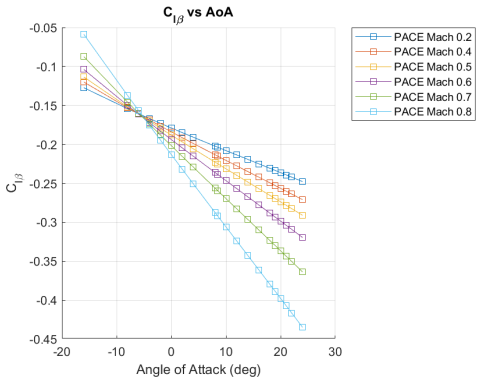


(a) Variation of rolling moment coefficient with sideslip angle.

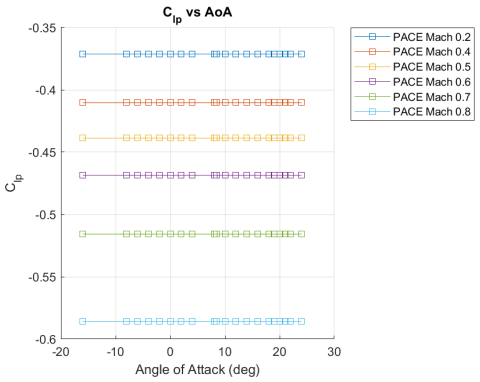


(b) Variation of rolling moment coefficient with roll rate.

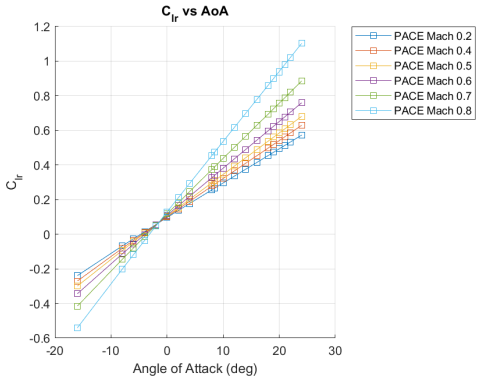


(c) Variation of rolling moment coefficient with yaw rate.

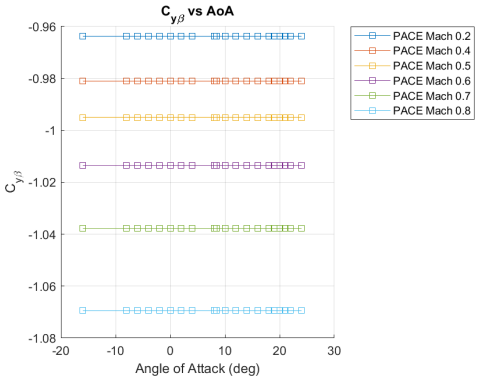


(d) Variation of side force coefficient with sideslip angle.

Figure 7.2: Pacelab APD Workbench Boeing 747-400 model's aerodynamic derivatives results

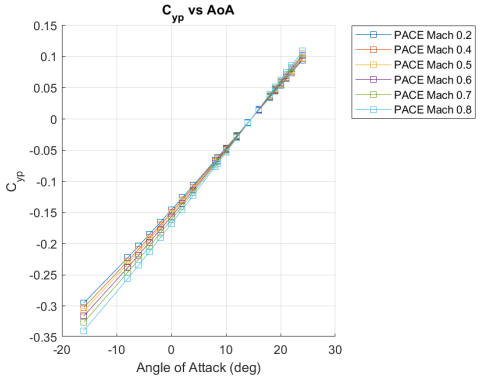


(e) Variation of side force coefficient with roll rate.

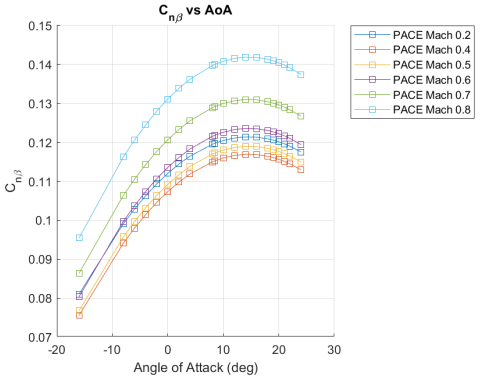


(f) Variation of yawing moment coefficient with sideslip angle.

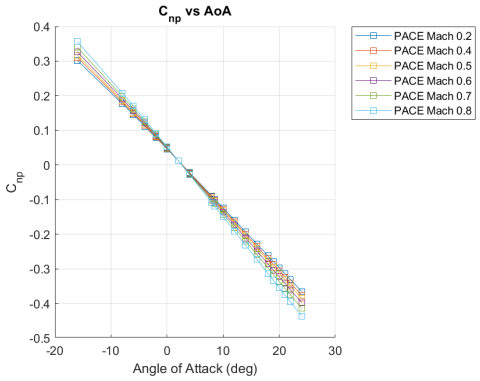


(g) Variation of yawing moment coefficient with roll rate.

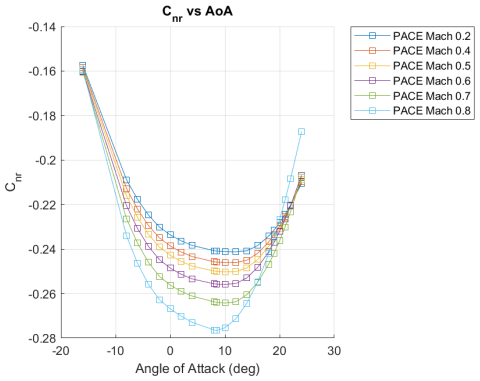


(h) Variation of yawing moment coefficient with yaw rate.

Figure 7.2: Pacelab APD Workbench Boeing 747-400 model's aerodynamic derivatives results

## 7.4 Results for steady roll rate criteria

The steady roll of the Boeing 737-800 was assessed by incorporating the calculated control derivative $Cl_{\delta_a}$ estimated through Digital DATCOM, in conjunction with the derivatives computed using the methods implemented in Pacelab APD Engineering Workbench.

The parameters for the ailerons used in the Digital DATCOM model were approximated values since no data regarding the positioning, chord, and span of the Boeing 737-800 ailerons was provided by the manufacturer or any of the literature reviewed in this thesis. Therefore, the creation of the aileron model for Digital DATCOM involved scaling its parameters based on available figures in the literature and comparing them with the geometry sizing in the Pacelab APD model.

It's worth mentioning that the input method for the ailerons in Digital DATCOM does not allow for multiple span wise stations with a mix of plain ailerons and deferentially deflected ailerons, which is the case for the Boeing 737-800. Instead, an approximate model of an oppositely symmetrical aileron was implemented, taking into account the same approximate area as the ailerons on the actual airplane.

The Digital DATCOM simulation was performed with aileron deflections of $\pm 20°$, $\pm 15°$, $\pm 10°$ and $\pm 5°$. The ailerons on each side are deflected asymmetrically, giving combined deflections of 40°, 30°, 20° and 10° respectively. For the steady roll rate, the $Cl_{\delta_a}$ used was calculated with a total deflection of 20°, ($\delta a_r + \delta a_l = 20°$) and 40°, ($\delta a_r + \delta a_l = 40°$). Figure 7.3 below shows the results obtained.

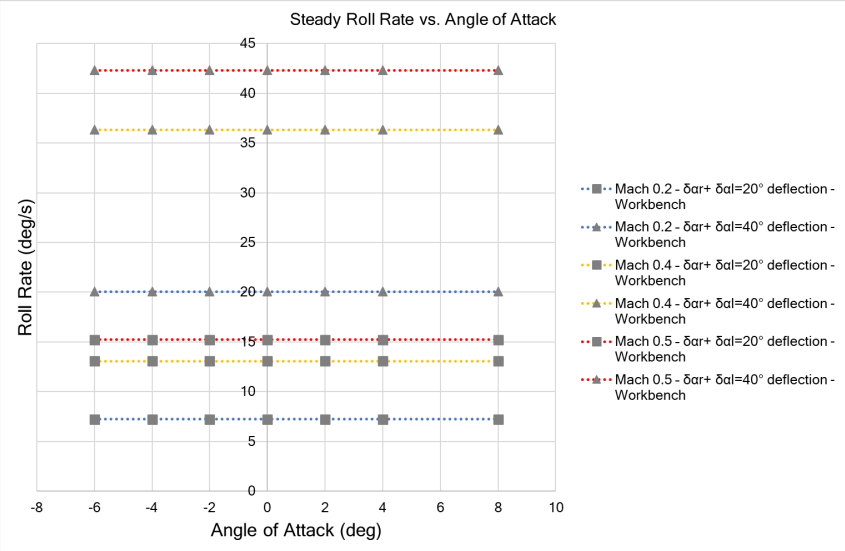


Figure 7.3: Steady roll rate for the Pacelab APD Workbench Boeing 737-800 model

The results show a steady roll rate varying from 7 [deg/s] for a 20° aileron deflection up to 20 [deg/s] for a 40° aileron deflection at Mach 0.2. At Mach 0.5, the steady roll rate varies between 15 [deg/s] and 42 [deg/s]. It is noticeable that the angle of attack does not influence the roll rate in this model since the $Cl_{\delta_a}$ coefficient exhibits very little variation through different angles of attack, and the $Cl_p$ for the Boeing 737-800 are equal at these Mach numbers.

## 7.5 Results for departure susceptibility criteria

Like the steady roll rate criteria, the departure criteria, seen in figure 7.4, was calculated using Digital DATCOM's $Cl_{\delta_a}$ and $Cn_{\delta_a}$ for the same reasons mentioned in the steady roll rate section 7.4. The aileron deflection angle used in this evaluation is ($\delta a_r + \delta a_l = 40°$), also with the same configuration as mentioned in the steady roll rate section 7.4. The variation of LCDP and $Cn_{\beta_{\text{dynamic}}}$ is related to the angle of attack, which was used between $-16°$ to 12°.

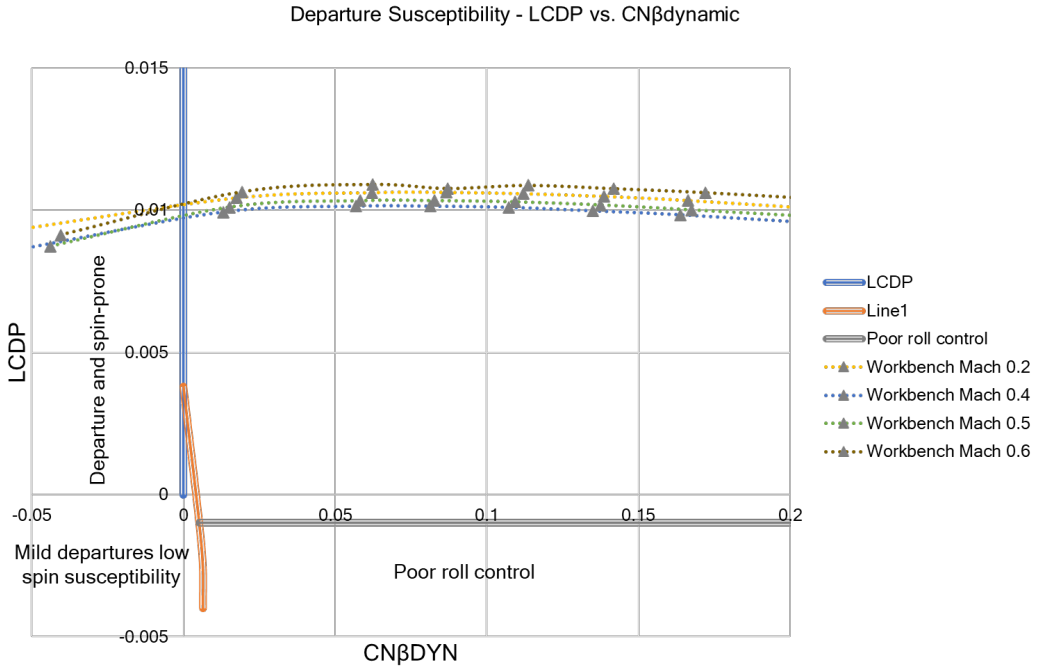


Figure 7.4: Departure susceptibility criteria for the Pacelab APD Workbench Boeing 737-800 model

The results show that the airplane is almost entirely within the no departure zone, as expected. Since the variation of the control derivatives with respect to the angle of attack used in this simulation is small, the progression of the airplane's departure characteristics mostly depends on the variations of $Cl_\beta$ and $Cn_\beta$ with respect to the angle of attack.

# Chapter 8

# Validation

## 8.1 Validation data for stability derivatives

Among the available literature concerning methods to predict stability derivatives, few authors provide data and results from template calculations that can be used to validate a model and when provided, they are related to out of production commercial airplanes or decommissioned military airplanes.

It is comprehensible that such values are kept under secrecy since their disclosure can allow a competitor manufacturer to obtain valuable information on the airplane's flying qualities. Roskam [10] and Napolitano [8] provide in their books data for calculating stability derivatives.

In order to validate the model to calculate the stability derivatives in Pacelab APD Workbench, one of the provided airplanes in the software has to be used, since it is both difficult to find geometrical and mass data for any airplane as it is to implement regarding the time constraint of the thesis.

Two aircraft that are available in the used version of Pacelab APD Workbench are the Boeing 747-400 and the Boeing 737-800. The 747-200 has its stability derivatives calculated for three different flying conditions by both [10] and [8], as in table B.1. Even though the 737-800 has no available data, it is a easy-to-find airplane model for Digital DATCOM [12] and OpenVSP[15].

Though the Boeing 747-200 and 747-400 are different in terms of geometry and mass, the overall shape of both airplanes are similar enough that the 747-200 provided data can be used for validation, considering the previously mentioned difficulties to find reliable flight mechanics data on the available airplanes models from Pacelab APD Workbench.

## 8.2 Digital DATCOM and OpenVSP

In order to validate the results generated by Pacelab Engineering Workbench, models for the Boeing 747-400 and Boeing 737-800 were generated using third-party software Digital DATCOM [12] and OpenVSP [15], in addition to the provided data for the Boeing 747-200 from [10] and [8]. These models were created to match the geometrical aspects of the models provided by Pacelab Engineering Workbench. Figure 8.1 shows the Boeing 747-400 model created with OpenVSP, while figures 8.2 and 8.3 show the Boeing 747-400 and Boeing 737-800 models respectively, created with Digital DATCOM. This approach for validation was necessary since the available data for the used airplanes could not be found, except for the three Boeing 747-200 flight conditions mentioned in section 7.

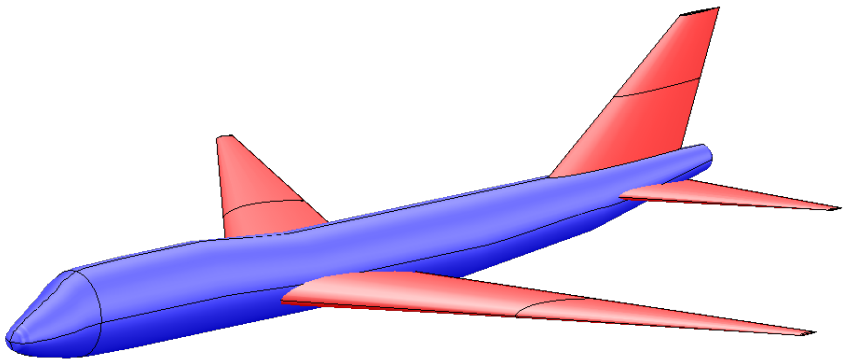

Figure 8.1: Visualization of the Boeing 747-400 model created for OpenVSP

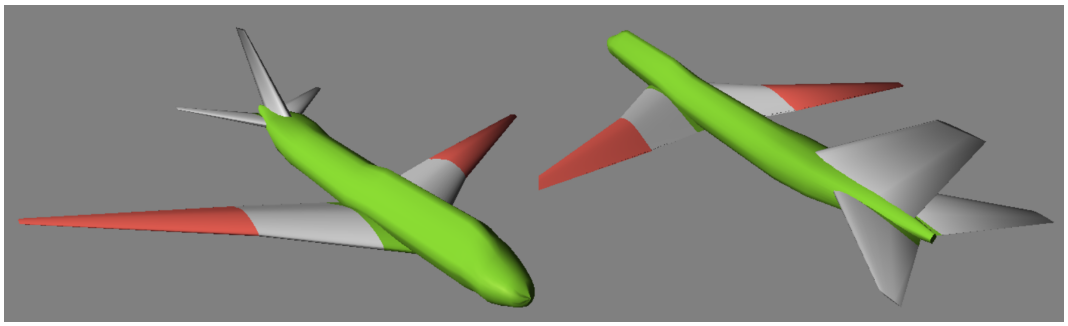

Figure 8.2: Visualization of the Boeing 747-400 model created for Digital DATCOM

## 8.3 Validation of static stability derivatives

The aerodynamic derivatives for both the Boeing 747-400 and Boeing 737-800 were calculated using the same flight conditions as in section 7.1. For the Digital DATCOM files generated for both airplane models, a maximum of sixteen points was used to describe the fuselage shape, while forty-nine

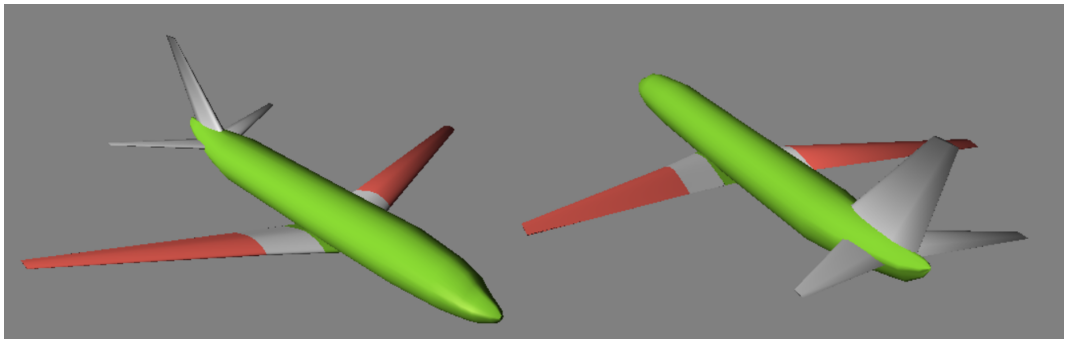

Figure 8.3: Visualization of the Boeing 737-800 model created for Digital DATCOM

points were used to describe the airfoil shape. In OpenVSP, there is no limit on the number of sections for the fuselage, but it does not allow for user-defined airfoils. The only choice available in OpenVSP is to use NACA 4-digit or 5-digit airfoils. To match the airfoil lift-curve slope used in the Pacelab Workbench models, the selected airfoils were set as NACA 22012, since both airplane models had a lift-curve slope of 6 [1/rad] and a maximum camber of 2%, which is similar to the NACA 22012 airfoil.

### 8.3.1 Validation of stability derivatives: B747-400

The lateral aerodynamic derivatives for the Boeing 747-400 were provided as follows in figure 8.4.

Considering the provided data for the Boeing 747-200 from [10] and [8], not all of the derivatives show a good correlation with the models from Digital DATCOM and OpenVSP, considering the previously mentioned differences from the 747-200 and 747-400 models.

OpenVSP was able to reasonably predict the behavior of $Cn_p$ and $Cl_r$, which matched the expected values from the literature. The derivatives $Cn_r$ and $Cy_\beta$ also showed more reasonable results compared to Digital DATCOM, although they were still far from the expected values. However, for $Cl_\beta$, $Cl_p$, $Cn_\beta$, and $Cy_p$, the results were far from the expected values in terms of both magnitude and progression of values along the angle of attack.

Digital DATCOM provided a better prediction for $Cl_\beta$, $Cl_p$, $Cl_r$, and $Cy_p$ compared to OpenVSP. Although the slope of $Cl_\beta$ was not as expected, it was still a closer result compared to OpenVSP. However, the results for $Cn_\beta$ and $Cn_p$ were equally far from the expected values, similar to OpenVSP. Additionally, the predictions for $Cn_r$ and $Cy_\beta$ were not any closer to the expected values from the literature.

Overall, the model from Pacelab Workbench exhibited better performance

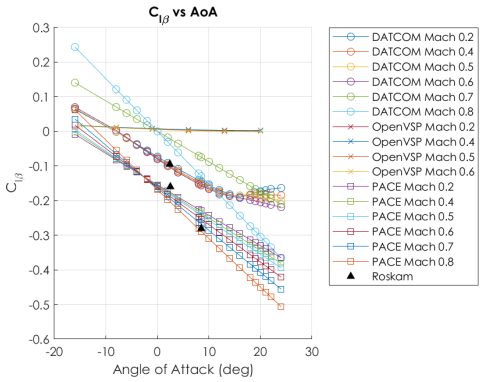


(a) Variation of rolling moment coefficient with sideslip angle.

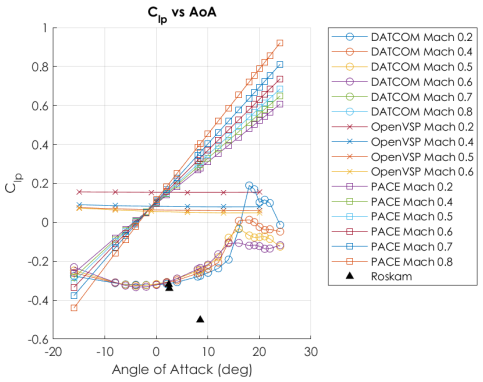


(b) Variation of rolling moment coefficient with roll rate.

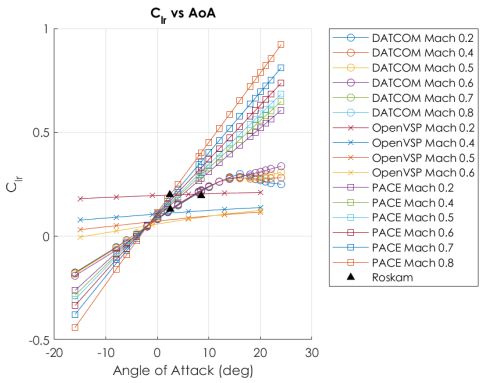


(c) Variation of rolling moment coefficient with yaw rate.

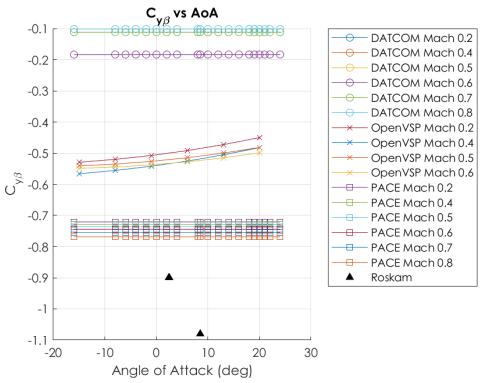


(d) Variation of side force coefficient with sideslip angle.

Figure 8.4: Boeing 747-400 model's aerodynamic derivatives results

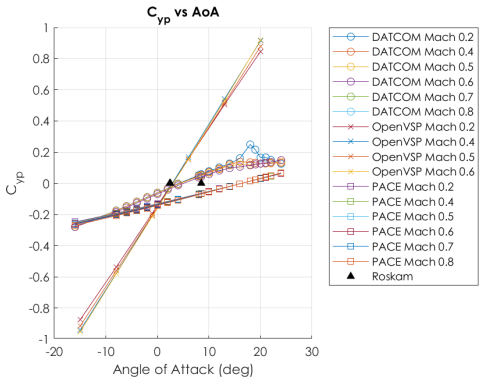


(e) Variation of side force coefficient with roll rate.

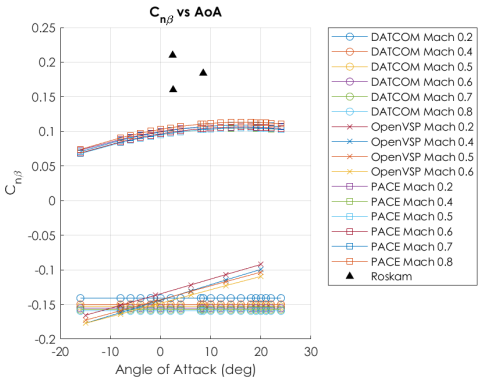


(f) Variation of yawing moment coefficient with sideslip angle.

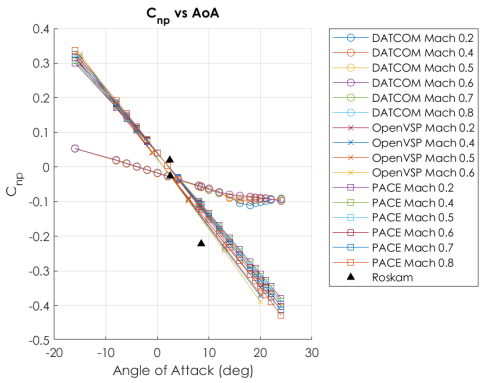


(g) Variation of yawing moment coefficient with roll rate.

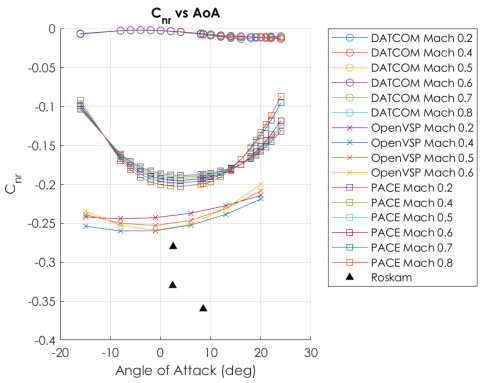


(h) Variation of yawing moment coefficient with yaw rate.

Figure 8.4: Boeing 747-400 model's aerodynamic derivatives results

in predicting the lateral stability derivatives compared to the previous validation models when considering the literature values. However, it should be noted that the $Cl_p$ derivative was overestimated in the Pacelab implemented model.

### 8.3.2 Validation of stability derivatives: B737-800

The lateral aerodynamic derivatives for the Boeing 737-800 were provided as follows in figure 8.5.

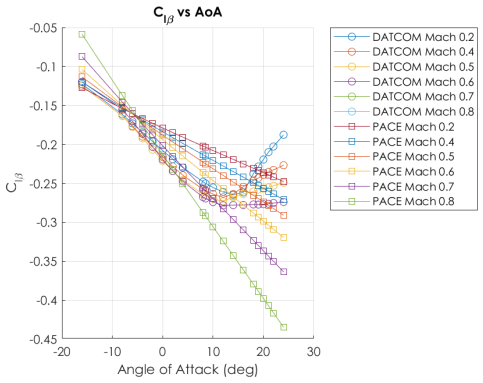


(a) Variation of rolling moment coefficient with sideslip angle.

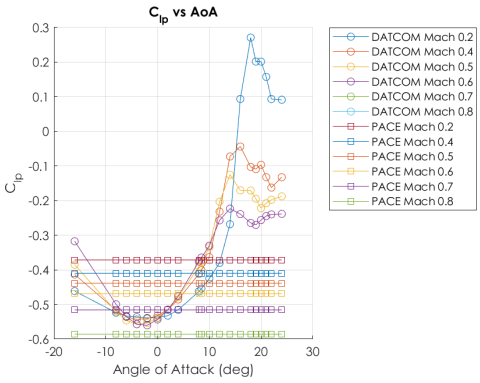


(b) Variation of rolling moment coefficient with roll rate.

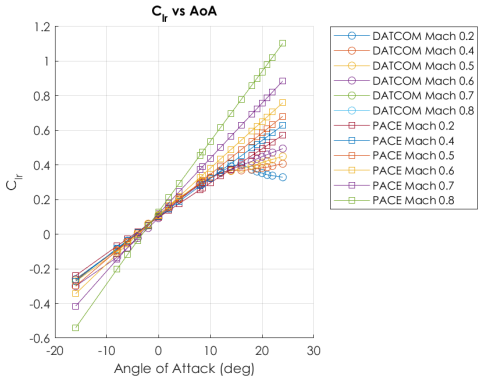


(c) Variation of rolling moment coefficient with yaw rate.

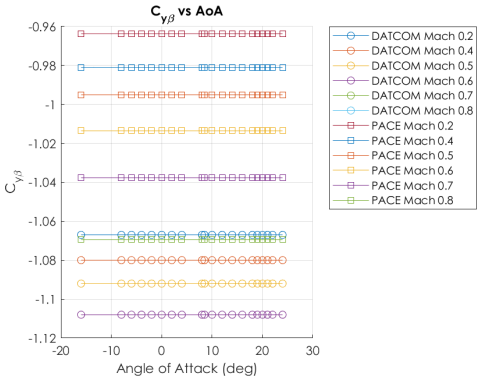


(d) Variation of side force coefficient with sideslip angle.

Figure 8.5: Boeing 737-800 model's aerodynamic derivatives results.

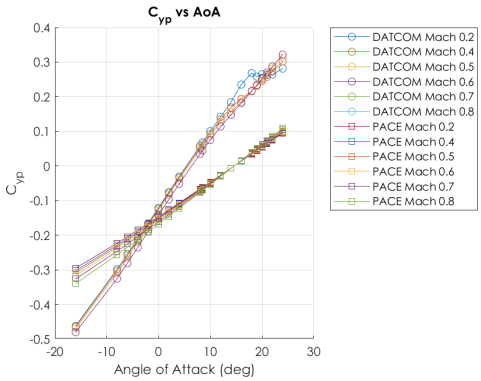


(e) Variation of side force coefficient with roll rate.

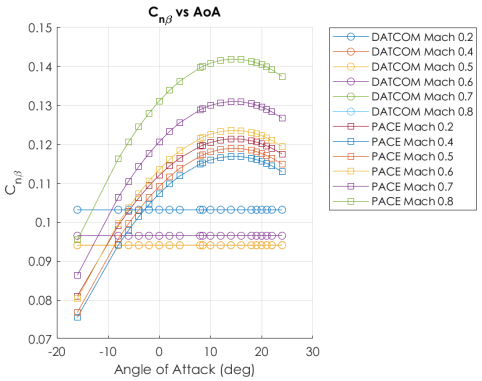


(f) Variation of yawing moment coefficient with sideslip angle.

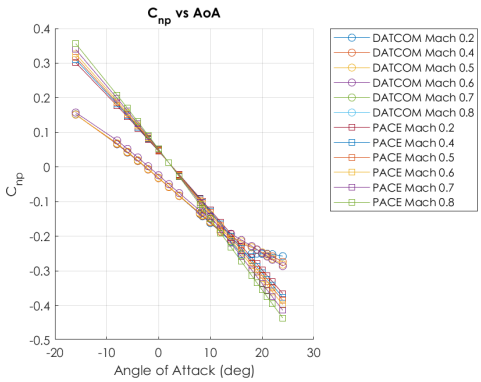


(g) Variation of yawing moment coefficient with roll rate.

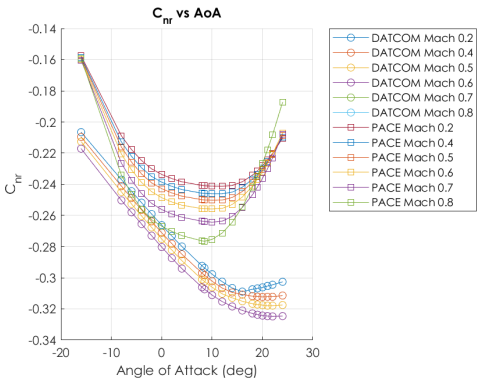


(h) Variation of yawing moment coefficient with yaw rate.

Figure 8.5: Boeing 737-800 model's aerodynamic derivatives results.

Since there are no available data from the literature specifically for the Boeing 737-800, it is not possible to conduct a quantitative evaluation of the results. However, considering the knowledge gained from the previous study with the Boeing 747-400, including the slopes and required magnitudes of the derivatives, and taking into account the differences between a wide-body airliner and a narrow-body airliner, the lateral stability derivative results for the Boeing 737-800 can provide a new set of data for comparison between the Pacelab Workbench and Digital DATCOM models.

## 8.4 Validation of steady roll rate criteria

The steady roll rate results generated by Digital DATCOM differ from the ones predicted in Pacelab Workbench in magnitude as the coefficients calculated by Digital DATCOM are different from the model implemented in figure 8.6. There is also a change in the roll rate for higher angles of attack when both models are compared due to the non-linear lift-curve slope of the Digital DATCOM model.

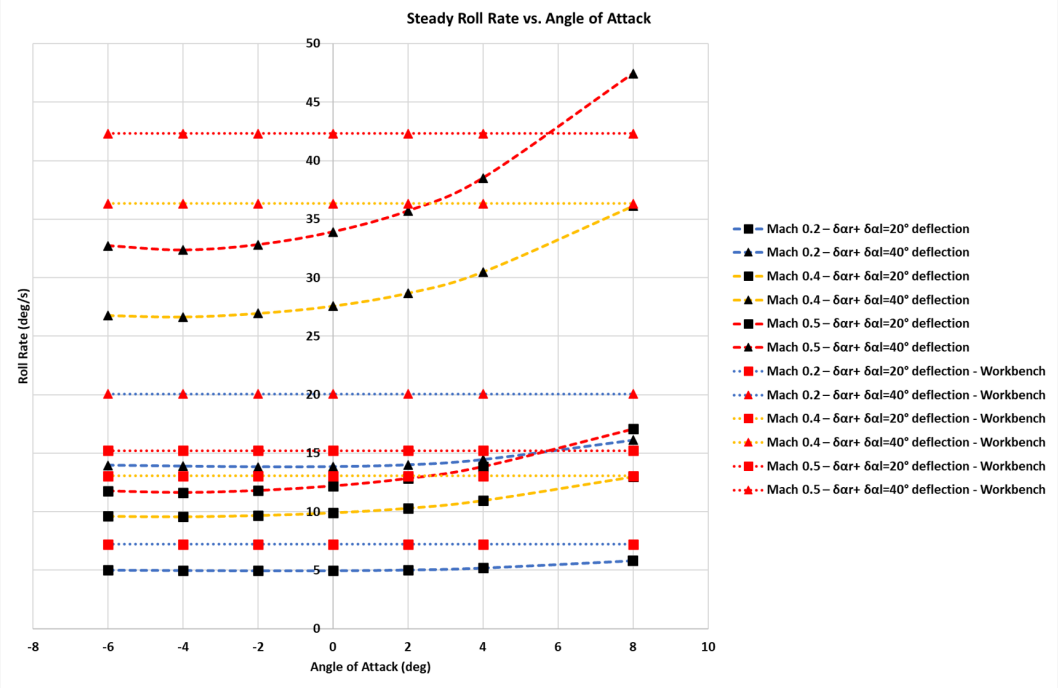


Figure 8.6: Steady roll rate for the Pacelab Workbench and Digital DATCOM Boeing 737-800 models

## 8.5 Validation of departure susceptibility criteria

The departure susceptibility model generated by Digital DATCOM yields similar results as the one generated by the implemented model in Pacelab Workbench though with slightly smaller LCDP and $Cn_{\beta_{\text{dynamic}}}$ values. This criteria is reliant on $Cl_\beta$ and $Cn_\beta$. The first coefficient has similar values for both models within angles of attack between $-16°$ and $0°$ while Pacelab Workbench model results between $0°$ and $15°$ are overestimated. The second coefficient has overrated values from Pacelab Workbench model compared to the Digital DATCOM model. Therefore it is expected that both LCDP and $Cn_{\beta_{\text{dynamic}}}$ values may be higher for the Pacelab Workbench prediction.

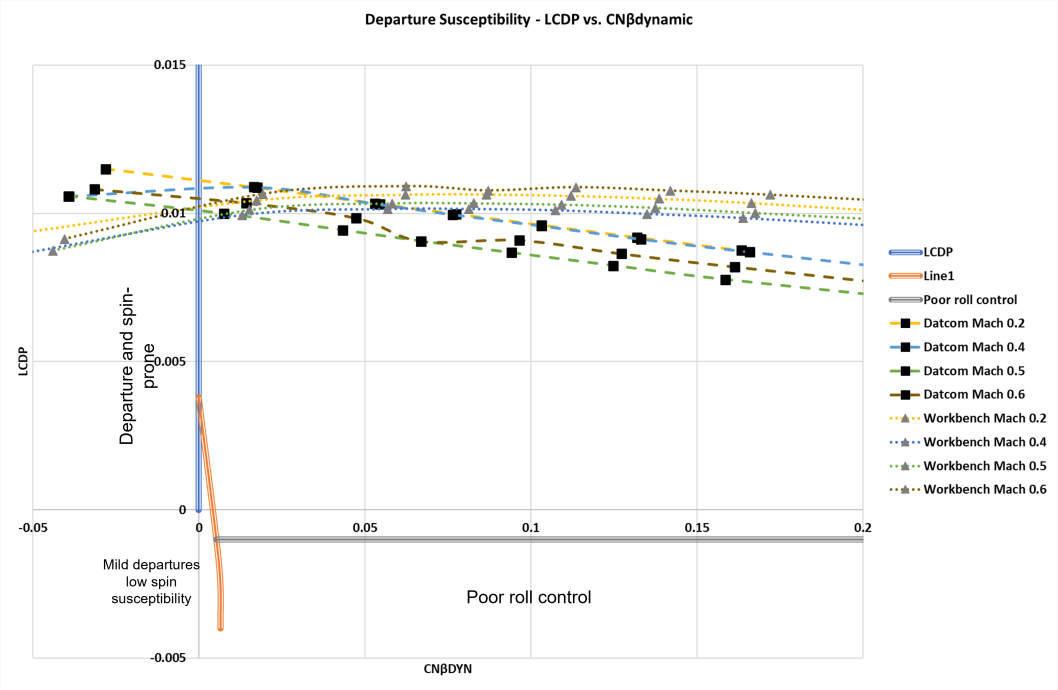


Figure 8.7: Departure susceptibility criteria for the Pacelab Workbench and Digital DATCOM Boeing 737-800 models

# Chapter 9

# Discussion

## 9.1 Discussion on stability derivatives: B747-400

Understanding the stability derivatives results of a simulation, either for a conceptual design phase or through a more advanced phase, is essential for assessing the dynamic behavior of the aircraft, including its roll, yaw, and sideslip responses.

The results for the static stability derivatives provided by the simulations performed in Pacelab APD Engineering Workbench (Pacelab EWB) showed unexpected behavior in terms of the evolution and magnitude of certain derivatives when compared to the values from Roskam [10].

The first important stability derivative to be analyzed is the variation of the side force coefficient with sideslip angle, $Cy_{\beta}$. More specifically, the contribution from the vertical stabilizer, $Cy_{\beta_v}$, is crucial as it affects other stability derivatives.

The vertical tail contributions $Cn_{\beta_v}$ (equation 4.19) of $Cn_{\beta}$, $Cl_{p_v}$ (equation 4.24) of $Cl_p$, $Cn_{p_v}$ (equation 4.29) of $Cn_p$, $Cy_r$ (equation 4.30), $Cl_{r_v}$ (equation 4.35) of $Cl_r$ and $Cn_{r_v}$ (equation 4.39) of $Cn_r$ are all influenced by $Cy_{\beta_v}$.

A small contribution from $Cy_{\beta_v}$ can underestimate the mentioned derivatives and cause a misinterpretation of the results. For the estimation of $Cy_{\beta_v}$, the term $\left(1 + \frac{d\sigma}{d\beta}\right) n_v$ calculated from equation 4.6 has the variable $d$ as an input, which is calculated as the maximum fuselage height along the chord-line of the wing/fuselage intersection and $Z_w$, which is the vertical distance from the wing root quarter chord point to the fuselage center line. When implementing a model which relies on very specific geometrical features of the aircraft, the resolution and precision of the points to describe the geometry need a high

level of fidelity with the original model, in this case as an evaluation of the derivatives of a known airplane, or an accurate description of the fuselage geometry of a conceptual design is of extreme importance since such seemingly simple parameters might greatly affect the results of other derivatives.

In the particular case of the Boeing 747-400, the fuselage possesses a variation in height in the forward section to account for the second deck, as seen in figure 9.1, which can influence in the final value of $Cy_{\beta_v}$.

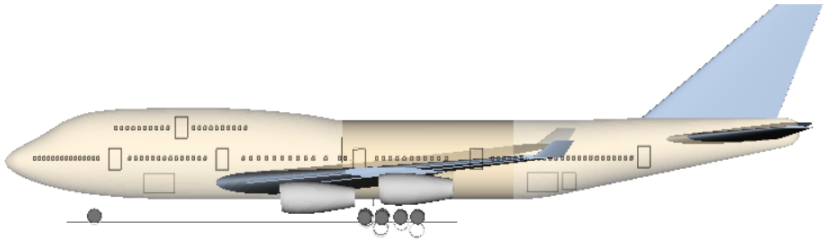

Figure 9.1: Side view of the Boeing 747-400 model from Pacelab EWB. The fuselage height changes in the forward section due to the second deck.

The accurate position where the fuselage height changes relative to the wing chord as well as the height variation might or might not be precisely implemented in the model implemented in Pacelab EWB. Since the accurate description of the fuselage geometry is not available from the manufacturer, checking the dimensions of the provided models is not possible. Also, considering the large dimensions of the Boeing 747-400 as a wide-body airliner, the height difference can vary greatly along the fuselage to account for the second deck. According to the model from Pacelab EWB, the central fuselage section has a height of 9.1 [m] while the maximum height for the forward fuselage is 10.2 [m], a 1.1 [m] difference.

It is important to point out that the $2r_1$ parameter, regarded as twice the Z-component length between the vertical tail and the fuselage bottom at the vertical tail's quarter chord, used to interpolate in plots A.2 and A.3 to estimate aspect ratio factors to be used in the Polhamus equation 4.7 is also dependent on the accuracy of the geometry description and modeling of the fuselage. A different slope and/or height at the after fuselage section can influence the vertical tail's $C_{L_\alpha}$ and therefore the $Cy_{\beta_v}$ contribution.

According to the results in the validation chapter 8, the Pacelab EWB model as well as the OpenVSP model underestimates the $Cy_\beta$ compared to the Roskam provided values. Digital DATCOM results are considerably underestimated and are certainly not describing the expected behavior of the airplane regarding the stability for the side force with sideslip angle. Well this low value for $Cy_\beta$ can be interpreted as the model not having enough vertical tail contribution to the side force from sideslip, which is known to be incorrect as pointed by Napolitano [8] in Chapter 4.2, "A substantial contribution to $Cy_\beta$ is instead provided by the vertical tail". The Boeing 747-400 has a con-

siderable area that should react to the relative wind when in a sideslip angle flight path, matching the prediction of values by Roskam.

The derivatives $Cn_\beta$, $Cn_r$ are greatly influenced by $Cy_{\beta_v}$ in their vertical stabilizer contribution for being yawing related derivatives. As expected from the Digital DATCOM model, since $Cy_\beta$ was underestimated, this derivatives were underestimated as well. Other contributing factors for estimation of this derivative are the fuselage side area, fuselage length and fuselage height at 1/4 of the length and at 3/4 of the length according to equation 4.17. As previously mentioned, once again the need for a precise description of the geometry of the fuselage is needed since many different factors that influence the final value of this derivative contribution are reliant on precise geometries.

$Cl_p$ and $Cl_r$ on the other hand are not heavily influenced by the $Cy_{\beta_v}$ contribution [11], but rather the wing-body and horizontal tail contributions as seen in equations 4.21 and 4.31, thought the equations contain the $Cy_{\beta_v}$ contribution. It is visible in figure 8.4c that the predicted values for $Cl_r$ are within the expected regions provided by Roskam for both Pacelab EWB and Digital DATCOM. $Cl_p$ results for Digital DATCOM shows that for lower angles of attack the values converge to Roskam predictions but for higher angles of attack, since the $Cy_{\beta_v}$ contribution was underestimated, its value should decrease with the increment of negative $Cy_{\beta_v}$ values but the contrary is observed in figure 8.4b.

Regarding Pacelab EWB $Cl_p$ results, the unexpected slope might be due to the off values of the $Cy_{\beta_v}$ contribution and also for the lift coefficient model adopted by Pacelab EWB which the lift-curve slope is a user input rather than a calculated value from an airfoil shape like in Digital DATCOM. In the method provided by Roskam, it is stated that for the wing-body contribution of this derivative, the $K$ factor is the ratio of the average wing section lift curve slope $C_{L_\alpha}$ to $2\pi$. Since the lift curve slope changes with angle of attack, this coefficient should also change.

Lastly, OpenVSP did not provide accurate and realistic results when compared to the provided literature data and models from Pacelab EWB and Digital DATCOM except when predicting $Cn_p$ and $Cn_r$. Therefore the simulations are not regarded as reasonable values for any comparison. The reasons for such different results are unknown and are not addressed in this thesis because of the difficulty to either create a model in OpenVSP that represents correctly the airplane to be evaluated or to troubleshoot and check existing models. Otherwise, an interesting approach would be to evaluate more airplane models to identify weaknesses and points of interest worth of investigating in OpenVSP in order to create a model sufficiently accurate to be used to generate stability derivatives.

## 9.2 Discussion on stability derivatives: B737-800

The Boeing 737-800 was chosen as an additional aircraft to be evaluated using Pacelab EWB model and Digital DATCOM. The model is already implemented in Pacelab EWB and with its geometrical data, the Digital DATCOM model was created.

To generate the model, similarly to the Boeing 747-400 model, it was used 16 sections of the fuselage and 49 sections of the airfoil. Once again, the Pacelab EWB model does not have a prediction of lift for the wing by executing any physics model such as the panel method used by Digital DATCOM but rather relies on user inputs of lift coefficient curve-slope of the airfoil.

Starting this discussion also by evaluating the variation of side force coefficient with sideslip angle $Cy_\beta$ from both model predictions, the results now show closer proximity and reasonable values where $Cy_\beta$ was expected to be. A negative high magnitude value for $Cy_\beta$ represents that the lateral force acting in the opposite direction of the lateral axis (considering that the sideslip angle $\beta$ is positive from the right of the pilot) generated by the contribution from the dihedral angle of the wing, fuselage side area and vertical tail is being correctly represented. Also it is possible to see that by increasing the Mach in both models, the coefficient tends to increase as the force is also expected to increase.

Since the prediction for $Cy_\beta$ is more realistic in this airplane rather than with the 747-400 model, it is expected that the derivatives closely related to the $Cy_{\beta_v}$ contribution shall present more significant and reasonable values.

The variation of yawing moment coefficient with sideslip angle $Cn_\beta$ for the Boeing 737-800 has positive values for both Pacelab EWB and Digital DATCOM even thought DATCOM's prediction is still within smaller ranges than Pacelab's predictions. A high value of $Cn_\beta$ is desirable since it represents that the vertical tail of the aircraft has dominance over the wind and body contribution while creating a yawing moment towards the relative wind, therefore considered to have a directional stability.

$Cl_\beta$ behavior for both models is similar to the Boeing 747-400, with negative values (meaning a negative rolling moment) expected to increase in magnitude with the angle of attack since the wing lift also increases and the moment created by the wing contribution $Cl_{\beta_{wb}}$. The difference in the evolution for the angle of attack of the values between the two models is due to the variable lift coefficient curve-slope generated by Digital DATCOM and the fixed used input lift coefficient curve-slope from Workbench. The same effect from the fixed lift coefficient curve-slope can be noticed in the results for $Cl_p$.

$Cn_r$ results from Digital DATCOM shows higher magnitude compared to the 747-400 model, meaning that the $Cy_{\beta_v}$ contribution for this derivative is higher since the overall value of $Cy_\beta$ changed as well. The Dutch-roll mode of the airplane evaluated using a combination of $Cn_r$ and the other cross-coupled derivative $Cl_r$. The combination of $Cl_r$ and $Cn_r$ values helps to either stabilize or increase the oscillations causing excessive divergence or instability in the Dutch-roll mode. As the aircraft experiences yawing motion, $Cl_r$ generates a rolling moment in the same direction, which counteracts the yaw and stabilizes the rolling motion. Simultaneously, $Cn_r$ generates a yawing moment in the same direction as the yaw rate, contributing to the stability of the yawing motion.

The results between the two models for the variation of rolling moment coefficient with yaw rate $Cl_r$ and variation of side force coefficient with roll rate $Cy_p$ were similar as expected since none of the derivatives affected by the previous geometrical issues should interfere with the results.

In overall the predictions for the lateral stability derivatives of the Boeing 737-800 were more similar towards the predictions from Digital DATCOM than for the Boeing 747-400. The differences in values are expected not only because the methods to calculate the derivatives are different but also because of the different assumptions of the two software and the smooth constant fuselage geometry of the 737-800 model compared to the variable height forward fuselage of the 747-400 that prevents a wrong estimation of $Cy_{\beta_v}$. Although Pacelab EWB has a higher resolution of points to define the fuselage and more freedoms of placement and angles of the airplane's components compared to Digital DATCOM, the last has a embedded VLM model that predicts stalls for high angles of attack while also calculating the correct lift coefficient curve-slope for each angle of attack, a feature that is very important as seen in the results to provide realistic and reliable results for predicting the flight dynamics of an airplane.

Its worth pointing out that Roskam's method is based in DATCOM [12] methods for conventional subsonic aircrafts and as such, correcting the aforementioned differences in the two software should yield similar results, considering the limitations of geometry description from Digital DATCOM. Once Pacelab EWB has the ability to calculate lift coefficients by estimating through the geometry of the model rather than using a user input, results should not differ or should be minimal, related only to the resolution of geometry.

## 9.3 Discussion on steady roll rate: B737-800

The steady roll rate is the roll around the x-axis or of the airplane exclusively performed by aileron deflections and discounting any interference of rudder inputs. The Title 14, Code of Federal Regulations (14 CFR) §25.349 [16]

regulates the roll rate for transportation aircraft. However, according to [17], part 25 of the mentioned regulation is inadequate for addressing an airplane with electronic flight controls that affect maneuvering, as referencing to the Boeing 737-800. Based on pilot ratings in the technical report by Holleman [18], a reasonable roll rate is defined at between 15 [deg/s] and 20 [deg/s].

The military standard MIL8785C [19] states that a category II airplane (medium to heavy transport) at a Category B (cruise) should be able to bank the airplane 45° in a time between 1.9[s] and 3.8[s]. During a Category C (Take-off / Approach) it should be able to bank the airplane 30° between 1.8 [s] and 3.6 [s].

The estimated steady roll rate in section 8.4 for the studied model is between 7 [deg/s] and 20 [deg/s] at Mach 0.2 for the Digital DATCOM simulation and between 5 [deg/s] and 14 [deg/s] at Mach 0.2 for the Pacelab EWB simulation. For a Mach 0.5 velocity, the steady roll rate is between 13 [deg/s] and 47 [deg/s] for the Digital DATCOM simulation and between 15 [deg/s] and 43 [deg/s] for the Pacelab EWB simulation.

Even though these values are within the specification of the standard, they cannot be validated due to the lack of data until the end of this thesis regarding the steady roll rates for the Boeing 737-800.

## 9.4 Discussion on departure susceptibility criteria: B737-800

As stated by [14], static aerodynamic data can only predict the susceptibility to depart, but not the departure motion itself. The models used for this thesis have their static stability derivatives estimated together with the aileron yawing moment derivative and rolling moment derivative. Besides, departure susceptibilities are more prone to happen at high-angle-of-attack situations where large deflections of ailerons and/or rudders can induce a spin or roll reversal. Under such conditions, it becomes necessary to utilize more sophisticated aerodynamic coefficients and incorporate a wing stall prediction model, along with an accurate methodology for calculating control stability derivatives. None of the aspects are present within the implemented method in Pacelab EWB and therefore the calculated departure susceptibility does not provides reliable results for the user. It is proposed that for the future, besides the implementation of a more precise aerodynamic model, control derivatives should be implemented so the current user input is not used but rather calculated according to the correct methods.

## 9.5 Research questions

- To what extent are the selected methods efficient and accurate in estimating the aerodynamic coefficients of the aircraft?

The methods for calculating lateral stability derivatives assessed in this thesis have proven to be reasonably reliable to estimate lateral aerodynamic coefficients if limitations for low angles-of-attack, sub-sonic and steady flight are considered. More information is needed to validate the implemented model such as wind-tunnel testing and CFD simulations since information from manufactures from embedded airplanes on Pacelab APD about aerodynamic characteristics are scarce or non. The efficiency and accuracy is also connected to the available detail in the geometry of the airplane.

- What are the most important and commonly used criteria that can be derived from the aerodynamic derivatives and coefficients of the aircraft?

Each stability derivative has its importance, however some can provide more information to the designer about the flying qualities of the airplane such as described on the Discussion sections 9.2 and 9.1. $Cy_{\beta_v}$ is the most important coefficient contribution as it is used and many of the stability derivatives and can heavily influence the results for other coefficients. $Cn_r$ and $Cl_r$ are important derivatives for lateral-directional stability and are considered cross-coupled derivatives. They directly affect the Dutch-Roll mode of the aircraft.

# Chapter 10

# Conclusion

## 10.1 Pacelab APD implementation

In conclusion, the implementation framework of Pacelab APD provides a robust system for modeling, analyzing, and designing aircraft systems efficiently. The framework consists of two main programs: PACE Engineering Workbench (EWB) and PACE Knowledge Designer (KD). EWB allows for the geometrical modeling of the aircraft and displays the data resulting from solving the data model. KD serves as the software where new feature implementation is done and contains the aircraft's data model. The project structure within Pacelab APD allows the user to customize the methods and applications for the design evaluation. However, the unique characteristics of KD regarding the EO and FO require a certain amount of training from the user to correctly implement the methods, functions while connecting the correct inputs to make sure it can be used for other projects/airplanes.

## 10.2 Results and validation

Calculating stability derivatives by using a semi-empirical method is a challenging task for its considerable amount of parameters that interfere with the final results. The details into the creation of a model are directly connected with the quality of the final results, where few parameters in certain coefficients can have a significant impact on other coefficients. Also the lack of precise aerodynamic model in Pacelab ADP impacts on the final results and should be addressed in the future if the software is supposed to be used with the implemented methods for predicting the aerodynamic coefficients.

Besides the impacts caused by these particularities of Pacelab APD, semi-empirical methods offer simplicity and ease of use but with inherent limitations

that can affect the accuracy and reliability of the stability derivative calculations. One of the main difficulties is the reliance on empirical data and assumptions. Semi-empirical methods are based on experimental data obtained from wind tunnel tests, flight testing, or historical aircraft data. These data may not fully capture the complexities of the aerodynamic interactions and phenomena occurring during flight, especially for unconventional or novel aircraft designs. As a result, the accuracy and applicability of the derived stability derivatives may be limited, leading to potential discrepancies between the calculated and actual aircraft behavior.

The B747-400 model analyzed in the previous section 9.2 showed many incongruities to the expected literature values as due to differences in geometrical aspects and other coefficients related estimations embedded in Pacelab Workbench such as lift-curve slope as a user input. Pinpointing the reasons for such different values proved to be time consuming and due to the limited time and in order to remain within schedule, the best option would be to evaluate Pacelab Workbench's prediction of stability derivatives with another airplane, therefore the B737-800 was used. However, the lack of common available models for both Pacelab Workbench and Digital DATCOM as well as literature values for other airplanes proved as a challenge as well to model. The interface for modeling an airplane and its flying conditions for a Digital DATCOM simulation is not user friendly. Inputting the data is still done in FORTRAN and requires a high level of attention and time for checking all necessary information for a reasonable simulation. The small amount of points to describe a fuselage (maximum twenty points) is a limited amount for more complex shape airplanes and since the software considers aerodynamic interference of the fuselage, wrong results can be yield from the simulations.

Another challenge is the assumption of linearity in the aircraft's response. Semi-empirical methods often assume that the aircraft's behavior can be linearized around a particular operating point or within a specific flight envelope. However, this assumption may not hold true for extreme flight conditions, such as high angles of attack, stall, or departure regimes. In these cases, non-linear effects can significantly influence the stability derivatives, and relying solely on linear approximations may lead to inaccurate predictions of the aircraft's dynamic behavior.

Additionally, semi-empirical methods generally lack the ability to account for complex flow phenomena and three-dimensional effects accurately. While they may capture the overall aerodynamic trends reasonably well, they often fail to accurately model flow separation, vortex shedding, and other intricate flow features that can have a substantial impact on stability derivatives. This limitation can particularly affect derivatives that are sensitive to local flow conditions or aircraft configurations, such as those associated with control surfaces.

In contrast, CFD and VLM methods offer more detailed and comprehen-

sive representations of the flow physics around the aircraft. CFD simulations solve the governing fluid equations numerically and can capture complex flow phenomena with high fidelity. VLM methods use a simplified panel representation of the aircraft and solve the potential flow equations to estimate the aerodynamic forces and moments. Both approaches can provide more accurate predictions of stability derivatives, especially in challenging flow conditions and for unconventional aircraft designs.

However, CFD and VLM methods come with their own challenges, such as computational complexity, time requirements, and the need for expertise in fluid dynamics and numerical simulations. They require detailed geometric representations, extensive meshing, and often demand substantial computational resources. As a result, semi-empirical methods remain attractive due to their simplicity, speed, and ease of implementation, especially for initial design and analysis purposes.

In summary, while semi-empirical methods offer practicality and convenience in estimating stability derivatives, they are limited by the reliance on empirical data, assumptions of linearity, and the inability to capture complex flow phenomena accurately. The choice of method should depend on the specific requirements of the analysis and the available resources, considering the trade-offs between accuracy and computational cost. For a conceptual design phase when little details of the airplane have been established, the use of Roskam's method can provide insightful information about the aircraft's behavior to the design engineers if limitations such as subsonic (and sub-critical Mach), low angle of attack and trimmed flight conditions are considered. Conditions outside of these should be addressed by other methods that better describe the aerodynamic effects and its implications of the aircraft motion and behavior.

# References


[1] Saab AB. URL: www.saab.com (cit. on p. 2).

[2] PACE Aerospace Engineering and Information Technology GmbH. *Preliminary Design Pacelab APD*. English. Consulted: 12/May/2023. 2023. URL: https://pace.txtgroup.com/products/preliminary-design/pacelab-apd/ (cit. on p. 2).

[3] David E Bossert et al. *Introduction to Aircraft Flight Mechanics: Performance, Static Stability, Dynamic Stability, and Classical Feedback Control*. American Institute of Aeronautics and Astronautics, 2003 (cit. on p. 5).

[4] JEAN M. DéLERY. *Chapter 8.3 - Shock Wave/Boundary Layer Interactions*. Ed. by GABI BEN-DOR, OZER IGRA, and TOV ELPERIN. Burlington: Academic Press, 2001, pp. 205–I. DOI: https://doi.org/10.1016/B978-012086430-0/50024-5. URL: https://www.sciencedirect.com/science/article/pii/B9780120864300500245 (cit. on p. 5).

[5] Daniel P. Raymer. *Aircraft Design a Conceptual Approach. a Conceptual Approach*. American Institute of Aeronautics & Astronautics, 2018 (cit. on pp. 8, 10, 16, 35–37).

[6] Jose Pedro Magraner Rullan. *Tema 01 - Ecuaciones de la Dinámica de un Avión Rígido*. Tech. rep. Universitat Politècnica de València, Feb. 2021 (cit. on pp. 11, 12).

[7] Brian L Stevens, Frank L Lewis, and Eric N Johnson. *Aircraft Control and Simulation: Dynamics, Controls Design, and Autonomous Systems. Dynamics, Controls Design, and Autonomous Systems*. John Wiley & Sons, 2015, p. 768 (cit. on p. 13).

[8] MR Napolitano. *Aircraft Dynamics: From Modeling to Simulation, 2012. from modeling to simulation*. John Wiley & Sons, 2012 (cit. on pp. 16, 20, 22, 38, 54–56, 64, 97).

[9] Jose Pedro Magraner Rullan. *Tema 02-A - Método de Estudio y de Cálculo de la Dinámica del Movimiento No Estacionario de un Avión. Linealización de las Ecuaciones de Bryan. Movimiento Longitudinal*. Tech. rep. Universitat Politècnica de València, Feb. 2021 (cit. on pp. 16–18).

[10] Jan Roskam. *Airplane Flight Dynamics and Automatic Flight Controls Part I*. 2001 (cit. on pp. 19, 54–56, 63, 97).

[11] Jan Roskam. *Methods for Estimating Stability and Control Derivatives of Conventional Subsonic Airplanes*. 1971 (cit. on pp. 22, 23, 25, 28, 31, 34, 44, 49, 65).

[12] DE Hoak and RD Finck. *USAF Stability and Control DATCOM*. National Technical Information Service, 1978 (cit. on pp. 22, 54, 55, 67, 77–89, 91–93, 95).

[13] Inc. AAT Bioquest. *Quest Graph™ Linear, Logarithmic, Semi-Log Regression Calculator. AAT Bioquest*. May 2023. URL: https://www.aatbio.com/tools/linear-logarithmic-semi-log-regression-online-calculator (cit. on p. 28).

[14] R. WEISSMAN. *Status of Design Criteria for Predicting Departure Characteristics and Spin Susceptibility*. DOI: 10.2514/6.1974-791. eprint: https://arc.aiaa.org/doi/pdf/10.2514/6.1974-791. URL: https://arc.aiaa.org/doi/abs/10.2514/6.1974-791 (cit. on pp. 37, 68).

[15] Robert A. McDonald and James R. Gloudemans. *Open Vehicle Sketch Pad: An Open Source Parametric Geometry and Analysis Tool for Conceptual Aircraft Design*. DOI: 10.2514/6.2022-0004. eprint: https://arc.aiaa.org/doi/pdf/10.2514/6.2022-0004. URL: https://arc.aiaa.org/doi/abs/10.2514/6.2022-0004 (cit. on pp. 54, 55).

[16] Federal Aviation Regulations. *Part 23 Airworthiness Standards: Normal, Utility, Acrobatic and Commuter Category Airplanes*. 1989 (cit. on p. 67).

[17] National Archives and Records Administration. *Special Conditions: The Boeing Company, Model 737-8 Airplanes; Design Roll-Maneuver Requirements*. Nov. 2016. URL: https://www.federalregister.gov/documents/2016/02/11/2016-02762/special-conditions-the-boeing-company-model-737-8-airplanes-design-roll-maneuver-requirements (cit. on p. 68).

[18] Euclid C Holleman. *Flight Investigation of the Roll Requirements for Transport Airplanes in Cruising Flight*. Tech. rep. 1970 (cit. on p. 68).

[19] USAF MIL. *8785C: Military Specification*. 1980 (cit. on p. 68).

# Appendices

# Appendix A

# Empirical plots used for aerodynamic derivatives calculation

## A.1 Plots used sideslip angle derivatives

Figure A.1: Wing-body interference factor for wing-body sideslip derivative $Cy_\beta$ (reproduced from figure 7.1 [12])

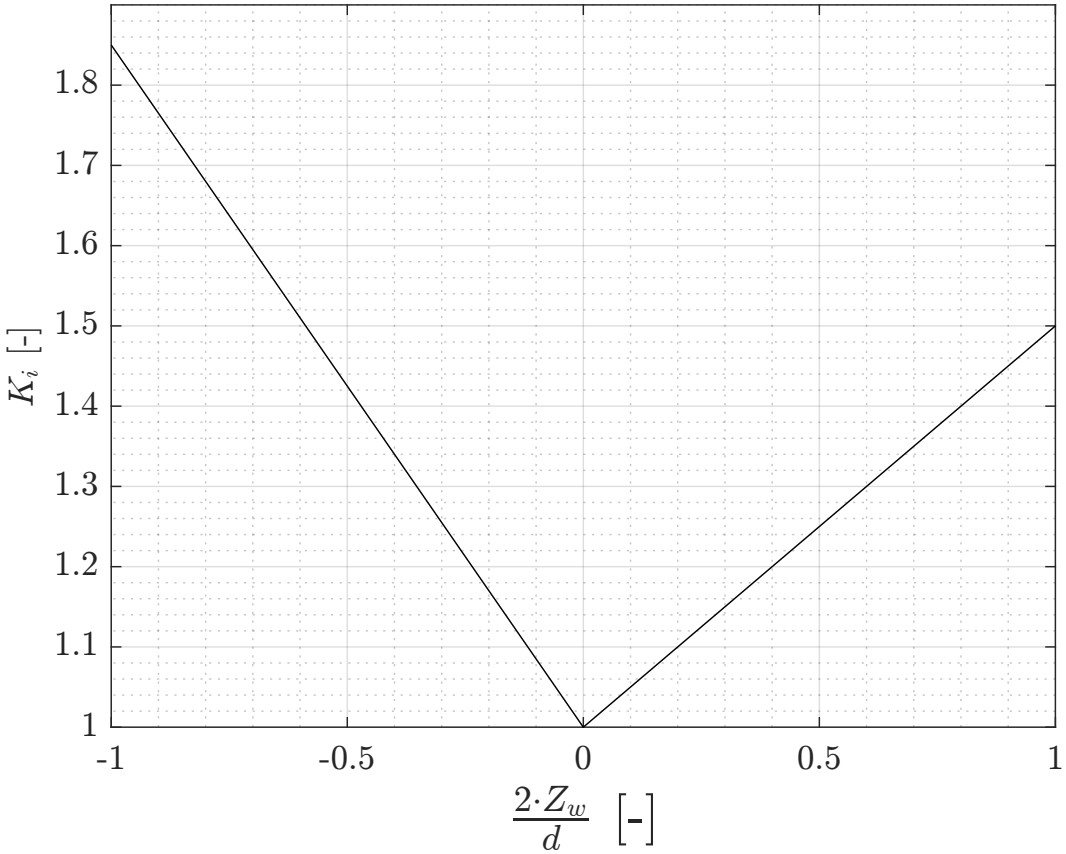

Figure A.2: Aspect ratio factor due to body interference (reproduced from figure 7.3 [12])

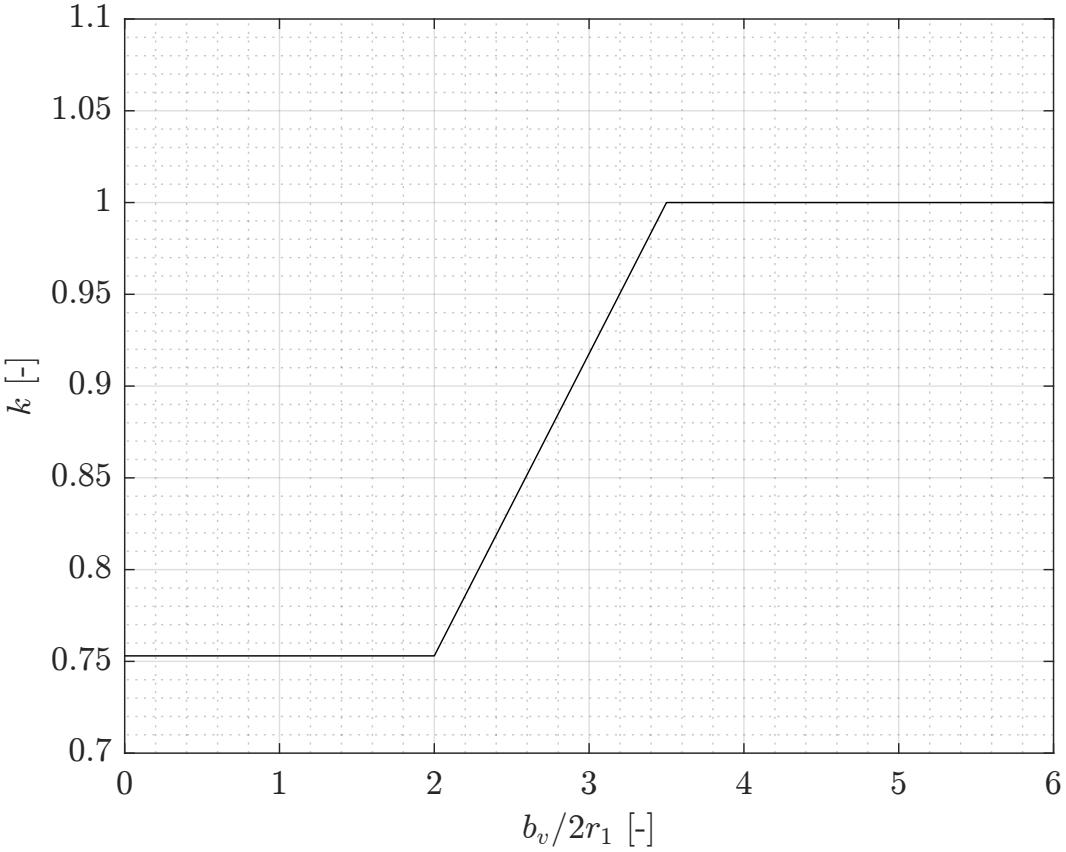

Figure A.3: Aspect ratio factor due to body interference (reproduced from figure 7.5 [12])

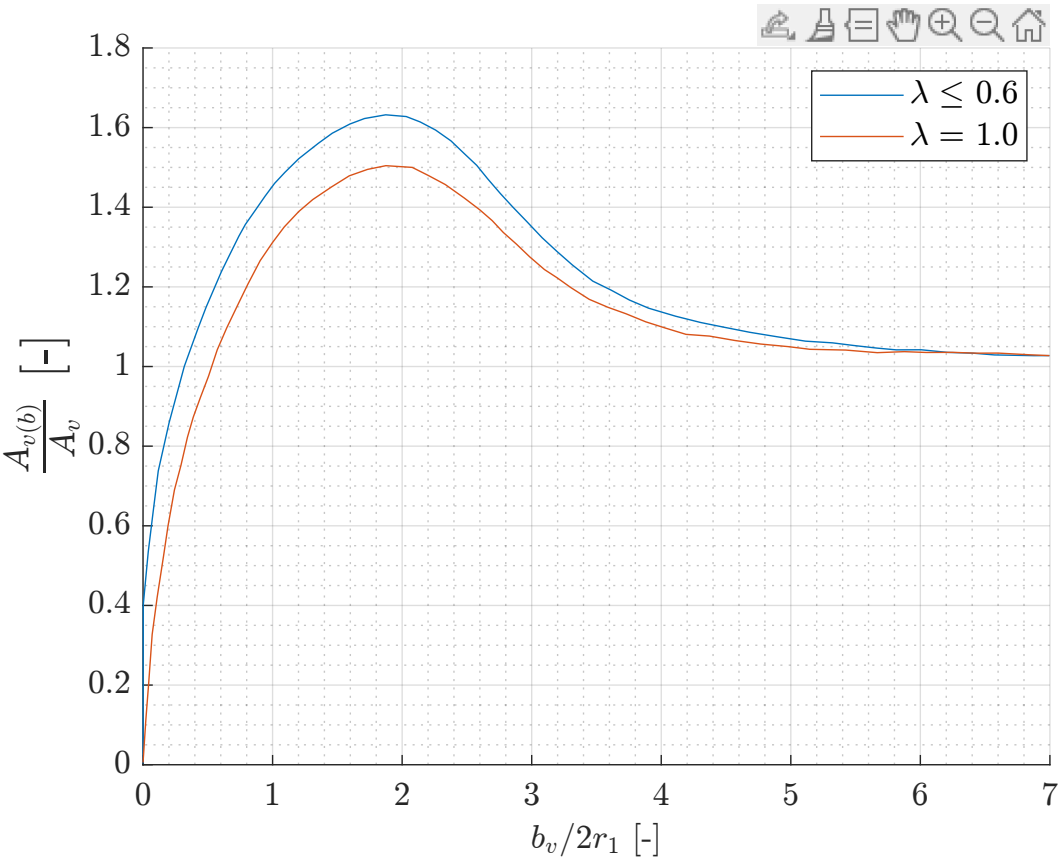

Figure A.4: Aspect ratio factor due to horizontal tail interference (reproduced from figure 7.6 [12])

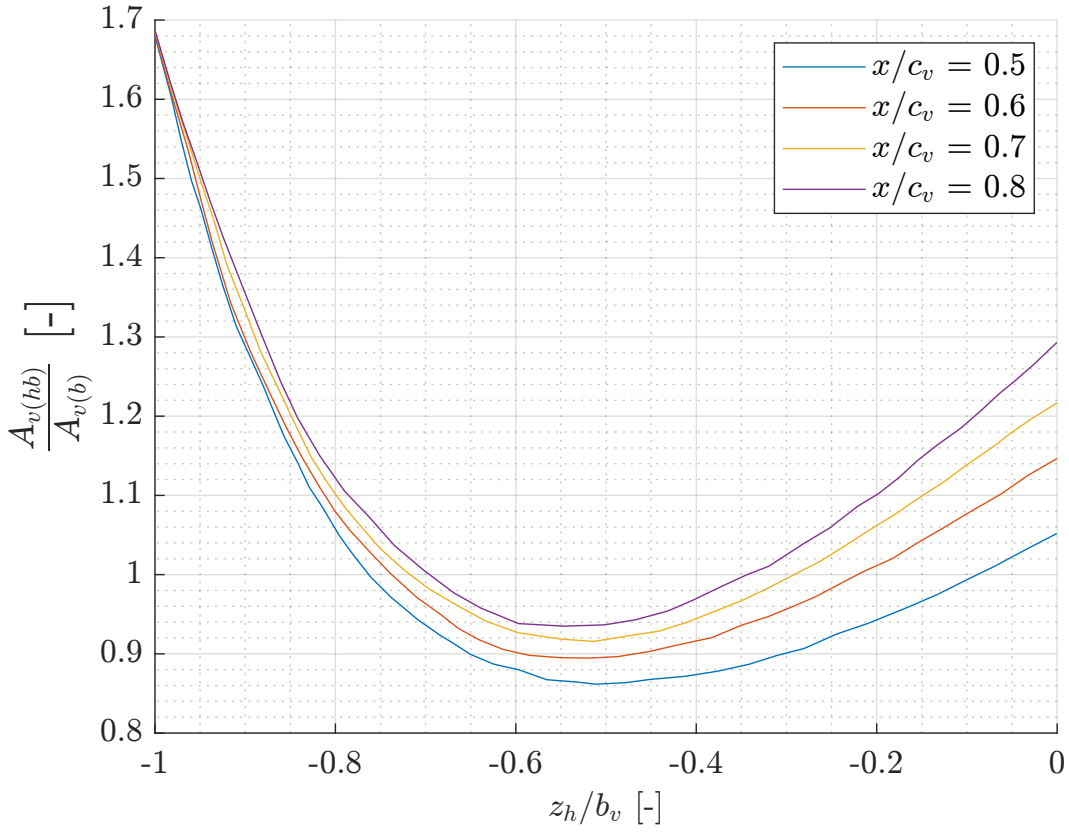

Figure A.5: Factor accounting for relative size of horizontal and vertical tails (reproduced from figure 7.7 [12])

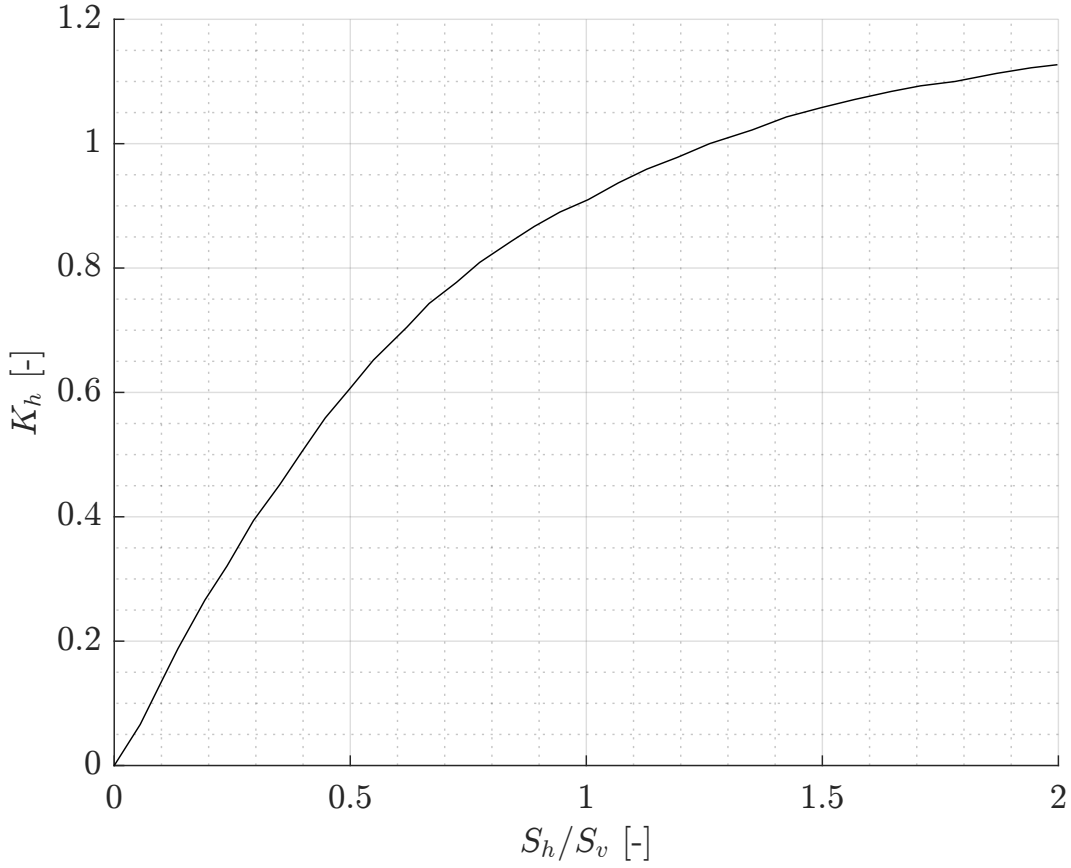

Figure A.6: Wing sweep contribution to $Cl_\beta$ (reproduced from figure 7.11 [12])

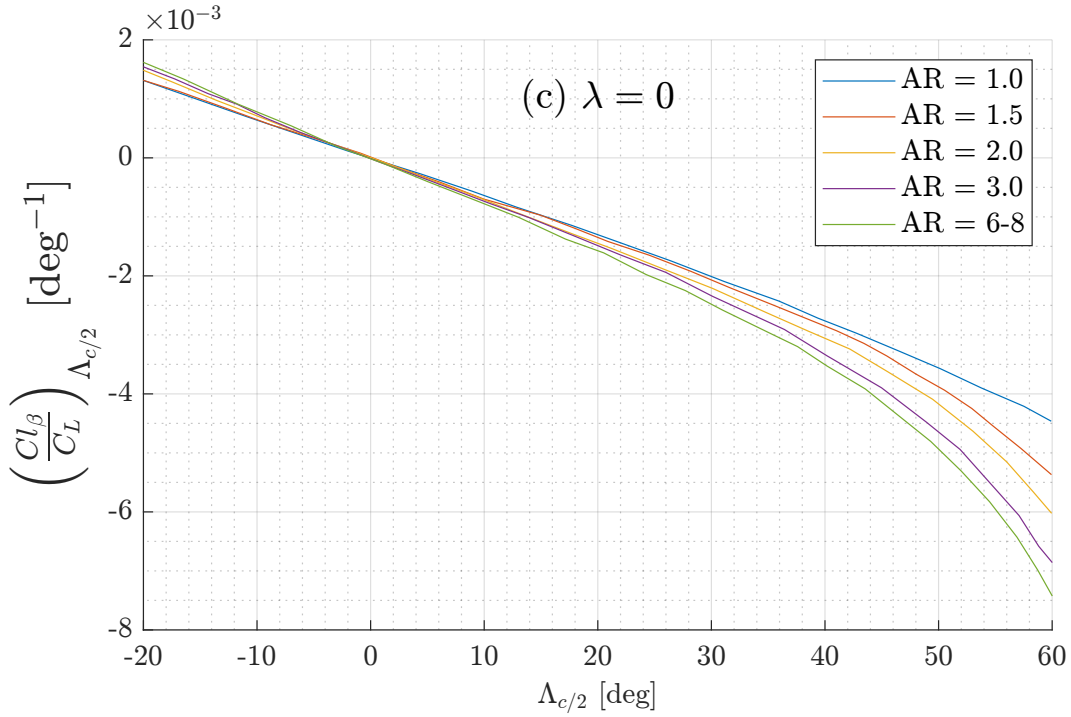


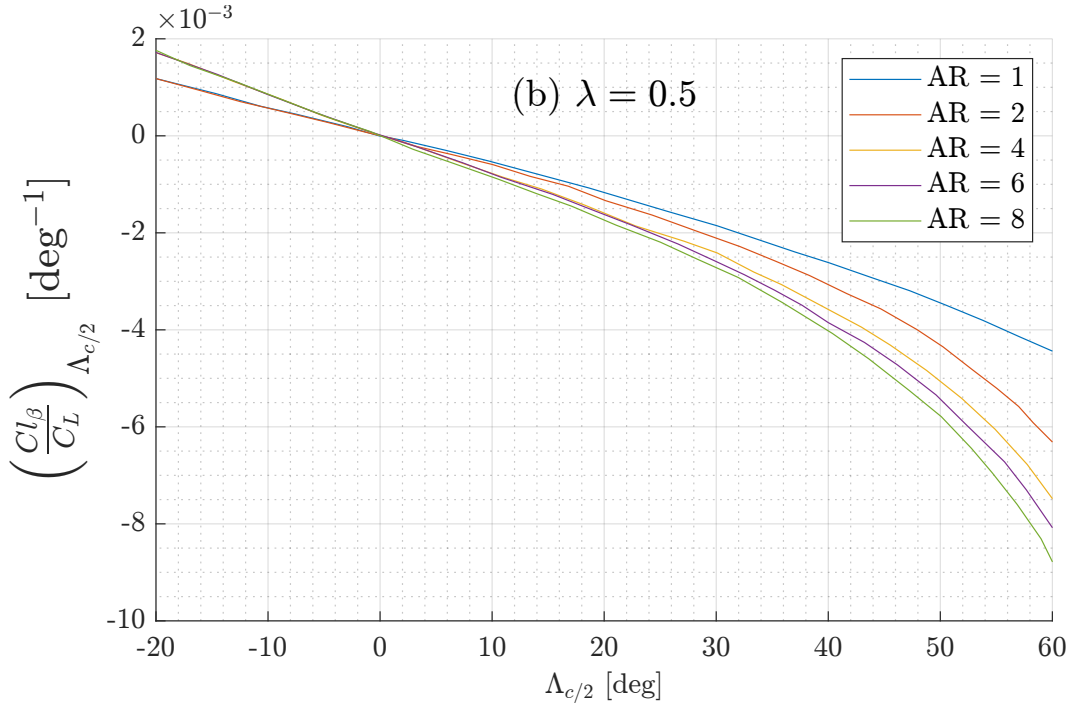

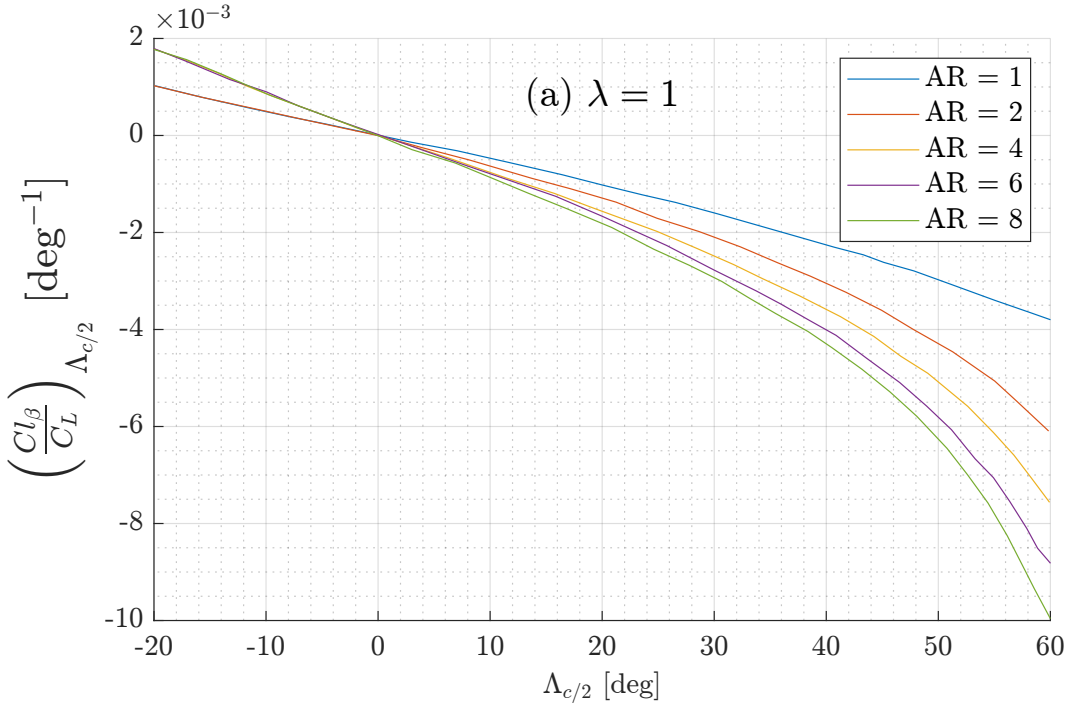


Figure A.7: Compressibility correction factor to sweep contribution to wing $C_{l_\beta}$ (reproduced from figure 7.12 [12])

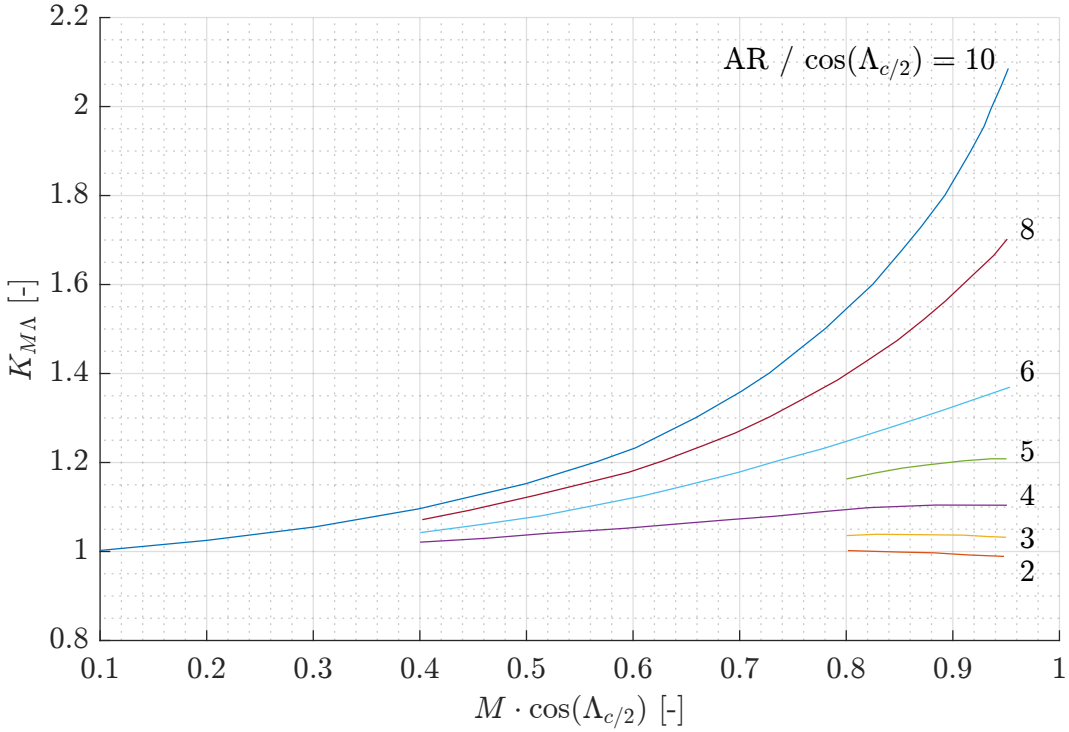

Figure A.8: Fuselage correction factor(reproduced from figure 7.13 [12])

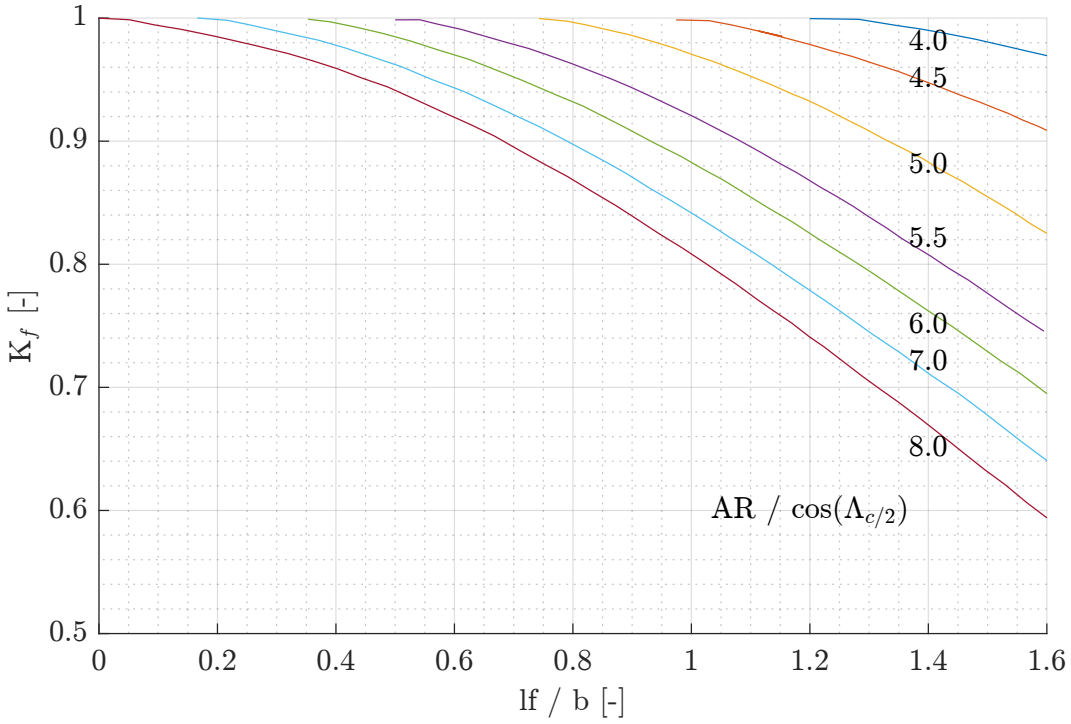


Figure A.9: Aspect ratio contribution to wing $Cl_\beta$ (reproduced from figure 7.14 [12])

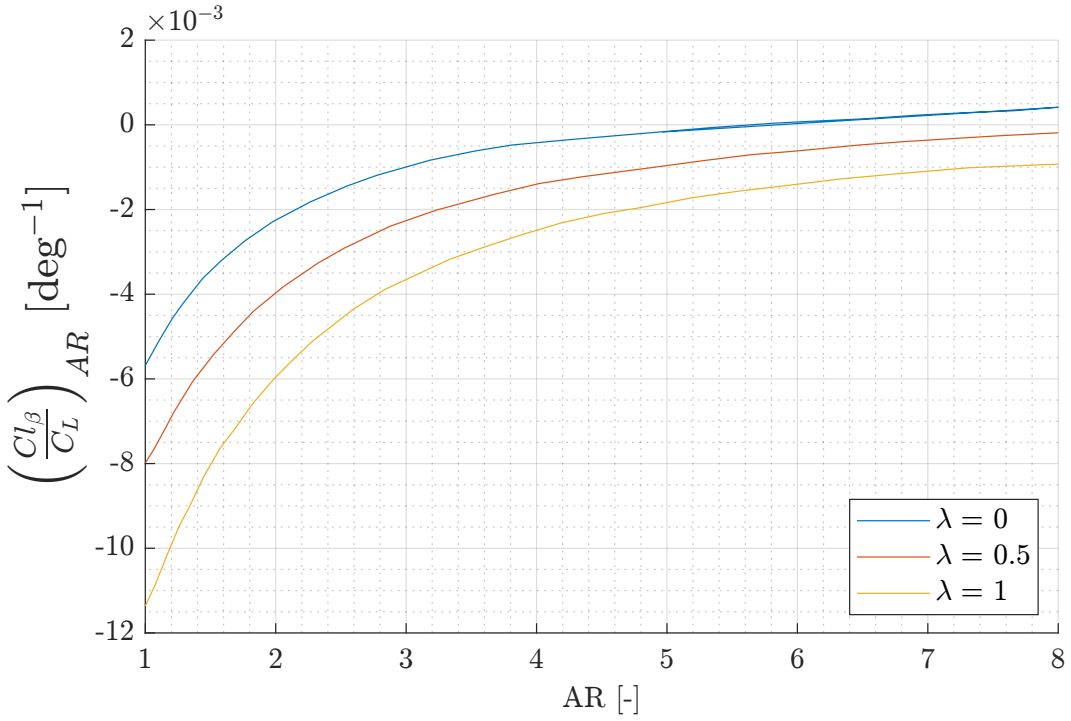

Figure A.10: Effect of uniform geometric dihedral on wing $Cl_\beta$ (reproduced from figure 7.15 [12])

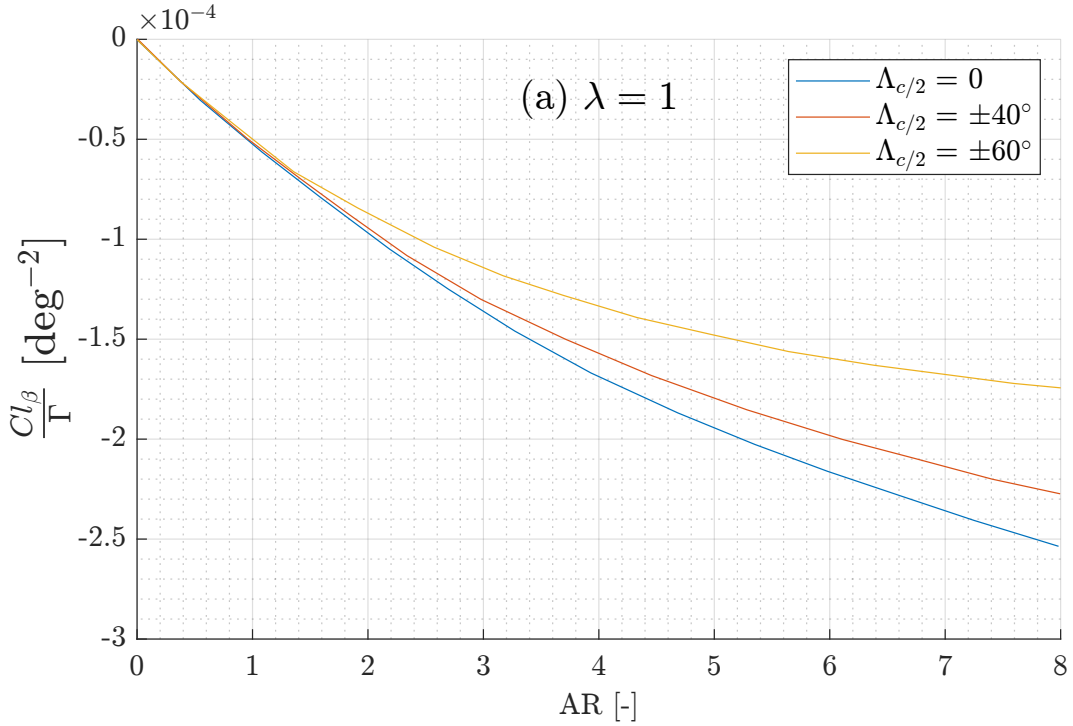


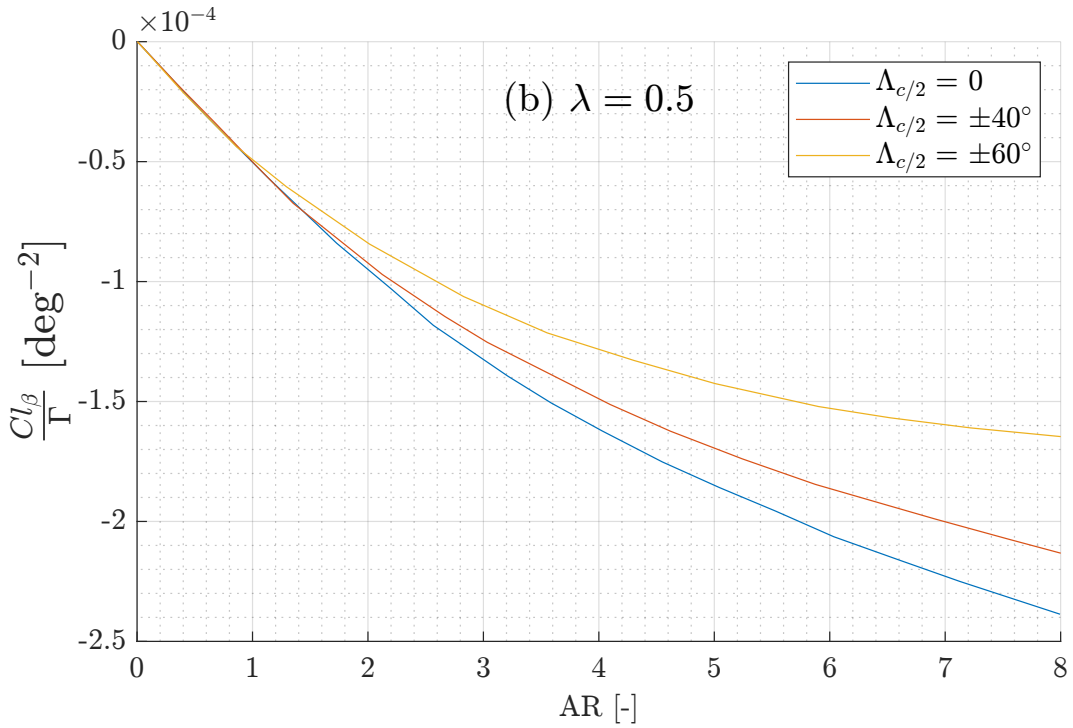

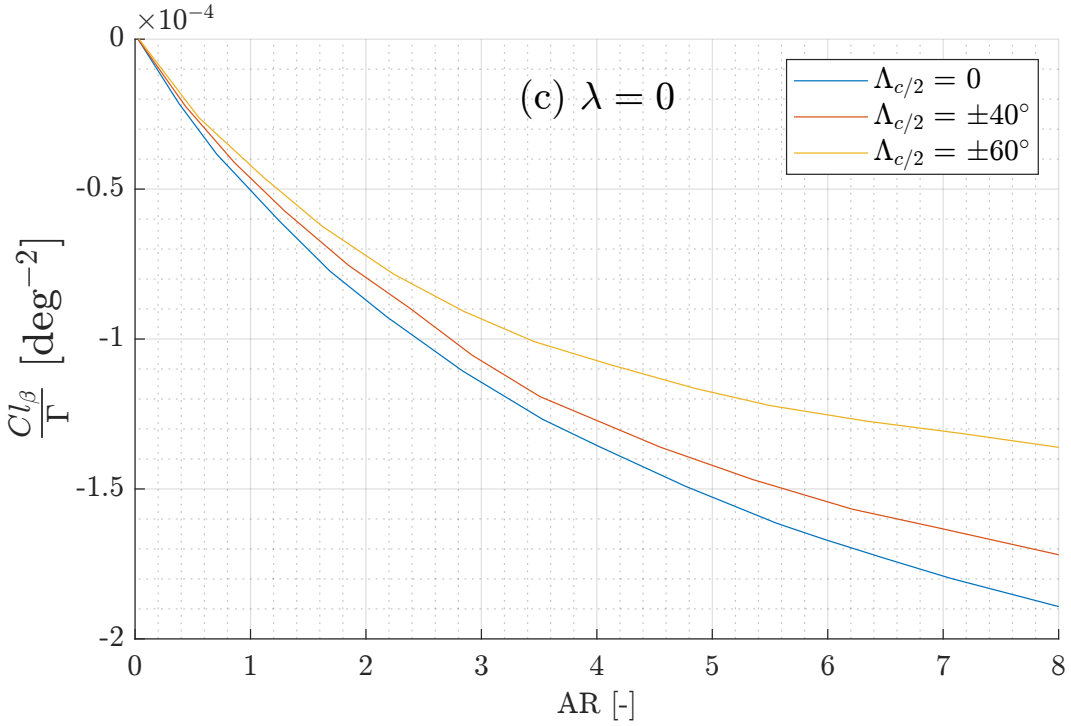


Figure A.11: Compressibility correction to dihedral effect on wing $Cl_\beta$ (reproduced from figure 7.16 [12])

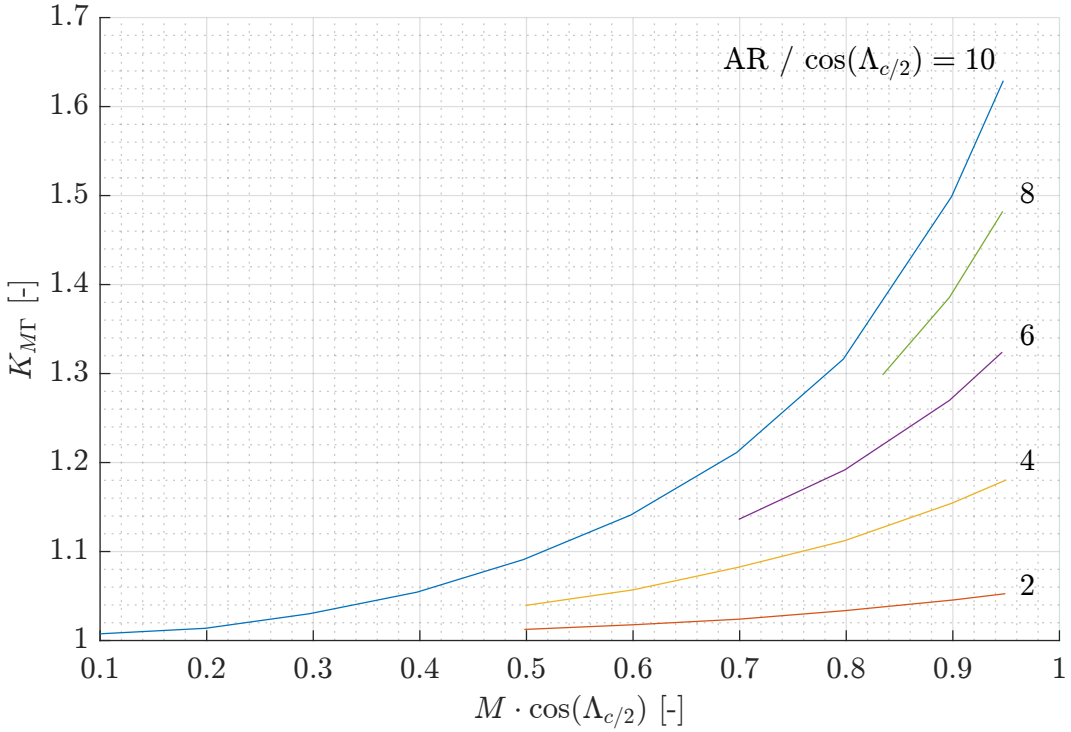

Figure A.12: Effect of wing twist on wing $Cl_\beta$ (reproduced from figure 7.17 [12])

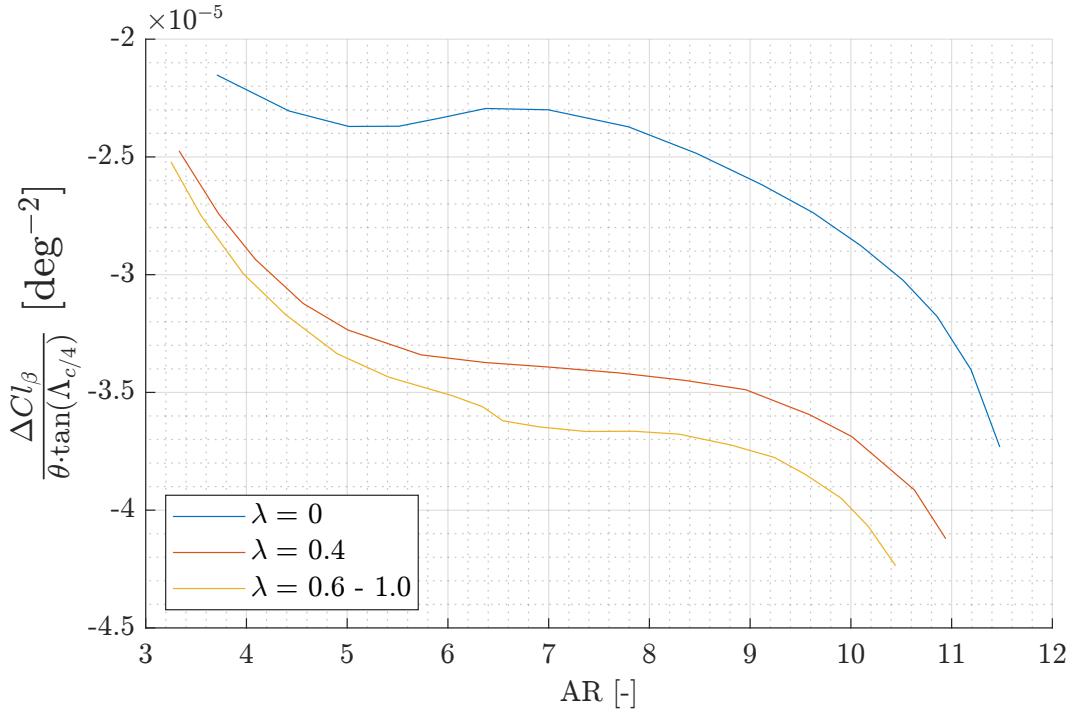

Figure A.13: Empirical factor Kn related to sideslip derivative $Cn_\beta$ for body+wing-body interference (reproduced from figure 7.19 [12])

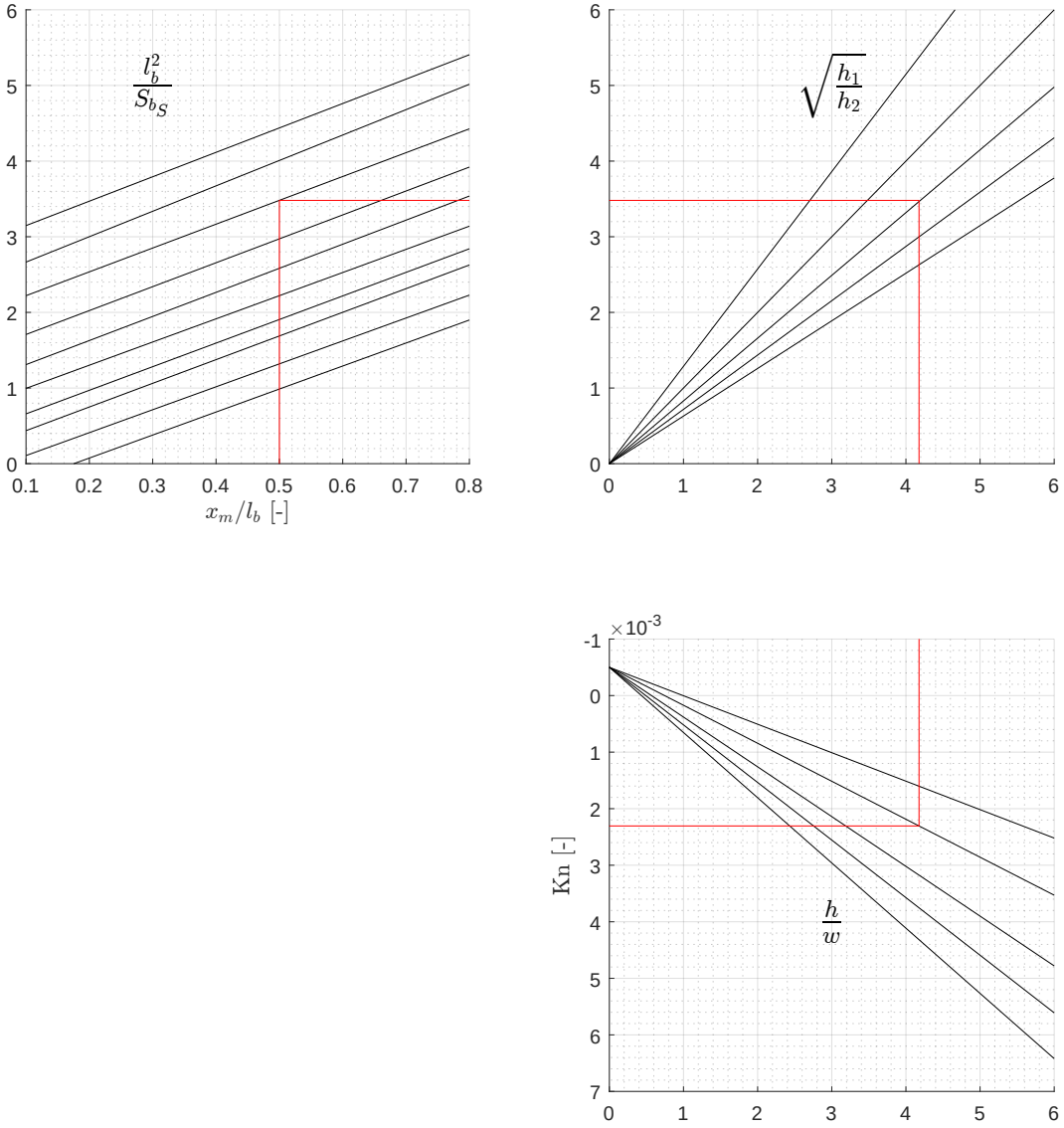

## A.2 Plots used roll rate derivatives

Figure A.14: Roll damping parameter (reproduced from figure 8.1 [12])

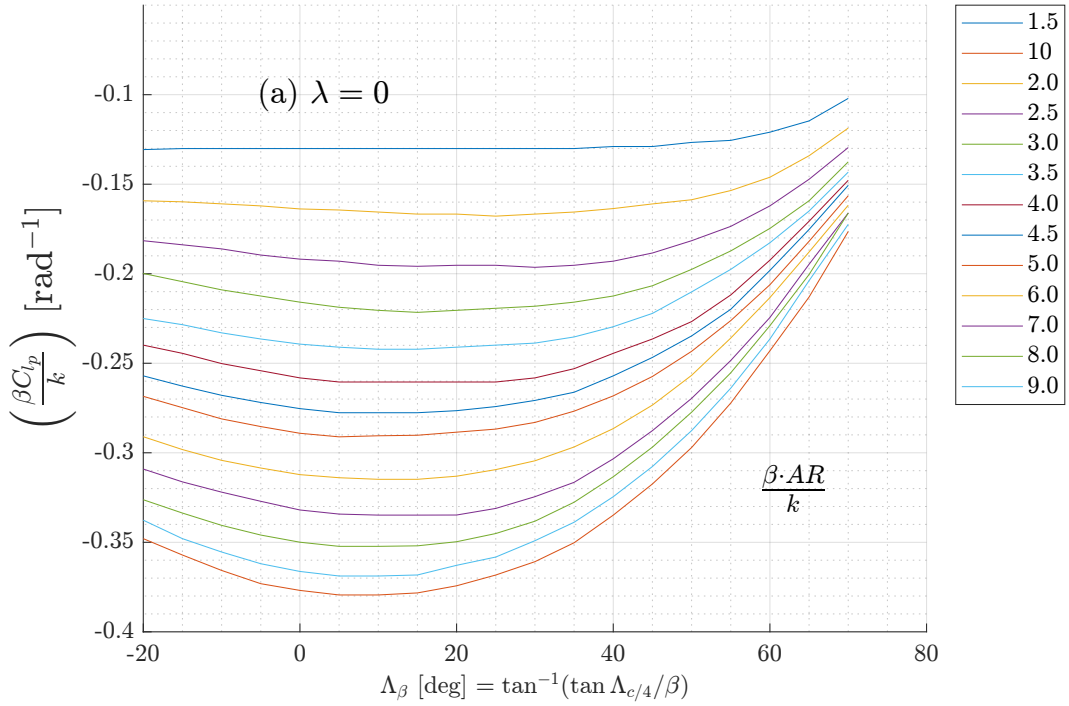

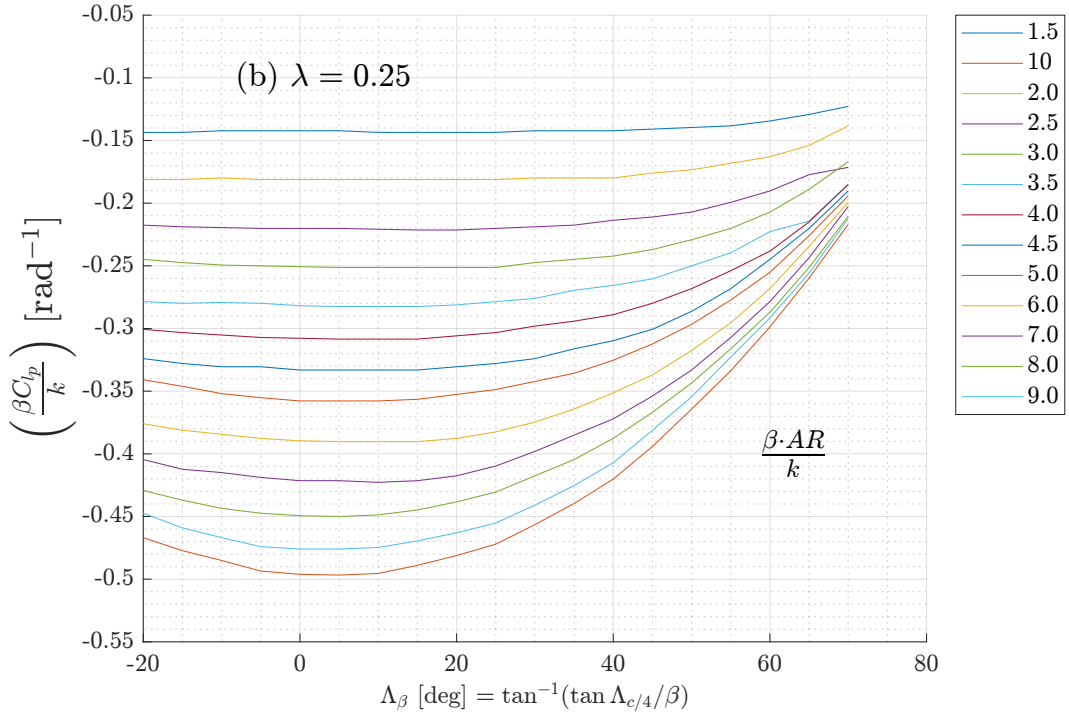
(b) $\lambda = 0.25$
$\left(\frac{\beta C_{l_p}}{k}\right)$ [rad$^{-1}$]
$\frac{\beta \cdot AR}{k}$
$\Lambda_\beta$ [deg] $= \tan^{-1}(\tan \Lambda_{c/4}/\beta)$
-0.05
-0.1
-0.15
-0.2
-0.25
-0.3
-0.35
-0.4
-0.45
-0.5
-0.55
-20
0
20
40
60
80
1.5
10
2.0
2.5
3.0
3.5
4.0
4.5
5.0
6.0
7.0
8.0
9.0

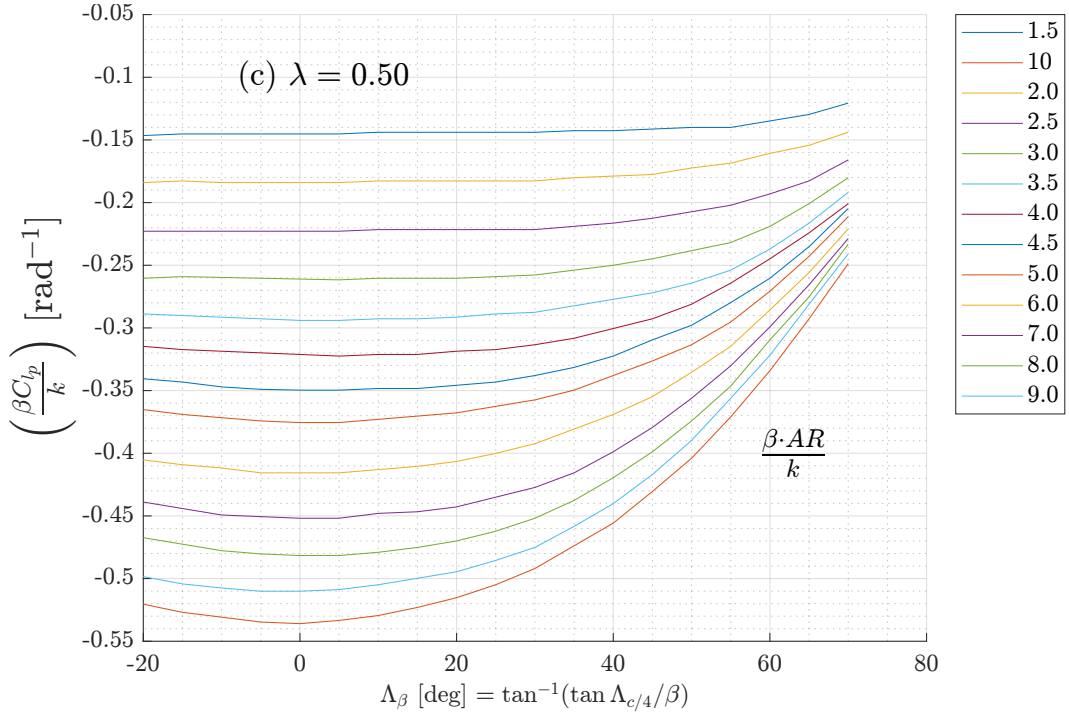
(c) $\lambda = 0.50$
$\left(\frac{\beta C_{l_p}}{k}\right)$ [rad$^{-1}$]
$\frac{\beta \cdot AR}{k}$
$\Lambda_\beta$ [deg] $= \tan^{-1}(\tan \Lambda_{c/4}/\beta)$
-0.05
-0.1
-0.15
-0.2
-0.25
-0.3
-0.35
-0.4
-0.45
-0.5
-0.55
-20
0
20
40
60
80
1.5
10
2.0
2.5
3.0
3.5
4.0
4.5
5.0
6.0
7.0
8.0
9.0

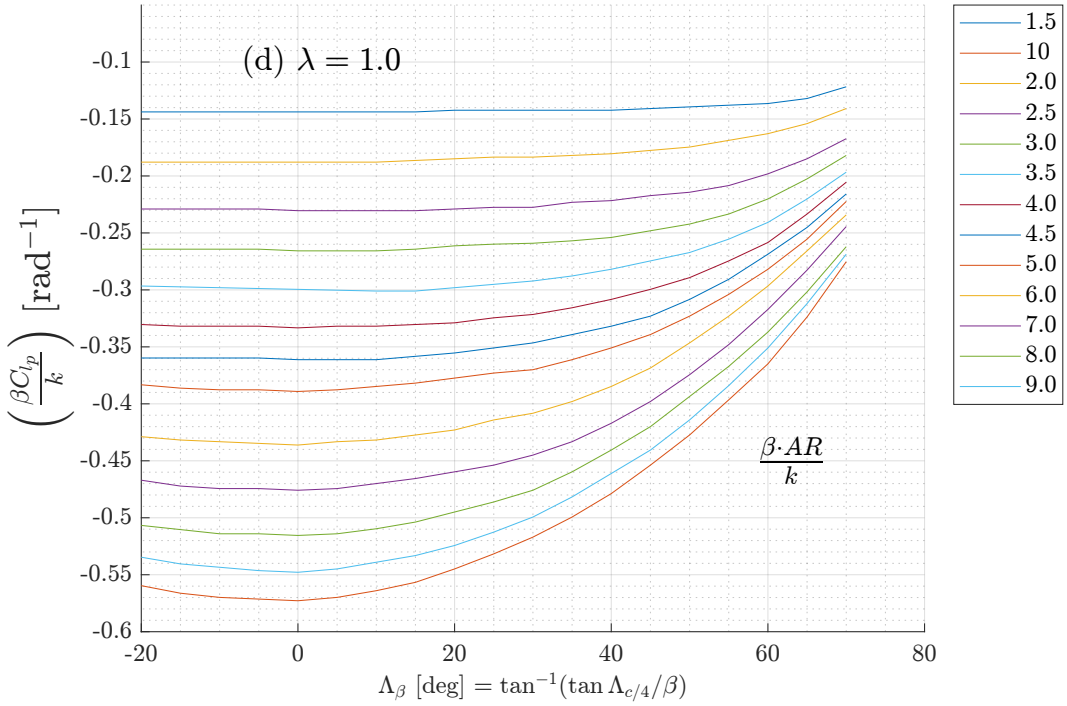


Figure A.15: Effect of wing twist on wing rolling derivative $Cn_p$ (reproduced from figure 8.2 [12])

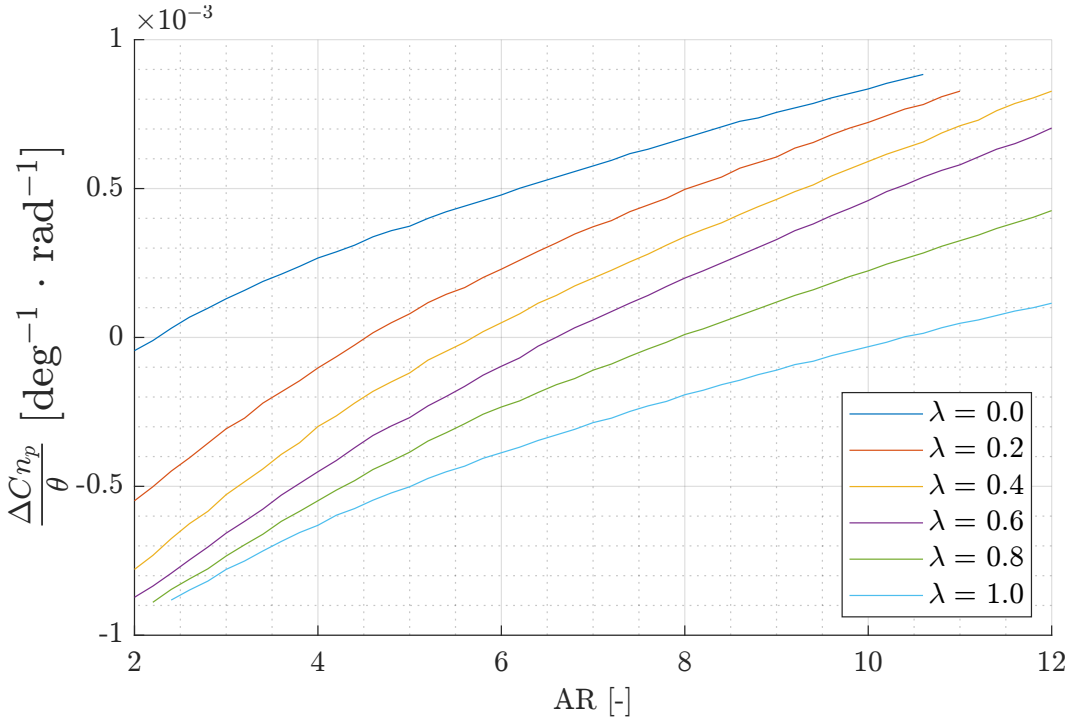

## A.3 Plots used yaw rate derivatives

Figure A.16: Wing yawing derivative $Cl_r$ (reproduced from figure 9.1 [12])

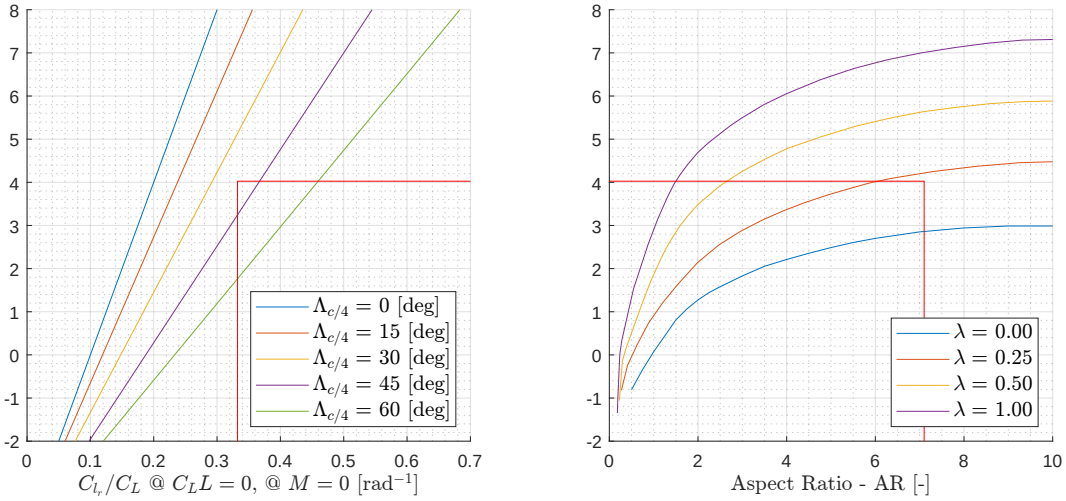

Figure A.17: Effect of wing twist on wing yawing derivative $Cl_r$ (reproduced from figure 9.2 [12])

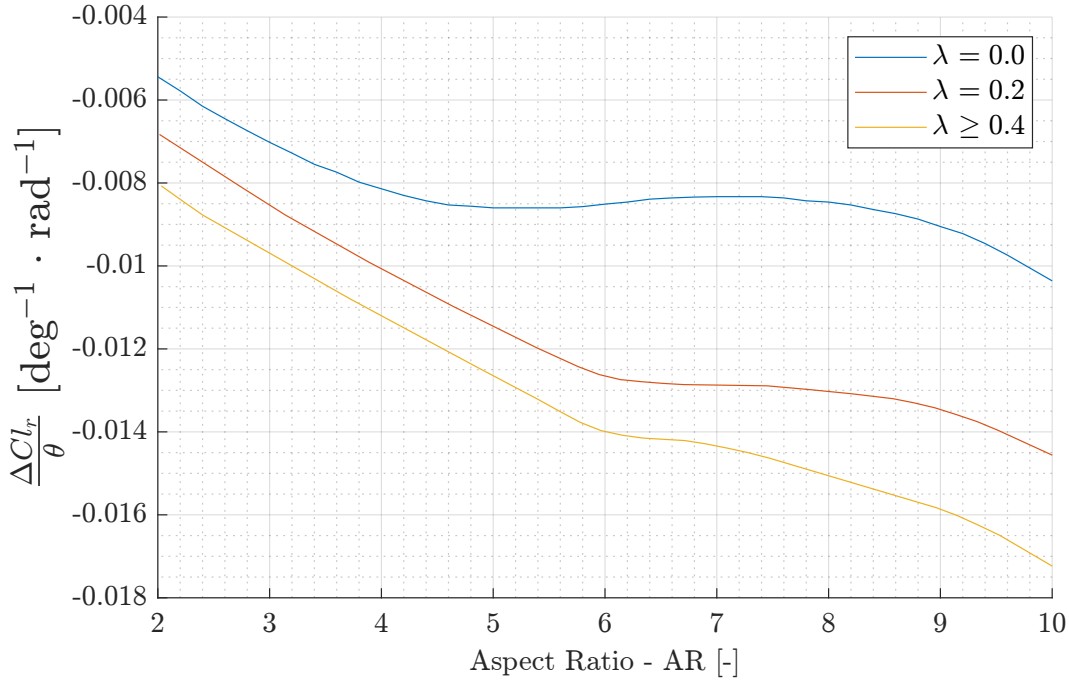


Figure A.18: Low speed drag-due-to-lift yaw-damping parameter (reproduced from figure 9.4 [12])

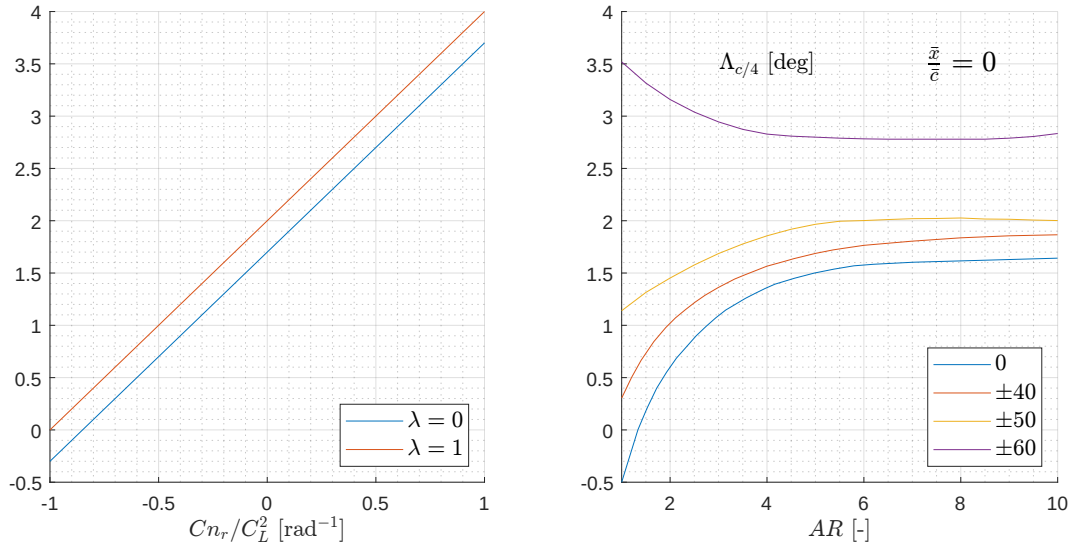

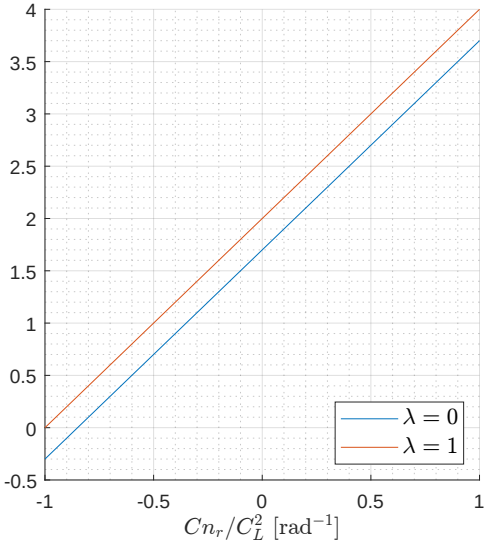
$\lambda = 0$
$\lambda = 1$
$Cn_r/C_L^2$ [rad$^{-1}$]

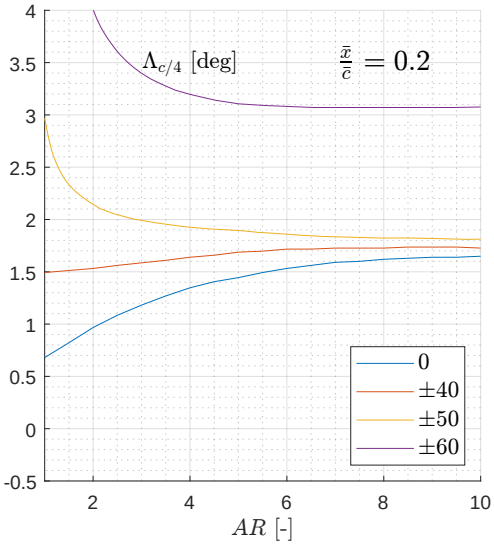
$\Lambda_{c/4}$ [deg]
$\frac{\bar{s}}{\bar{c}} = 0.2$
0
±40
±50
±60
$AR$ [-]

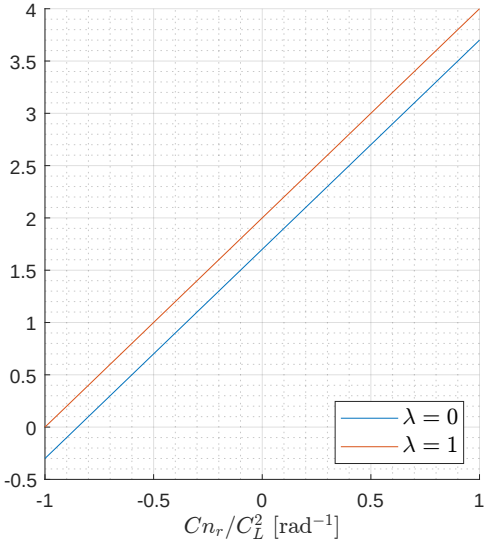
$\lambda = 0$
$\lambda = 1$
$Cn_r/C_L^2$ [rad$^{-1}$]

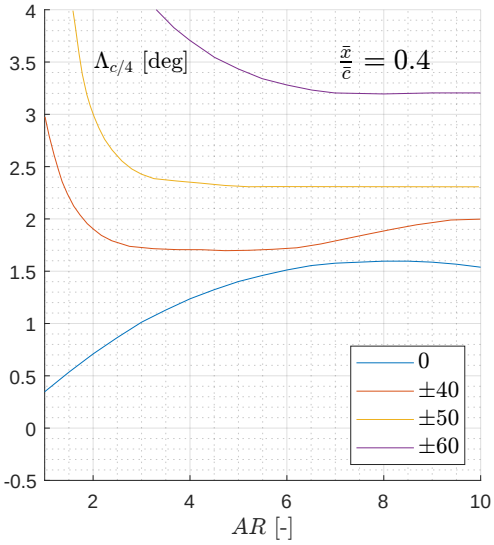
$\Lambda_{c/4}$ [deg]
$\frac{\bar{s}}{\bar{c}} = 0.4$
0
±40
±50
±60
$AR$ [-]

Figure A.19: Low speed profile-drag yaw-damping parameter (reproduced from figure 9.5 [12])

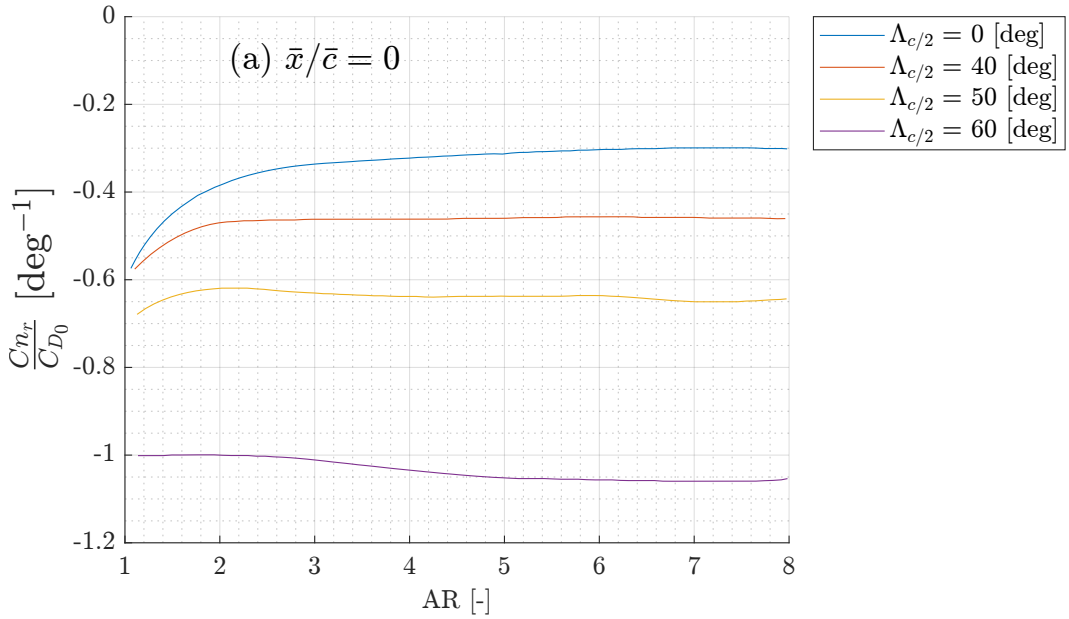


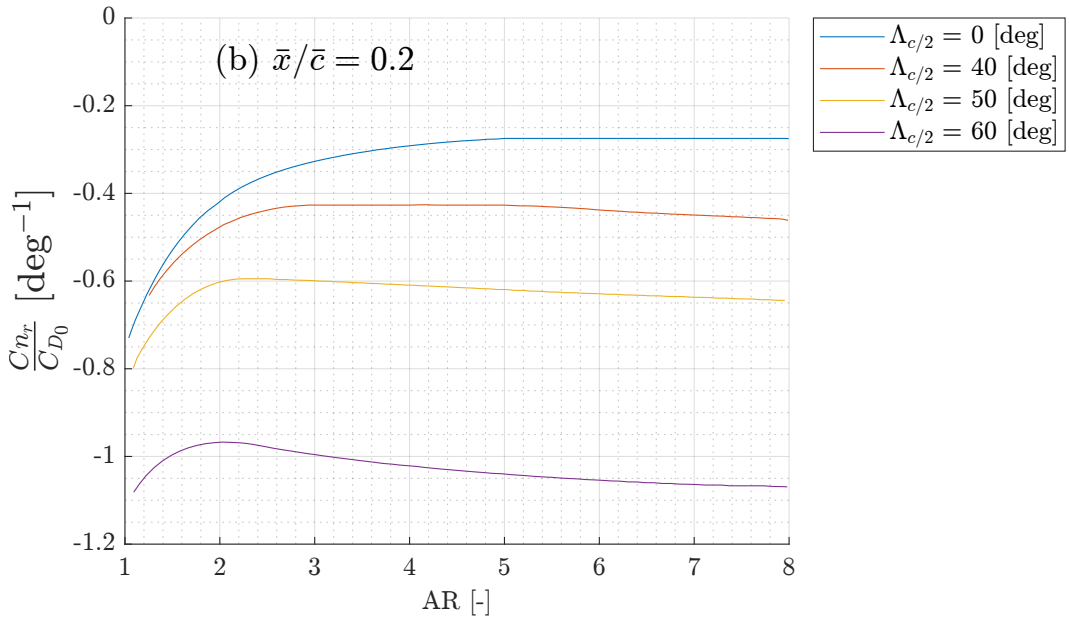

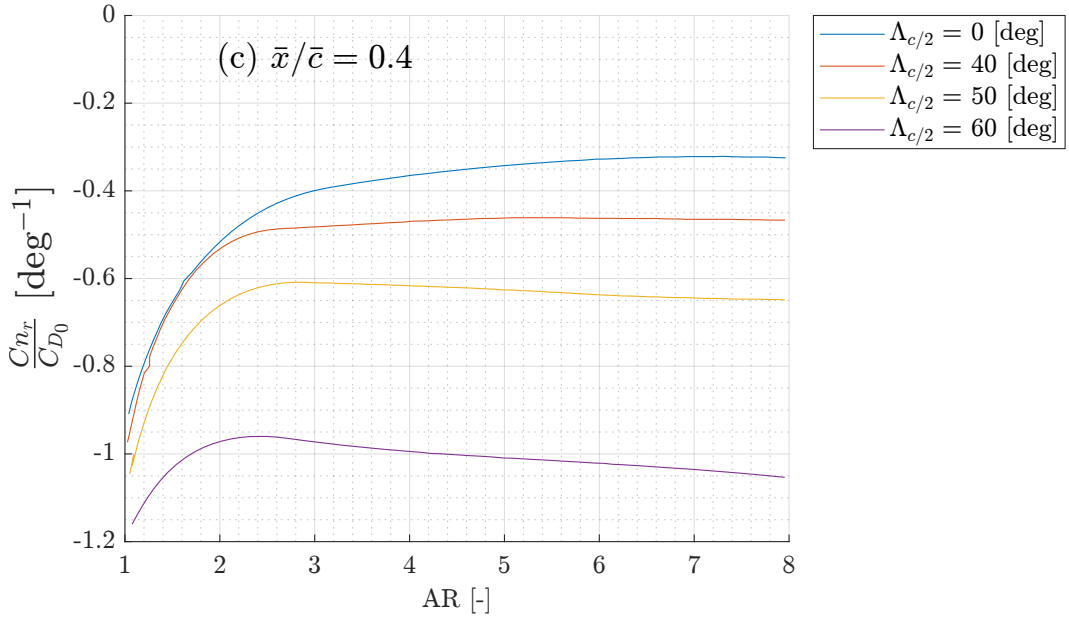
(c) $\bar{x}/\bar{c} = 0.4$
$\frac{Cn_r}{C_{D_0}}$ [deg$^{-1}$]
AR [-]
0
-0.2
-0.4
-0.6
-0.8
-1
-1.2
1
2
3
4
5
6
7
8
$\Lambda_{c/2} = 0$ [deg]
$\Lambda_{c/2} = 40$ [deg]
$\Lambda_{c/2} = 50$ [deg]
$\Lambda_{c/2} = 60$ [deg]

# Appendix B

# Aircraft data

## B.1 Boeing 747-200 data

Table B.1: Provided data for the Boeing 747-200 by [8] and [10]

| | | | |
|---|---|---|---|
| Wing Surface ($ft^2$) | | 5.5 | |
| Mean Aerodynamic Chord (MAC) ($ft$) | | 27.3 | |
| Wing Span ($ft$) | | 196 | |
| | Approach | Cruise (low) | Cruise (high) |
| Altitude ($ft$) | 0 | 20,000 | 40,000 |
| Mach Number | 0.198 | 0.65 | 0.90 |
| True Airspeed ($ft/sec$) | 221 | 673 | 871 |
| Dynamic Pressure ($lbs/ft^2$) | 58 | 287.2 | 222.8 |
| Location of CG % MAC | 0.25 | 0.25 | 0.25 |
| Steady state angle of attack ($deg$) | 8.5 | 2.5 | 2.4 |
| Mass ($lbs$) | 564,000 | 636,636 | 636,636 |
| Moment of Inertia x-axis ($slugft^2$) | 13,700,000 | 18,200,000 | 18,200,000 |
| Moment of Inertia y-axis ($slugft^2$) | 30,500,000 | 33,100,000 | 33,100,000 |
| Moment of Inertia z-axis ($slugft^2$) | 43,100,000 | 49,700,000 | 49,700,000 |
| Product of inertia xz-plane ($slugft^2$) | 830 | 970 | 970 |
| | Approach | Cruise (low) | Cruise (high) |
| Steady State | | | |
| $C_{L1}$ | 1.76 | 0.4 | 0.52 |
| $C_{D1}$ | 2,630 | 250 | 450 |
| $C_{m1}$ | 0 | 0 | 0 |
| $CT_{X1}$ | 2,630 | 250 | 450 |
| $Cm_T$ | 0 | 0 | 0 |
| Stability Derivatives | | | |
| $CD_0$ | 0.751 | 0.164 | 0.305 |

| | | | |
|---|---|---|---|
| $CD_u$ | 0 | 0 | 0 |
| $CD_0$ | 1.13 | 0.20 | 0.50 |
| $CT_{Xu}$ | -5,523 | -55 | -950 |
| $CL_O$ | 0.92 | 0.21 | 0.29 |
| $CL_U$ | -0.22 | 0.13 | -0.23 |
| $CL_\alpha$ | 5.67 | 4.4 | 5.5 |
| $CL_{\dot{\alpha}}$ | 6.7 | 7.0 | 8.0 |
| $CL_q$ | 5.65 | 6.6 | 7.8 |
| $Cm_0$ | 0 | 0 | 0 |
| $Cm_u$ | 71 | 13 | -0.09 |
| $Cm_\alpha$ | -1.45 | -1.00 | -1.60 |
| $Cm_{\dot{\alpha}}$ | -3.3 | -4.0 | -9.0 |
| $Cm_q$ | -21.4 | -20.5 | -25.5 |
| $Cm_T$ | 0 | 0 | 0 |
| $Cm_{T\alpha}$ | 0 | 0 | 0 |
| | Control Derivatives | | |
| $CD_{\delta E}/CD_{IH}$ | 0/0 | 0/0 | 0/0 |
| $CL_{\delta E}/CL_{IH}$ | 0.36/0.75 | 0.32/0.70 | 0.30/0.65 |
| $CM_{\delta E}/CM_{IH}$ | -1.40/-3.0 | -1.30/-2.70 | 1.20/-2.50 |
| | Approach | Cruise (low) | Cruise (high) |
| | Stability Derivatives | | |
| $C_{l\beta}$ | -0.281 | -0.160 | -0.95 |
| $C_{lp}$ | -0.502 | -0.340 | -0.320 |
| $C_{lr}$ | 0.195 | 0.130 | 0.200 |
| $C_{y\beta}$ | -1.08 | -0.90 | -0.90 |
| $C_{yp}$ | 0 | 0 | 0 |
| $C_{yr}$ | 0 | 0 | 0 |
| $C_{n\beta}$ | 0.184 | 0.160 | 0.210 |
| $C_{nT\beta}$ | 0 | 0 | 0 |
| $C_{np}$ | -0.0222 | -0.026 | 0.02 |
| $C_{nr}$ | -0.360 | -0.280 | -0.330 |
| | Control Derivatives | | |
| $C_{l\delta\alpha}$ | 0.053 | 0.013 | 0.014 |
| $C_{l\delta r}$ | 0 | 0.08 | 0.05 |
| $C_{Y\delta\alpha}$ | 0 | 0 | 0 |
| $C_{Y\delta r}$ | 0.0179 | 0.0120 | 0.060 |
| $C_{n\delta\alpha}$ | 0.083 | 0.018 | -0.028 |
| $C_{n\delta r}$ | -0.113 | -0.10 | -0.95 |